

---

Wayne State University Theses


---

1-1-2016

# Targeted Delivery Of Nrf2 Sirna Using Modular Polymeric Micellar Nanodelivery System For Efficient Target Gene Knockdown In Hepatocellular Carcinoma

Shaimaa Mohamed Ibrahim Yousef  
*Wayne State University,*

Follow this and additional works at: [https://digitalcommons.wayne.edu/oa\\_theses](https://digitalcommons.wayne.edu/oa_theses)

 Part of the [Medicinal Chemistry and Pharmaceutics Commons](#), [Nanoscience and Nanotechnology Commons](#), and the [Polymer Chemistry Commons](#)

---

## Recommended Citation

Yousef, Shaimaa Mohamed Ibrahim, "Targeted Delivery Of Nrf2 Sirna Using Modular Polymeric Micellar Nanodelivery System For Efficient Target Gene Knockdown In Hepatocellular Carcinoma" (2016). *Wayne State University Theses*. 514.  
[https://digitalcommons.wayne.edu/oa\\_theses/514](https://digitalcommons.wayne.edu/oa_theses/514)

This Open Access Thesis is brought to you for free and open access by DigitalCommons@WayneState. It has been accepted for inclusion in Wayne State University Theses by an authorized administrator of DigitalCommons@WayneState.

**TARGETED DELIVERY OF NRF2 SIRNA USING MODULAR POLYMERIC  
MICELLAR NANODELIVERY SYSTEM FOR EFFICIENT TARGET GENE  
KNOCKDOWN IN HEPATOCELLULAR CARCINOMA**

by

**SHAIMAA YOUSEF**

**THESIS**

Submitted to the Graduate School

of Wayne State University,

Detroit, Michigan

in partial fulfillment of the requirements

for the degree of

**MASTER OF SCIENCE**

2016

MAJOR: PHARMACEUTICAL SCIENCES  
(Pharmaceutics)

Approved By:

---

Advisor

Date

**© COPYRIGHT BY**

**SHAIMAA YOUSEF**

**2016**

**All Rights Reserved**

## DEDICATION

### *To my beloved family*

*I would like to dedicate this work to my beloved family, my parents: Dr. Mohamed Yousef and Dr. Fatheai El Dessokey, my brother: Dr. Omar Yousef, my sister: Dr. Asmaa Yousef, my husband: Ahmed Negmeldin, and my son: Hamza Negmeldin. All of you were supporting me tremendously throughout this whole work, without your help I wouldn't have completed this achievement and today I wish to share this success with you.*

## ACKNOWLEDGEMENTS

It's my pleasure to give deep thanks to everyone who helped me throughout this whole work. Thank you very much my father and my mother for teaching me to love science and thanks for your continuous support, and encouragement. My lovely husband, you were amazing, without your endless support emotionally and scientifically, I couldn't have reached this success. My son you were helpful, thank you sweetie.

Special appreciation and thanks to my advisor Dr. Arun Iyer for giving me the chance to be a member of your research team. You were always ambitious and encouraged me to aim higher and do my best. Thank you for your motivation, support and guidance. Also, I would like to extend my appreciation to my committee members Dr. Randall Commissaris and Dr. Arun Rishi for all your help, suggestions and insightful comments.

It's a pleasure to express my gratitude to Dr. Olivia Merkel and Dr. Duska Separovic for all the experimental techniques I learnt in your labs during my lab rotations, these were really beneficial and helped me a lot throughout my research work. Many thanks to Dr. Prashant Kesharwani and Dr. Rahul Deshmukh the present and past postdocs in our lab for teaching me different lab techniques and for their continuous support. My helpful labmates Duy Luong, Hashem Alsaab, Kaustubh Gawde, and Zhaoxian Wang, thanks for all your help.

Thanks Dr. Zhi Mei for TEM imaging, and Daniel DeSantis for CLSM imaging. Special thanks to Dr. Anna Moszczyńska for using the luminescent image analyzer in her lab. Thanks a lot Dr. Timothy Stemmler for using the FPLC system

in your lab with deep thanks to Lindsey Thompson for help in using it. Many thanks to Dr. Olivia Merkel for using the Flow cytometer in her lab, and thanks to Yuran Xie for assistance in its use for running my samples.

Finally, I would like to convey my sincere acknowledgment to all my professors and lecturers back home in Egypt, College of Pharmacy, Cairo University for all their help and support during my undergraduate study years.

Thank you all.

## TABLE OF CONTENTS

DEDICATION.....	ii
ACKNOWLEDGEMENTS.....	iii
LIST OF TABLES.....	ix
LIST OF FIGURES.....	x
LIST OF SCHEMES.....	xiii
CHAPTER 1 INTRODUCTION.....	1
1.1 Cancer as a Disease.....	1
1.2 Liver Cancer.....	2
1.2.1 Hepatocellular Carcinoma Risk Factors.....	2
1.2.2 Hepatocellular Carcinoma Therapeutic Strategies.....	2
1.3 Cancer Cells Chemoresistance.....	4
1.4 Nrf2 (nuclear factor erythroid 2-related factor 2) Transcription Factor.....	5
1.4.1 Nrf2 Mechanism of Action.....	5
1.4.2 Dual Role of Nrf2 in Cancer.....	6
1.4.3 Nrf2 in Hepatocellular Carcinoma.....	7
1.5 Small Interfering RNA (siRNA) Therapy.....	8
1.5.1 Mechanism of Action.....	8
1.5.2 Systemic Delivery Barriers.....	9
1.6 Nanocarriers, Drugs/Genes Delivery Systems, As Solution to Chemotherapy Problems.....	9
1.6.1 Polymeric Micelles.....	10
1.6.2 Multifunctional Polymeric Micelles for Cancer Therapy.....	11
1.7 Poly(styrene-co-maleic anhydride partial iso-octyl ester) (SMAPIE) Copolymer, As a Micellar Core Building Block.....	12

1.8 Branched Polyethylenimine (PEI) Polymer, As a Micellar Shell Building Block .....	13
1.9 Copper Free “Click” Chemistry Application in Micellar Surface Functionalization.....	14
1.10 Galactosamine as Efficient Targeting Ligand for Selective HCC Therapy .....	16
CHAPTER 2 EXPERIMENTAL DESIGN .....	19
2.1 Materials .....	19
2.2 Cell Culture .....	20
2.3 Synthesis and Characterization of SMAPIE-PEI-N3 and SMAPIE-PEI-Gal Micelles.....	21
2.3.1 Synthesis of SMAPIE-PEI-N3 Micelles Forming Block Copolymer.....	21
2.3.2 Synthesis of Targeting Ligand Conjugated SMAPIE-PEI-Gal Micelles Forming Block Copolymer .....	22
2.4 Size Exclusion Chromatography (SEC).....	24
2.5 Copper Assay .....	24
2.6 Determination of Critical Micelle Concentration (CMC).....	25
2.7 Preparation of siRNA Micelleplexes or Polyplexes .....	26
2.8 SYBER Gold Assay .....	26
2.9 Size and Zeta Potential Measurements: Light Scattering (LS) .....	27
2.10 Size and Morphology Measurements: Transmission Electron Microscopy (TEM).....	28
2.11 Buffering Capacity Measurements.....	28
2.12 Biological Evaluation of SMAPIE-PEI-N3 and SMAPEI-PEI-Gal Micelles	29
2.12.1 Cytotoxicity Assay Using Human Liver Cancer Cells .....	29
2.12.2 Cellular Uptake Quantification by Flow Cytometry .....	30
2.12.3 Cellular Uptake and Endosomal Escape by Confocal Laser Scanning Microscopy (CLSM).....	31



2.12.4 Transfection Efficiency and Nrf2 Gene Knockdown by Western Blot Analysis.....	33
CHAPTER 3 RESULTS .....	37
3.1. Synthesis and Characterization of SMAPIE-PEI-N3 and SMAPIE-PEI-Gal Micelles.....	37
3.1.1 Synthesis of SMAPIE-PEI-N3 Micelles Forming Block Copolymer.....	37
3.1.2 Synthesis of Targeting Ligand Conjugated SMAPIE-PEI-Gal Micelles Forming Block Copolymer .....	37
3.2 Size Exclusion Chromatography (SEC) .....	40
3.3 Copper Assay .....	41
3.4 Determination of Critical Micelle Concentration (CMC).....	42
3.5 SYBER Gold Assay .....	44
3.6 Size and Zeta Potential Measurements: Light Scattering (LS) .....	45
3.7 Size and Morphology Measurements: Transmission Electron Microscopy (TEM).....	49
3.8 Buffering Capacity Measurements.....	50
3.9 Biological Evaluation of SMAPIE-PEI-N3 and SMAPEI-PEI-Gal Micelles .	52
3.9.1 Cytotoxicity Assay Using Human Liver Cancer Cells .....	52
3.9.2 Cellular Uptake Quantification by Flow Cytometry .....	53
3.9.3 Cellular Uptake and Endosomal Escape by Confocal Laser Scanning Microscopy (CLSM).....	56
3.9.4 Transfection Efficiency and Nrf2 Gene Knockdown by Western Blot Analysis.....	59
CHAPTER 4 DISCUSSION .....	62
4.1 Synthesis and Characterization of SMAPIE-PEI-N3 and SMAPIE-PEI-Gal Micelles.....	62
4.1.1 Synthesis of SMAPIE-PEI-N3 Micelles Forming Block Co-polymer ....	62

4.1.2 Synthesis of Targeting Ligand Conjugated SMAPIE-PEI-Gal Micelles Forming Block Copolymer .....	68
4.2 Size Exclusion Chromatography (SEC) .....	70
4.3 Copper Assay .....	71
4.4 Determination of Critical Micelle Concentration (CMC).....	72
4.5 SYBER Gold Assay .....	74
4.6 Size and Zeta Potential Measurements: Light Scattering (LS) .....	75
4.7 Size and Morphology Measurements: Transmission Electron Microscopy (TEM).....	76
4.8 Buffer Capacity Measurements.....	77
4.9 Biological evaluation of SMAPIE-PEI-N3 and SMAPEI-PEI-Gal micelles..	79
4.9.1 Cytotoxicity Assay Using Human Liver Cancer Cells .....	79
4.9.2 Cellular Uptake Quantification by Flow Cytometry .....	80
4.9.3 Cellular Uptake and Endosomal Escape by Confocal Laser Scanning Microscopy (CLSM).....	83
4.9.4 Transfection Efficiency and Nrf2 Gene Knockdown by Western Blot analysis .....	85
SUMMARY .....	88
REFERENCES .....	92
ABSTRACT.....	112
AUTOBIOGRAPHICAL STATEMENT .....	114

## LIST OF TABLES

Table 3.1. Polydispersity indexes of plain SMAPIE-PEI-N3 and SMAPIE-PEI-Gal micelles. Results are presented as average from three independent samples (n=3) $\pm$ standard deviation.....	47
Table 3.2. Polydispersity indexes of SMAPIE-PEI-N3/siRNA, SMAPIE-PEI-Gal/siRNA micelleplexes and PEI 10 KDa/siRNA polyplexes at the specified N/P ratios. Results are presented as average from three independent samples (n=3) $\pm$ standard deviation.....	48

## LIST OF FIGURES

Figure 1.1. Schematic illustration of Nrf2 roles in enhancing cancer cell proliferation and development of chemoresistance to anticancer chemotherapeutic drugs. ....	7
Figure 1.2. Schematic illustration of different types of polymeric nanomicelles. .	12
Figure 1.3. Schematic illustration of the strain-promoted alkyne-azide cycloaddition copper free “click” reaction (SPAAC) and the copper-catalyzed alkyne-azide cycloaddition “click” reaction (CuAAC). ....	15
Figure 1.4. Schematic illustration of galactosamine conjugation to the modular polymeric SMAPIE-PEI-N3 micelles, the SMAPIE-PEI-Gal micelleplexes formation followed by their uptake in HCC cells via receptor mediated endocytosis to achieve siRNA mediated Nrf2 gene knockdown.....	18
Figure 3.1. Size exclusion chromatogram of SMAPIE-PEI-N3 micelles.....	40
Figure 3.2. Standard curve of log molecular weights of protein standards versus standards $V_e/V_o$ (elution volume/ column void volume), showing SMAPIE-PEI-N3 relative molecular weight determination.....	41
Figure 3.3. Standard curve of absorbance of cuprammonium complex at different PEI 10 KDa concentrations, showing PEI composition analysis of SMAPIE-PEI-N3 and SMAPIE-PEI-Gal micelles by copper assay.....	42
Figure 3.4. Fluorescence spectra of pyrene at different SMAPIE-PEI-N3 concentrations in water, showing bathochromic shift in pyrene excitation wavelength with increasing SMAPIE-PEI-N3 concentration.....	43
Figure 3.5. Critical micelle concentration (CMC) Plot of I339/I334 emission ratio versus Log concentration of SMAPIE-PEI-N3 copolymer.....	43
Figure 3.6. Condensation/Complexation behavior of polymers or micelles to siRNA by SYBER Gold fluorescence quenching assay at increasing N/P ratios.....	45
Figure 3.7. Hydrodynamic diameters (A) and zeta potentials (B) of plain SMAPIE-PEI-N3 and SMAPIE-PEI-Gal micelles.....	46
Figure 3.8. Hydrodynamic diameters of SMAPIE-PEI-N3/siRNA, SMAPIE-PEI-Gal/siRNA micelleplexes and PEI 10 KDa/siRNA polyplexes at the specified N/P ratios.....	47

- Figure 3.9. Zeta potentials of SMAPIE-PEI-N3/siRNA, SMAPIE-PEI-Gal/siRNA micelleplexes and PEI 10 KDa/siRNA polyplexes at the specified N/P ratios. ....48
- Figure 3.10. Transmission electron microscopy images illustrating size and morphology of SMAPIE-PEI-N3 micelles (without siRNA) (A and B), SMAPIE-PEI-Gal micelles (without siRNA) (C and D), SMAPIE-PEI-N3 micelleplexes (E), and SMAPIE-PEI-Gal micelleplexes (F). Micelleplexes were prepared at N/P ratio of 10. Micelles and micelleplexes were negatively stained with 3% uranyl acetate stain. ....50
- Figure 3.11. Acid base titration profile of non-targeted SMAPIE-PEI-N3, targeted SMAPIE-PEI-Gal micelles forming block copolymers and PEI polymers of different molecular weights (25, 10, 1.8 KDa) at pH range (11-2). ....52
- Figure 3.12. Plot showing cytotoxicity analysis of SMAPIE-PEI-N3, and SMAPIE-PEI-Gal copolymers in comparison with PEI 25 KDa and PEI 10 KDa as polymeric controls. Analysis was done on Hep G2 cells by MTT assay with concentration range (0 – 400 µg/mL) and incubation time of 48 hours.....53
- Figure 3.13. Histogram of flow cytometry analysis showing number of cells/channel on Y- axis versus the fluorescence intensity detected from FAM-labeled siRNA positive Hep G2 cells. A) Shows compared fluorescence intensity achieved at cellular uptake of SMAPIE-PEI-Gal or SMAPIE-PEI-N3 micelleplexes prepared with FAM-labeled siRNA, to that achieved in case of PEI 10 KDa polyplexes (positive control) and free FAM-labeled siRNA as well as untreated cells (negative controls). B) Shows different cellular uptake associated fluorescence intensity for SMAPIE-PEI-Gal micelleplexes in presence or absence of 20 Mm free galactosamine as competitor. ....55
- Figure 3.14. Plot of median fluorescent intensity of FAM- labeled siRNA positive Hep G2 cells for quantitative determination of cellular uptake of SMAPIE-PEI-N3, SMAPIE-PEI-Gal micelleplexes or polyplexes prepared with FAM-labeled siRNA at N/P ratio of 10. PEI 10 KDa polyplexes were used as positive control, while free FAM-labeled siRNA and untreated cells were as negative controls. As a competitive assay, SMAPIE-PEI-Gal micelleplexes uptake in the presence of 20 mM free galactosmine as a competitor of galactosamine in SMAPIE-PEI-Gal was detected. Results were obtained after 5 hours incubation of samples with cells, and are presented as (mean ± standard deviation of n=3, \*\*  $p < 0.01$ , ns = none statistically significant). ....56
- Figure 3.15. Confocal laser scanning microscopy images of Hep G2 cells treated with SMAPIE-PEI-Gal micelleplexes (column A), SMAPIE-PEI-Gal micelleplexes plus free galactosamine competitor (column B), SMAPIE-PEI-N3 micelleplexes (column C) and PEI 10 KDa polyplexes (column D), 22 hours after transfection. Micelleplexes or polyplexes were prepared with FAM-

labeled siRNA at N/P ratio of 10. The cells nuclei were stained with Hoechst 33342 stain (blue), acidic endosomal compartments with Lyso Tracker Deep Red dye (red), and siRNA was labeled with FAM (green). ..... 58

Figure 3.16. Plot illustrating CLSM images green fluorescence quantification. Mean total corrected cellular fluorescence (MTCCF) of internalized green fluorescent FAM -labeled siRNA complexed with micelleplexes or polyplexes in Hep G2 cells was calculated per image and plotted on Y axis against treatment type on X axis. .... 59

Figure 3.17. Western blot bands of Nrf2 and GAPDH protein levels detected in Hep G2 cells after 24 hours transfection with SMAPIE-PEI-Gal micelleplexes or PEI 10 KDa polyplexes condensing 50 nM Nrf2-siRNA or negative control siRNA (Ncr-siRNA) at N/P ratio of 10 (A). Estimation of Nrf2 gene silencing efficiency accomplished by SMAPIE-PEI-Gal micelleplexes versus PEI 10 KDa polyplexes through quantification of the above western bands intensities, data presented as mean of (GAPDH normalized Nrf2 protein level/GAPDH normalized Nrf2 protein level in case of NCr-siRNA plexes treatment)  $\pm$  standard deviation, n=3, and \*  $p < 0.05$  statistical significance (B)..... 61

Figure 4.1. Illustration of targeting ligand attachment to SMAPIE-PEI-N3 micelles via strain promoted alkyne azide cycloaddition (SPAAC) “click” reaction. .... 63

Figure 4.2. FT/IR spectra of PEI polymer (green), SMAPIE copolymer (blue), and SMAPIE-PEI-N3 micelles forming block copolymer (red). .... 65

Figure 4.3. <sup>1</sup>H NMR spectra of (A) SMAPIE in DMSO (B) PEI in D<sub>2</sub>O (C) PEI-N3 in D<sub>2</sub>O (D) SMAPIE-PEI in CD<sub>3</sub>OD (E) SMAPIE-PEI-N3 in CD<sub>3</sub>OD. .... 67

Figure 4.4. <sup>1</sup>H NMR spectra of (A) Galactosamine in D<sub>2</sub>O (B) SMAPIE-PEI-Gal in D<sub>2</sub>O. .... 70

## LIST OF SCHEMES

Scheme 3.1. Synthesis of non-targeted SMAPIE-PEI-N3 micelles forming block copolymer (3). .....	38
Scheme 3.2. Synthesis of ligand targeted SMAPIE-PEI-Gal micelles forming block copolymer (7). .....	39

## CHAPTER 1 INTRODUCTION

### 1.1 Cancer as a Disease

Cancer is a group of diseases characterized by uncontrolled cell proliferation, resistance to cell death, evasion of immune system destruction, angiogenesis, invasion as well as metastasis<sup>1,2</sup>. Various genetic mutations in oncogenes or tumor suppressor genes together with many epigenetic factors such as changes in DNA methylation are considered as contributors to the disruption of cell signaling, cell growth, and cell proliferation control, which leads to tumorigenesis and cancer development<sup>3-7</sup>.

Cancer is considered as a serious killer. According to the world health organization (WHO) 8.2 million individuals died from cancer in 2012 and the number of new cancer patients is expected to increase by around 70% in the coming 20 years. In the United States, cancer is the second leading cause of death just after the cardiovascular diseases as reported by the National Center for Health Statistics (NCHS) for the year 2014<sup>8</sup>. American Cancer Society estimated that there will be 1,685,210 new cancer cases and 595,690 cancer deaths, in 2016 in USA alone<sup>9</sup>.

Different therapeutic interventions are available to overcome cancer and increase patient's survival rates. Among these, surgery and radiation therapy are the first line therapeutic strategies for cancer, however, for metastatic cancers they are not effective as standalone therapy. Chemotherapy, on the other hand, is one of the most commonly used therapeutic strategies to fight both local and metastatic cancers either alone or as adjuvant therapy<sup>10,11</sup>. However two major limitations for



cancer chemotherapeutic drugs are toxicity towards rapidly growing normal cells, as well as the emergence of multi drug resistance (MDR) mechanisms, leading to poor therapeutic outcomes<sup>1</sup>.

## **1.2 Liver Cancer**

Liver cancer is a type of neoplasm that affects the hepatic tissues. According to WHO, liver cancer was the second most common lethal cancer worldwide in 2012<sup>12</sup>. In contrast to the declining trend among most cancer types, liver cancer showed increase in incidence and mortality rates, indicating its poor prognosis<sup>9,13</sup>. American cancer society, estimated 39,230 new cases of liver cancer to occur in the US during 2016, approximately three-fourths of which will be hepatocellular carcinoma (HCC)<sup>14</sup>.

### **1.2.1 Hepatocellular Carcinoma Risk Factors**

Hepatocellular carcinoma is the most prevailing histological type of liver cancer<sup>15</sup>. It occurs mostly in inflamed and cirrhotic liver, with the most common causes being the Hepatitis B (HBV) and Hepatitis C (HCV) viral infections<sup>15,16</sup>. Other risk factors correlated with HCC are aflatoxin B1 ingestion, alcohol and tobacco consumption, non-alcoholic fatty liver disease, iron overload in hemochromatosis<sup>17</sup> and type 2 diabetes<sup>18</sup>.

### **1.2.2 Hepatocellular Carcinoma Therapeutic Strategies**

There are multiple treatment strategies for HCC depending on liver function, the tumor size, number of lesions and stage. Surgical liver resection to remove the tumor with some healthy tissues around it is mostly performed in case of non-cirrhotic, single tumor lesion as opposed to the cases of cirrhosis or multiple

invasive tumor lesions. The latter cases are more susceptible to post resection recurrence of tumor<sup>19,20</sup>. Non-surgical but invasive therapeutic approaches include percutaneous ethanol injection (PEI)<sup>21</sup>, radiofrequency ablation (RFA)<sup>22</sup>, local radiotherapy (LR) and trans arterial chemoembolization (TACE)<sup>23</sup>, that are used for patients who are not candidates for resection. Liver transplantation is another therapeutic modality for HCC with limitations of being a big and expensive procedure. In addition it takes long time to find a well matched liver donor, and requires immunosuppressive treatment post operation to avoid new liver rejection<sup>19,24</sup>. Unfortunately, the majority of HCC patients (>80%) are diagnosed at an advanced stage where the above curative therapeutic options would not be effective<sup>25,26</sup>. Systemic chemotherapies such as cytotoxic drugs or antiangiogenic agents are mostly the treatment of choice for patients with advanced late stage HCC, in addition to their application as adjuvant therapies with other treatment options. Systemic cytotoxic small molecule treatments such as doxorubicin, epirubicin, cisplatin, 5-fluorouracil, etoposide and their combinations were used for advanced HCC, however very low efficacy with no more than 20% response rate was achieved<sup>25,26</sup>. On the other hand, newer therapies using sorafenib or erlotinib have demonstrated antiangiogenic activity as a result of being tyrosine kinase inhibitors. Bevacizumab is antiangiogenic monoclonal antibody against vascular endothelial growth factor (VEGF). They work by inhibiting the VEGF or EGF signaling and hence suppress the tumor's ability to generate new blood vessels<sup>27,28</sup>. In terms of cancer chemotherapy, there are several physicochemical factors such as the molecular weight, stability, and hydrophobicity of drugs as well

as pathophysiological and anatomical factors such as their inefficient accumulation in tumor tissues, the involvement of various chemo-resistance mechanisms by cancer cells among others, that contribute to the inefficient therapeutic outcomes of the HCC systemic chemotherapy<sup>28-31</sup>.

### **1.3 Cancer Cells Chemoresistance**

Cancer cells are found to have tremendous ability to develop various resistance mechanisms to chemotherapeutic agents and to upregulate specific molecular targets and proteins that have essential roles in increasing tumor growth, invasiveness, and metastasis<sup>32,33</sup>.

Chemoresistance mechanisms are various and principally include: Overexpression of P-glycoprotein (Pgp) and multidrug resistance associated proteins (MRP) that form efflux pumps which export the chemotherapeutic agents out of the cancer cells and help cells evade their cytotoxic effect<sup>34,35</sup>. The overexpression of growth factors and amplification of survival signals in response to chemotherapy induced stress, induction of enzymes metabolizing anticancer drugs, alteration of the drug target proteins so they have less binding affinity to the drug or alterations in the downstream signaling proteins, and downregulation of the drugs cellular transporters which decrease their effective concentration in cancer cells<sup>33,36</sup>.

As a result, cancer cells no longer respond to chemotherapy, which consequently leads to treatment failure. Use of anticancer drugs which have different mechanisms of action in combination, or the use of drugs and

genes/siRNA combination could be an alternative approach to overcome tumor cells resistance and restore their therapeutic responsiveness<sup>36,37</sup>.

#### **1.4 Nrf2 (nuclear factor erythroid 2-related factor 2) Transcription Factor**

Nrf2 is a key transcription factor that has a fundamental role in the cellular defense against different toxicants, xenobiotics and any internal or external oxidative insults.

##### **1.4.1 Nrf2 Mechanism of Action**

Nrf2 works in the Nrf2- Keap1 (Kelch-like erythroid cell-derived protein1) - ARE (antioxidant response element) signaling pathway. Under normal conditions, the transcription factor Nrf2 binds to its repressor protein Keap1 which marks it for ubiquitination and subsequent proteasomal degradation<sup>38,39</sup>. However when cells are exposed to oxidative stress, the Keap1 protein gets covalently and conformationally modified in a way that no longer promotes Nrf2 ubiquitination and degradation with subsequent Nrf2 stabilization and accumulation in the cytoplasm<sup>40,41</sup>. The accumulated free Nrf2 in the cytoplasm then translocates to the nucleus where it dimerizes with Maf (masculoaponeurotic fibrosarcoma) protein and binds to the AREs in regulatory region of many metabolic, antioxidant and cytoprotective genes to induce their transcription<sup>42</sup>. Among the genes which Nrf2 promotes their transcription are the genes of : GSH (glutathione) forming and metabolizing enzymes, antioxidant proteins, reactive oxygen species neutralizing enzymes, drug metabolizing enzymes, efflux pump multidrug resistance protein 1 (MRP1)<sup>43</sup>. All these proteins are known to participate in the cellular protection and detoxification processes.

### 1.4.2 Dual Role of Nrf2 in Cancer

There is dual role noted for Nrf2 and it may be considered as a double-edged sword. While on one hand Nrf2 helps to protect the normal cells from neoplastic transformation (when exposed to various carcinogens), by reducing the reactive oxygen species (ROS) burden and by acting against DNA damage in cells, on the other hand, it promotes the cancer cells survival and increases their chemo and radio resistance. As a consequence, high levels of Nrf2 in cancer patients were reported to be an indicator of poor prognosis<sup>44,45</sup>.

Nrf2 was found to be constitutively elevated and activated in many cancer types including: breast<sup>46,47</sup>, hepatocellular<sup>48,49</sup>, prostate<sup>50</sup>, gall bladder<sup>51</sup>, oesophageal<sup>52</sup>, pancreatic<sup>53</sup> and non-small-cell lung<sup>54</sup> carcinomas. As illustrated in figure 1.1, Nrf2 promotes cancer cells proliferation and chemoresistance. In various carcinomas, elevated Nrf2 level promotes cells aggressive proliferation and anabolism through induction of purine nucleotides (DNA and RNA forming units) synthesizing enzymes, glutathione (mitosis and cell cycle promotor) synthesizing enzymes<sup>55</sup> as well as glucose metabolizing enzymes expression<sup>56</sup>. Highly activated Nrf2 contributed to resistance development to many chemotherapeutic agents such as doxorubicin, cisplatin, and 5-fluorouracil (5-FU). Nrf2 mediated chemoresistance mechanisms reported include induction of expression of genes encoding antioxidant proteins, as well as drug detoxifying enzymes and increasing drug efflux pumps production<sup>44,45</sup>.

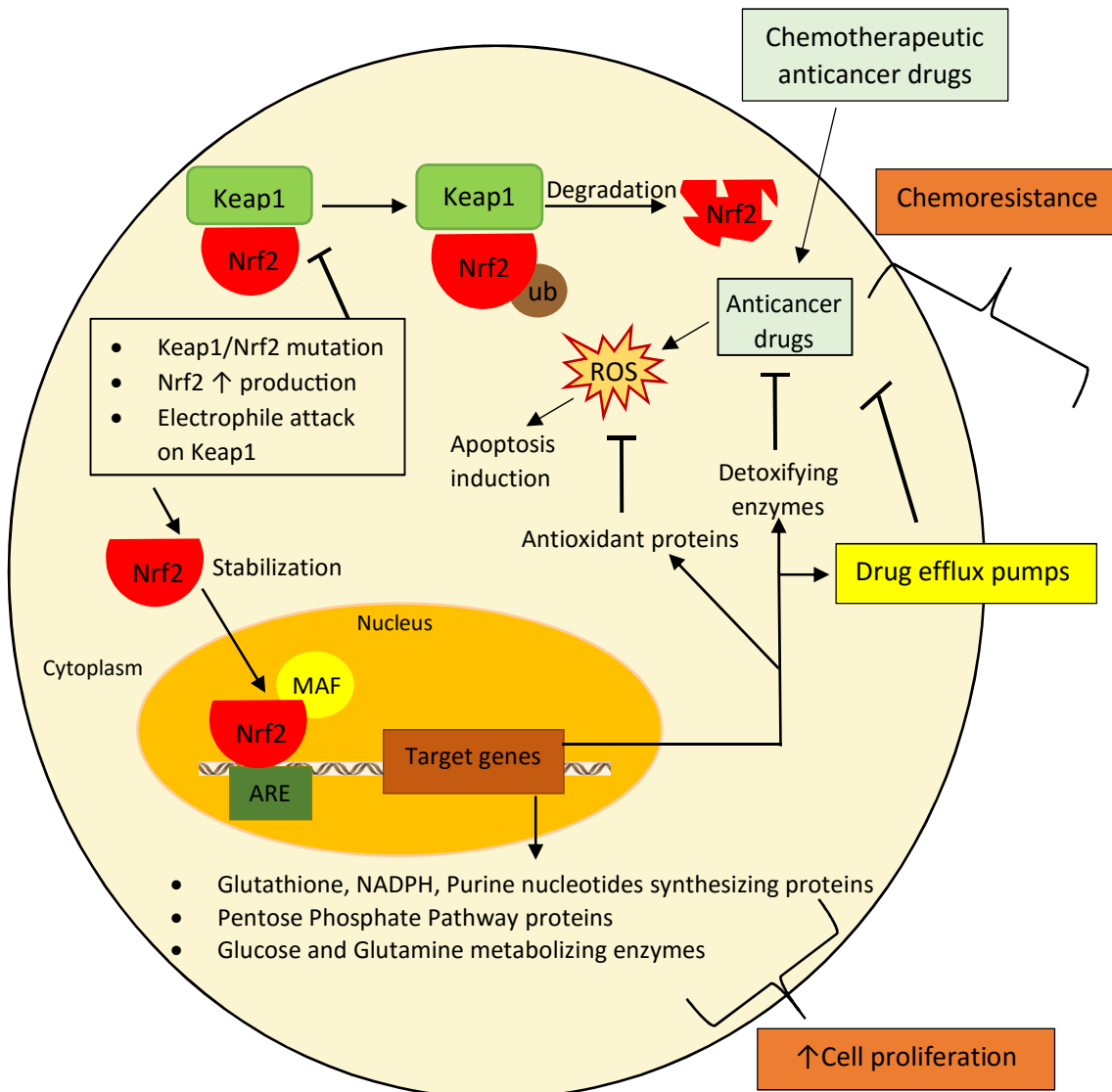


**Figure 1.1.** Schematic illustration of Nrf2 roles in enhancing cancer cell proliferation and development of chemoresistance to anticancer chemotherapeutic drugs.

### 1.4.3 Nrf2 in Hepatocellular Carcinoma

In addition, Nrf2 was reported to have a proven role in cancer proliferation, invasion and metastasis in HCC through regulation of Bcl-xL (antiapoptotic protein) and MMP-9 (matrix metalloproteinases-9, a protein regulating cell migration and invasion) expression<sup>49</sup>. Literature suggested that Nrf2 is involved in chemoresistance in HCC and its inhibition by sorafenib can sensitize cancer cells

to 5-FU<sup>57</sup>. It was also reported that Nrf2 down regulation by miRNA-340 reversed cisplatin resistance in Hep G2 /cisplatin resistant HCC cells<sup>58</sup>. In another study, it was documented that apigenin resensitized HCC BEL-7402/doxorubicin resistant cells to doxorubicin via reducing Nrf2 expression<sup>59</sup>. These results emphasize the importance of targeting Nrf2 in fighting HCC. In this study we applied RNA interference (RNAi) technique, using polymeric micelles loaded with Nrf2 siRNAs to knockdown Nrf2 gene in Hep G2 hepatocellular carcinoma cell line in which Nrf2 was reported to be mainly distributed in the cytoplasm<sup>60</sup>.

### **1.5 Small Interfering RNA (siRNA) Therapy**

RNA interference (RNAi) is an efficient post-transcriptional gene silencing process. RNAi through small interfering RNA (siRNA) is highly regarded as a promising therapeutic strategy to inhibit and silence specific genes involved in pathogenesis of different diseases<sup>61-64</sup>.

#### **1.5.1 Mechanism of Action**

siRNA is small double stranded RNA (21-23 nucleotides) that are able to target a specific mRNA of complementary sequence. In the cytoplasm, siRNA is loaded in RNA-induced silencing complex (RISC), where its sense strand (passenger strand) gets cleaved by the argonaute 2 (AGO 2) protein. The activated RISC carrying the antisense strand (guide strand) recognizes the complementary sequence in the target mRNA and mediates its degradation with consequent mRNA specific gene silencing<sup>65-68</sup>.

### **1.5.2 Systemic Delivery Barriers**

Researchers faced multiple challenges during the systemic delivery of naked siRNAs, which end up with insufficient accumulation in cytosol of target cells and hence result in poor therapeutic outcomes. These obstacles include: degradation in serum with the endonucleases after intravenous injection, short plasma half-life (< 10 minutes) and rapid renal clearance<sup>69</sup>, also its very large size and high negative charge prevents it from diffusion through the anionic cell membrane readily<sup>61,70</sup>. As a result, therapeutic application and significant clinical benefit of siRNA are dictated by the availability of safe, well designed, effective siRNA carriers or delivery systems<sup>70,71</sup>.

In this regard, several different nanocarriers have been used and studied for protecting and delivering siRNA efficiently to the cytoplasm of target cells. Among these, nanotechnology utility has helped to improve the biological stability of siRNAs, their pharmacokinetics as well as cellular uptake. Thus far, using such systems, satisfactory therapeutic outcomes have been obtained<sup>72,73</sup>.

### **1.6 Nanocarriers, Drugs/Genes Delivery Systems, As Solution to Chemotherapy Problems**

It is a well-known fact that delivery of siRNAs and drugs to the target organs and tissues has been a challenge. In terms of delivery strategies, many nanocarriers including dendrimers, liposomes, polymeric nanoparticles and polymeric micelles have been extensively studied to achieve either passive or active targeting of chemotherapeutic agents or siRNA/genes to the tumor tissues<sup>74,75</sup>.



These nanosystems not only accumulate in the cancerous tissue by exploiting the leaky tumor vasculature or the enhanced permeability and retention (EPR) effect but can also be internalized into the tumor cells by receptor mediated uptake<sup>76,77</sup>. Nanocarriers also protect the drugs/nucleic acids from burst release or degradation, improve their cargo pharmacokinetics, increase drug solubility, and reduce toxicity as well as unfavorable side effects thereby enhancing patient compliance<sup>74,75,78</sup>. Although several nanocarriers are under development or in the clinical trials stages, only a few have been approved by the FDA. These shortcomings necessitate the need to fast-track the development of delivery technologies, including the more promising and beneficial targeted nanodelivery systems<sup>1,79</sup>.

### **1.6.1 Polymeric Micelles**

Polymeric nanomicelles are one class of nanocarriers that are constructed from amphiphilic block copolymers that can self-assemble in aqueous environment to form spherical core-shell structures, at concentration above the critical micellar concentration (CMC)<sup>80,81</sup>. Amphiphilic copolymers are composed of hydrophilic and hydrophobic moieties and when CMC is reached the hydrophobic moieties start to come closer to each other and away from water to reach more favorable entropy forming the micellar core while the hydrophilic moieties form the micellar shell<sup>82</sup>. Different hydrophobic drugs have been loaded in micellar core through their interaction with the core hydrophobic groups. On the other hand, hydrophilic shell groups confer water solubility and diminish protein (opsonin) adsorption on micelles, which consequently improves the micelle's cargo blood stability and

circulation half-life<sup>83</sup>. It is proven that solubility, stability and circulation time of hydrophobic chemotherapeutic agents are enhanced by their encapsulation in the micellar core<sup>78,82,84</sup>. Being water soluble and of nanosize, micelles carrying hydrophobic anticancer drugs can be administered intravenously to achieve better drug penetration and passive accumulation in the tumors<sup>83,85</sup>. Functionalization of the micellar shell with targeting ligands not only allow their active accumulation selectively in tumor tissues, but also decrease the chemoresistance to their drug cargo through evasion of efflux pumps and achieving receptor mediated endocytosis<sup>75,86</sup>. Different types of polymeric nanomicelles are illustrated in figure 1.2.

### **1.6.2 Multifunctional Polymeric Micelles for Cancer Therapy**

Multifunctional polymeric micelles as the name suggests, are the ones in which more than one therapeutic agent, or therapeutic and diagnostic/imaging agents can be integrated on the same micellar carrier, with or without the attachment of targeting moieties for selective delivery<sup>80</sup>. It is well documented that multifunctional micellar nanocarriers can help achieve synergistic control over cancer growth by co-delivery of genes/ siRNA and chemotherapeutics at the same time<sup>87-89</sup>. Co-delivery of different therapeutic agents that work by different mechanisms of action is a desirable approach to overcome cancer chemoresistance and improve therapeutic efficacy<sup>90</sup>. Theranostic multifunctional polymeric micelles have been reported to perform both therapeutic and imaging functions through incorporation of imaging probes as well as therapeutic

drugs/genes in the micellar constructs<sup>91,92</sup>. Multifunctional micelles as a result, has a great potential for application in cancer therapy.

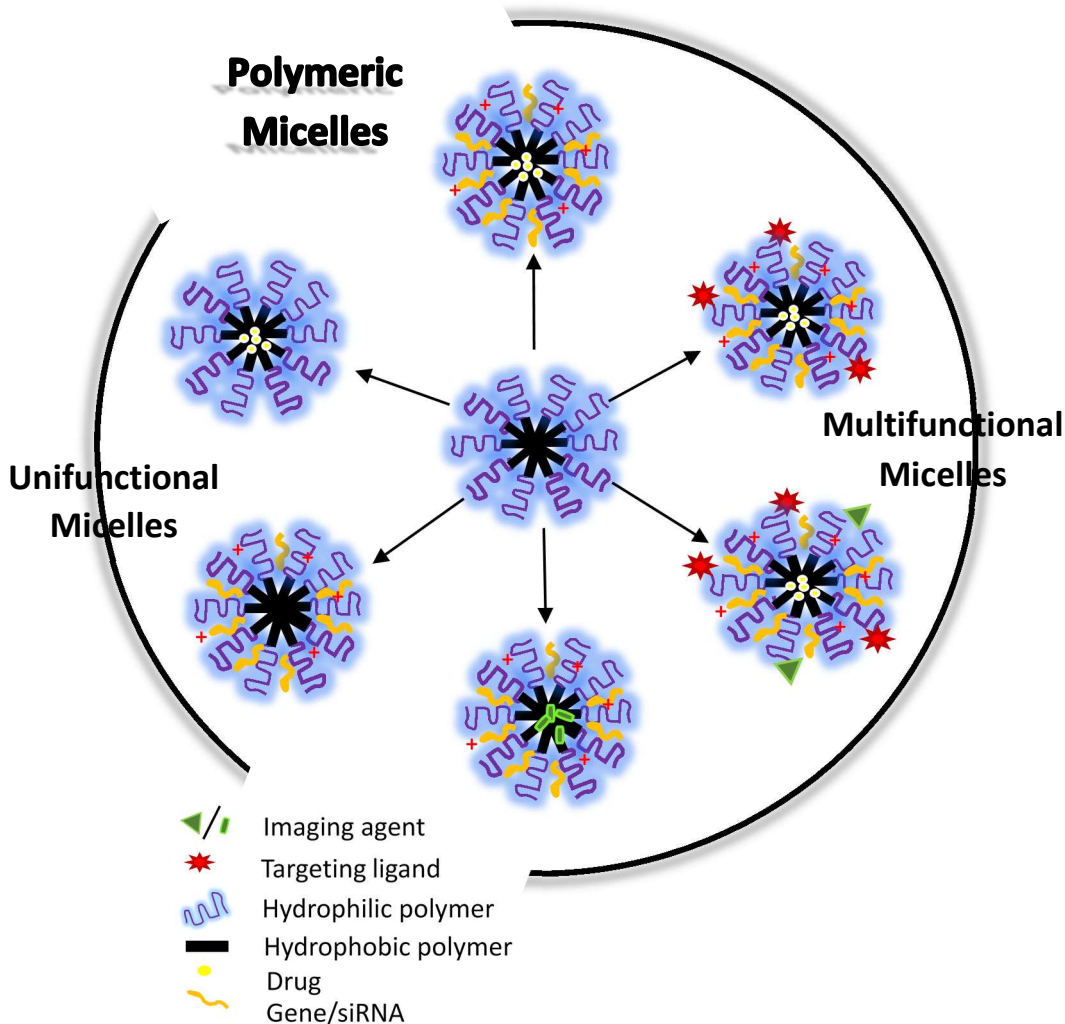


**Figure 1.2.** Schematic illustration of different types of polymeric nanomicelles.

### 1.7 Poly(styrene-co-maleic anhydride partial iso-octyl ester) (SMAPIE) Copolymer, As a Micellar Core Building Block

In terms of the nanomicellar carrier building polymers, poly(styrene-co-maleic anhydride partial iso-octyl ester) (SMAPIE) is a partial ester of the well-studied polystyrene-co-maleic anhydride (SMA) copolymer. It is established that the hydrophobic styrene groups in SMAPIE copolymer can participate in formation

of compact micellar core during fabrication of polymeric micellar delivery systems for efficient encapsulation and delivery of hydrophobic anticancer drugs<sup>93,94</sup>. In terms of the use of SMA for drug delivery applications, the base polymer has been proven to be safe for in vivo use. Indeed SMA polymer was used in the synthesis of many polymeric drug conjugates such as fenoprofen-SMA and gemfibrozil-SMA conjugates<sup>95</sup>, SMA-neocarzinostatin (also known as SMANCS)<sup>96</sup> and SMA conjugated YIGSR<sup>97</sup>. The micellar SMA-doxorubicin<sup>98</sup> and SMA-pirarubicin<sup>99</sup> also showed better pharmacokinetic and pharmacodynamic profiles compared to those of the free drug in animal tumor models.

### **1.8 Branched Polyethylenimine (PEI) Polymer, As a Micellar Shell Building Block**

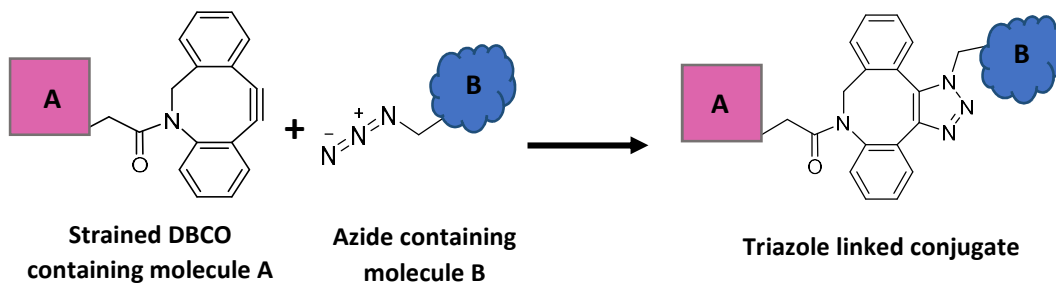
Polyethylenimine (PEI) polymer has many hydrophilic amine groups that can be used to form hydrophilic shell of a micellar system. In addition, PEI is one of the most efficient cationic polymers used for gene/siRNA delivery both in vitro and in vivo applications<sup>100–102</sup>. As a cationic polymer it is relatively safer, less immunogenic, simpler to prepare and cheaper than the viral vectors<sup>103</sup>. PEI cationic amine groups can efficiently condense anionic phosphate groups of nucleic acids via electrostatic interaction and improve their cellular uptake via endocytosis<sup>104</sup>. The intrinsic endosomolytic ability of PEI allows the endosomal escape of the delivery system cargo via the “*proton sponge*” mechanism and hence can increase transfection efficiency<sup>105</sup>. The “*proton sponge*” effect of the protonatable amine groups causes the protons and water influx in the endosomes, which results in the endosomal membrane rupture releasing the drugs/siRNA cargo into the cytoplasm after evasion of the lysosomal degradation<sup>71</sup>. In addition,

modification of some of the amine groups of PEI with targeting moieties can reduce its charge density, cytotoxicity and improve its targeting ability<sup>104,106</sup>. Modification of PEI with targeting ligands or imaging agents can be efficiently done using copper free “*click*” chemistry.

### **1.9 Copper Free “*Click*” Chemistry Application in Micellar Surface Functionalization**

Copper free “*click*” chemistry is a simple, rapid, highly selective, water compatible, and bioorthogonal chemical approach that involves ligation of two moieties through strain promoted 1, 3 dipolar azide alkyne cycloaddition<sup>107,108</sup>. Copper free “*click*” synthetic module is more useful compared to the copper catalyzed “*click*” reactions since copper free reactions don’t involve the oxidative damage and toxicity that could be caused to the cells and tissues due to residual copper catalyst remaining in the purified product<sup>109</sup>. As shown in figure 1.3, the driving force for the copper free “*click*” approach is the strain of alkyne encountering ring, as in the dibenzyl cyclooctyne (DBCO) ring instead of the copper catalyst in the copper catalyzed reaction<sup>108</sup>. The copper free “*click*” type reported by Bertozzi and co-workers is biocompatible and bioorthogonal reaction that can occur inside the living systems without inducing toxicity or interfering with native biological molecules or processes<sup>107</sup>.

### Copper free reaction



### Copper catalyzed reaction

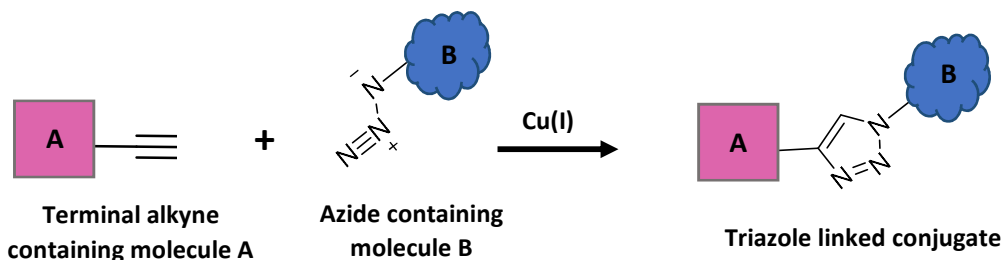


**Figure 1.3.** Schematic illustration of the strain-promoted alkyne-azide cycloaddition copper free “click” reaction (SPAAC) and the copper-catalyzed alkyne-azide cycloaddition “click” reaction (CuAAC).

“Click” chemistry has been used in many applications including biorthogonal imaging or labeling of different biomolecules as proteins or nucleic acids using alkynyl or azido sugars or amino acids probes<sup>110–114</sup>, in situ fragment based drug development with example of multivalent enzyme or receptor inhibitors construction<sup>115,116</sup>, synthesis of fluorescently labeled targeted drug nanocarriers for cancer therapy and imaging<sup>117</sup>.

In this study we synthesized azide modified modular micellar platform that can be decorated off-the-shelf with different cyclooctyne linked targeting moieties or imaging agents simultaneously using the same rapid copper free “click” reaction to arrive at nanomicelles suitable for theranostic and metastatic cancer therapy application. Importantly, the concept can be utilized to quickly assemble the

micellar nanocarriers constructed using off-the-shelf library of the synthesized azide/alkyne block co-polymers (containing various drug and gene payloads) decorated with various targeting ligands for treating multiple different cancers that overexpress several kinds of receptor domains.

### **1.10 Galactosamine as Efficient Targeting Ligand for Selective HCC Therapy**

Galactosamine is among the selective targeting ligands used for targeting hepatocellular carcinoma due to its high binding affinity to asialoglycoprotein receptor. Asialoglycoprotein receptors (ASGPRs), also known as (Ashwell receptor) are lectin receptors that were found to be over expressed in several human neoplastic hepatocytes<sup>118</sup> and HCC cell lines including Hep G2 and Huh7.5 cells<sup>119,120</sup>. ASGPRs selectively binds and internalize different molecules exposing carbohydrate residues as galactose, galactosamine, or N-acetylgalactosamine through clathrin type receptor mediated endocytosis<sup>121,122</sup>.

Galactosamine was proven to achieve ASGPR mediated efficient liver tumor targeting in phase I clinical trial of poly[N-(2-hydroxypropyl)methacrylamide] copolymer carrying doxorubicin and galactosamine, as reported by Peter J. Julyan and co workers<sup>123</sup>. In the same line, Zheyu Shen, *et al.* showed increased cellular uptake and cytotoxicity of galactosamine targeted doxorubicin loaded albumin nanoparticles compared to non-targeted counterparts<sup>124</sup>. Similarly, Yu Cai Wang *et al.* demonstrated that galactosamine conjugated micelles loaded with paclitaxel exhibited better drug internalization, cytotoxicity and induction of cell cycle arrest in contrast to the paclitaxel loaded micelles without galactosamine ligand<sup>125</sup>. As a result, galactosamine is a well-studied effective targeting moiety for hepatoma cells

expressing ASGPR. Galactosamine conjugated delivery systems could thus be very promising in achieving more effective HCC therapy, with better accumulation of therapeutic agents in the tumor tissue and lesser side effects.

In the present work, we engineered polymeric nanomicelles which can be multifunctional in use and can be utilized as modular platform for delivering chemotherapeutic drugs, imaging agents, and genes/siRNA simultaneously or individually, in a targeted manner to one or more cancer type. Our amphiphilic micellar copolymer is composed of SMAPIE copolymer grafted to hyperbranched PEI polymer, with the hydrophobic styrene groups forming the compact micellar core and the hydrophilic polyethylenimine amino branches forming the coronal layer. The role of PEI is for efficient complexation of siRNAs and genes. We partially converted primary amine groups in PEI polymer to azide groups, so that copper free “*click*” chemistry could be employed to conjugate targeting ligands or imaging moieties to decorate the nanomicelles. As a proof-of-concept in this study we synthesized galactosamine targeted nanomicelles for selective delivery of Nrf2 siRNA in HCC cells. As illustrated in figure 1.4, the targeted micelles were able to achieve selective high cellular uptake via ASGPR mediated endocytosis and statistically significant Nrf2 gene knockdown in the tested HCC.



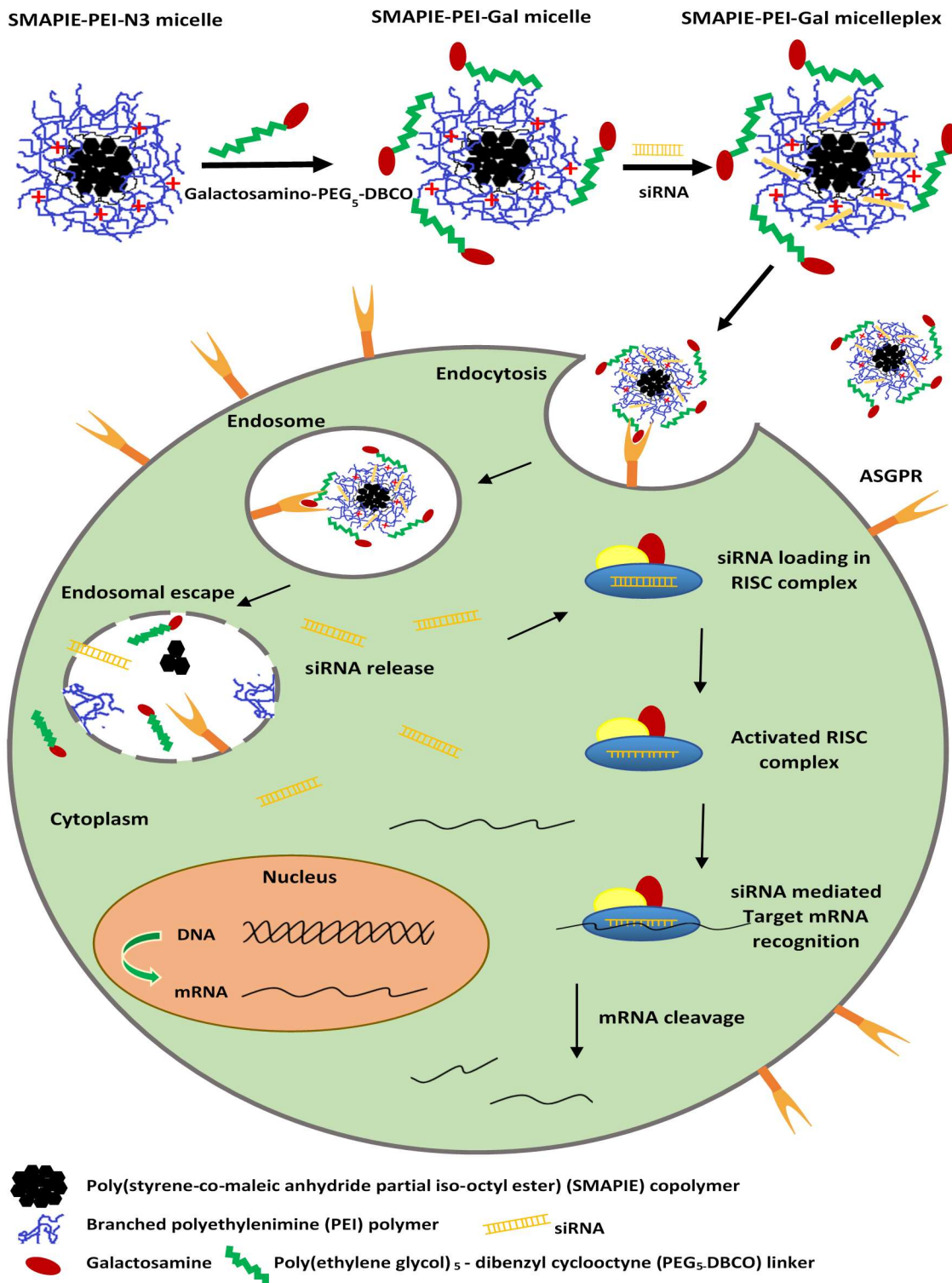


**Figure 1.4.** Schematic illustration of galactosamine conjugation to the modular polymeric SMAPIE-PEI-N3 micelles, the SMAPIE-PEI-Gal micelleplexes formation followed by their uptake in HCC cells via receptor mediated endocytosis to achieve siRNA mediated Nrf2 gene knockdown.

## CHAPTER 2 EXPERIMENTAL DESIGN

### 2.1 Materials

Branched polyethylenimine (PEI) with average molecular weight 10 KDa was purchased from polysciences (Warrington, PA). Branched polyethylenimine (PEI) with average molecular weight 25 KDa, Poly(styrene-co-maleic anhydride, partial iso-octyl ester) cumene terminated (SMAPIE) with average molecular weight 2.3 KDa,  $\beta$ -D(+)-Glucose, Glycine, Ammonium persulfate, Glycerol, Sodium dodecyl sulfate, 2-Mercaptoethanol, N,N,N',N'-Tetramethylethylenediamine, MISSION siRNA Universal Negative Control #2 (SIC002), and RNAase free water, were purchased from Sigma-Aldrich (St Louis, MO, USA). D-(+)-Galactosamine.HCl was obtained from MP BioMedicals, LLC (Solon, OH, USA). Dibenzyl cyclooctyne – (polyethylene glycol)<sub>5</sub> –N-hydroxy succinimide (DBCO-PEG<sub>5</sub>-NHS) ester was purchased from Click Chemistry Tools Bioconjugate Technology Company (Scottsdale, AZ, USA). Potassium carbonate was purchased from Fisher science education (Nazareth, PA, USA). Pyrene was from Acros (NJ, USA). SYBER Gold nucleic acid gel stain was obtained from Invitrogen life technologies (Carlsbad, CA, USA). Dulbecco's modified eagle medium (DMEM), FluoroBrite™ DMEM life cell fluorescence imaging medium, Phosphate-buffered saline (PBS), fetal bovine serum (FBS), penicillin-streptomycin (Pen-Strep), and Trypsin-EDTA (0.25%) with phenol red solution were from Gibco, Thermo Fisher Scientific (Waltham, MA, USA). Tris base (hydroxyl Methyl amino Methane), Pierce protease and phosphatase inhibitor mini tablets, and Super Signal West Pico chemiluminescent substrate were obtained

from Thermo Fisher Scientific (Waltham, MA, USA). Goat anti-mouse IgG-HRP sc-2005 secondary antibody, Nrf2 (A-10) sc-365949 mouse monoclonal primary antibody, GAPDH (G-9) sc-365062 mouse monoclonal primary antibody, and Nrf2 siRNA (h) sc-37030 were purchased from Santa Cruz Biotechnology, Inc. (Dallas, TX, USA). MTT (3-(4,5-Dimethylthiazol-2-yl)-2,5-Diphenyltetrazolium Bromide) was obtained from Gold Biotechnology (St Louis, MO, USA). Silencer® FAM™-Labeled Negative Control #1 siRNA was obtained from Applied Biosystems Ambion, Inc. (Austin, TX, USA). Lyso Tracker Deep Red fluorescent dye, and Hoechst 33342, Trihydrochloride Trihydrate nucleic acid stain were purchased from Life Technologies (Carlsbad, CA, USA). Bradford protein assay dye reagent concentrate, 10% Tween 20 solution, and 30% Acrylamide/Bis solution were bought from BIO-RAD (Hercules, CA, USA). Imidazole-1-sulfonylazide hydrochloride reagent was synthesized in our lab according to previously reported method<sup>126</sup>. All other reagents and Solvents were of analytical grade and were used without further purification.

## **2.2 Cell Culture**

The human HCC cell line (Hep G2) was a kind gift from Dr. John J. Reiners (Wayne State University, Detroit, MI, USA). Cells were cultured in DMEM medium supplemented with 10% fetal bovine serum (FBS), 4 mM L-Glutamine, (4.5 g/L D-glucose), (3.7 g/L sodium bicarbonate) and 1% penicillin-streptomycin solution at 37 °C in humidified air containing 5% CO<sub>2</sub>. Cells were maintained and sub-cultured every 3 to 4 days at approximately 80% confluency.

## **2.3 Synthesis and Characterization of SMAPIE-PEI-N3 and SMAPIE-PEI-Gal Micelles**

### **2.3.1 Synthesis of SMAPIE-PEI-N3 Micelles Forming Block Copolymer**

SMAPIE-PEI-N3 micelles were synthesized in two steps by one pot reaction method. First, previously reported method<sup>127</sup> was followed, with some modifications. Briefly, PEI 10 KDa (250 mg, 0.025 mmole) was dissolved in 47 mL methanol followed by addition of 23 mL DMSO to it. SMAPIE 2.3 KDa (57.5 mg, 0.025 mmole) was dissolved in 23 mL DMSO followed by addition of 47 mL methanol. Subsequently, SMAPIE solution was added in a dropwise fashion onto the PEI 10 KDa solution with continuous stirring using a magnetic stirrer. The dropping rate was fixed at about 12 drops/min. The reaction mixture was then kept under continuous stirring at room temperature overnight.

In the next step, conversion of some of the primary amine groups in PEI to azide groups was undertaken using a previously published method<sup>126</sup>, with some modifications. In brief, potassium carbonate (216.4 mg, 1.566 mmole) was added to the crude reaction mixture from the previous step while stirring on ice, followed by the portion wise addition of imidazole-1-sulfonylazide hydrochloride reagent (109.4 mg, 0.522 mmole). The ice bath was removed and the reaction was kept under stirring at room temperature for 24 hours. The reaction mixture was then dialyzed using dialysis bag (MWCO 10KDa, Spectra/Por, Spectrum Labs, San Diego, CA, USA) against deionized water for 2 days with frequent changes of the dialysis water to remove solvents, salts and any small molecular weight unreacted reagents. Then, the dialysis was continued against deionized water for another 6 hours using a dialysis bag (MWCO 12-14 KDa, Spectra/Por, Spectrum Labs, San

Diego, CA, USA) to get rid of unreacted PEI. The final dialyzed product was filtered using Whatman filter paper to remove any precipitate or crosslinked product. The dry SMAPIE-PEI-N3 product was obtained by lyophilization (yield 86%).

The successful synthesis of SMAPIE-PEI-N3 product was confirmed by Fourier transform infrared spectroscopy (JASCO, FT/IR - 4200 Fourier Transform Infrared Spectrometer, Japan) and Proton nuclear magnetic resonance ( $^1\text{H}$  NMR) spectroscopy (600 MHz, Agilent-NMR-inova600, Santa Clara, CA, USA).

FT-IR ( $\nu$ ,  $\text{cm}^{-1}$ ): 2500-3700 (carboxylic acid broad  $-\text{OH}$  stretch), 2105 (azide  $-\text{N}_3$  stretch), 1749 (ester  $-\text{C}=\text{O}$  stretch), 1700 (little shoulder of carboxylic acid  $-\text{C}=\text{O}$  stretch), 1671 (secondary amide  $-\text{C}=\text{O}$  stretch), 1519 (aromatic benzene ring  $\text{C}=\text{C}$  stretch).

$^1\text{H}$  NMR ( $d_4$ - $\text{CD}_3\text{OD}$ ):  $\delta$  (ppm) = 0.86 (overlapping peaks of:  $-\text{CH}_3$  in cumene terminal and  $-\text{CH}(\text{CH}_3)_2$  in iso-octyl chain), 1.15-1.8 (overlapping peaks of:  $-\text{CH}(\text{CH}_3)_2$ ,  $-\text{CH}_2-$  in iso-octyl chain and  $-\text{CH}_2\text{CHPh}$ ), 2.2-3 ( $-\text{CH}_2\text{CH}_2\text{NH}-$  in PEI), 3.1-3.6 (overlapping peaks of:  $-\text{COCH}-$ ,  $-\text{OCH}_2-$ ,  $-\text{CH}_2\text{NHCO}-$  and  $-\text{NHCH}_2\text{CH}_2\text{N}_3$  in PEI chain), 6.4-7.4 ( $\text{C}_6\text{H}_5-$  in cumene terminal and styrene residues).

### **2.3.2 Synthesis of Targeting Ligand Conjugated SMAPIE-PEI-Gal Micelles Forming Block Copolymer**

Galactosamine targeted micelles, SMAPIE-PEI-Gal, were synthesized by copper free “click” chemistry according to a protocol provided by Click Chemistry Tools company (Scottsdale, AZ, USA) in two steps, with some modifications. First, the galactosamine.HCl (20.2 mg, 0.0936 mmole) was dissolved in 3mL 1X phosphate buffer saline (PBS). Then, triethylamine ( $\text{Et}_3\text{N}$ ) (13  $\mu\text{l}$ , 0.0936 mmole) was added to the solution to obtain the galactosamine in its basic form so that it

can efficiently react with the NHS ester. DBCO-PEG<sub>5</sub>-NHS ester (21.65 mg, 0.0312 mmole) was dissolved in 400  $\mu$ l DMSO and then added to the solution containing galactosamine to obtain the product, galactosamino-PEG<sub>5</sub>-DBCO. The reaction mixture was kept under stirring at room temperature for 6 hours in order to allow the reaction to proceed to completion.

In the next step, galactosamino-PEG<sub>5</sub>-DBCO obtained in the first step was reacted with SMAPIE-PEI-N3 micelles as follows: SMAPIE-PEI-N3 (50 mg) was dissolved in 7 mL deionized water and added to the solution containing galactosamino-PEG<sub>5</sub>-DBCO obtained from step one. The reaction mixture was stirred at room temperature for 12 hours. The product was dialyzed using a dialysis bag (MWCO 10KDa, Spectra/Por, Spectrum Labs, San Diego, CA, USA) against deionized water for 1 day with frequent changes to the dialysis water to remove solvents, salts and any small molecular weight unreacted reagents. The dried final product, SMAPIE-PEI-Gal was obtained by lyophilization (yield 99%).

The successful synthesis of SMAPIE-PEI-Gal targeted micelles forming block copolymer was confirmed by proton nuclear magnetic resonance (<sup>1</sup>H NMR) spectra recorded on 600 MHz spectrometer (Agilent-NMR-inova600, Santa Clara, CA, USA).

<sup>1</sup>H NMR (*d*<sub>2</sub>-D<sub>2</sub>O):  $\delta$  (ppm) = 1.4 (overlapping peaks of: -CH<sub>3</sub> in cumene terminal and -CH(CH<sub>3</sub>)<sub>2</sub> in iso-octyl chain), 1.7 (overlapping peaks of: -CH<sub>2</sub>- in iso-octyl chain and -CH<sub>2</sub>CHPh), 2.2-3 (-CH<sub>2</sub>CH<sub>2</sub>NH- in PEI), 3-3.49 (overlapping peaks of: -COCH-, -OCH<sub>2</sub>- in SMAPIE, -CHNH<sub>2</sub> protons in galactosamine alpha and beta anomers and -OCH<sub>2</sub>CH<sub>2</sub>O- in PEG chain), 3.5-4 (-CH<sub>2</sub>CHCHOH, -NH<sub>2</sub>CHCHOH,

-CH<sub>2</sub>OH, -CHCH<sub>2</sub>- protons in galactosamine alpha and beta anomers), 4.5, 5 (-OCHOH alpha and beta anomeric protons in galactosamine), 6.4-7.6 (overlapping peaks of: -C<sub>6</sub>H<sub>4</sub> in substituted DBCO and -C<sub>6</sub>H<sub>5</sub> in cumene terminal and styrene residues).

## 2.4 Size Exclusion Chromatography (SEC)

Gel filtration chromatography (GFC), a type of size exclusion chromatography, was performed to determine the molecular weight of SMAPIE-PEI-N3 micelles relative to molecular weight of protein standards. Briefly, the samples were prepared in 0.45  $\mu$ m filtered deionized water (6 mg/mL) and sonicated using Branson 8210 ultrasonifier for 20 min. The sample was then injected in Hiload 16/600 Superdex 75 pg column in AKTA FPLC system (GE Healthcare Lifesciences, Pittsburgh, PA, USA). The sample was run at a flow rate 0.3 mL/min using (300 mM NaCl, 50 mM Na<sub>2</sub>HPO<sub>4</sub>/NaH<sub>2</sub>PO<sub>4</sub>, 10% acetonitrile) as running buffer (pH 7.2) at 4 °C. UV detector was set at 280 nm for detection of aromatic benzene ring in SMAPIE chain. Elution volume was used to calculate the relative molecular weight using standard curve of log molecular weights of protein standards versus standards  $V_e/V_o$  (elution volume/ column void volume).

## 2.5 Copper Assay

A copper based assay was performed to quantify the amount of PEI in SMAPIE-PEI-N3 and SMAPIE-PEI-Gal micelles according to previously described method<sup>128</sup>. Briefly, using a 96 well plate, 50  $\mu$ L of 20 mM copper acetate in 5% Na acetate solution was added to 50  $\mu$ L of either SMAPIE-PEI-N3 or SMAPIE-PEI-Gal solution (2 mg/mL) in deionized water. The intensity of the blue colored

cuprammonium complex was measured at 690nm on a synergy 2 microplate reader (BioTek Instrument, Winooski, VT, USA).

The concentration of PEI in targeted and non-targeted micelles was calculated based on the calibration curve constructed using PEI 10 KDa as standard at varied concentrations (2, 1, 0.5, 0.25, 0.125, 0.0625 mg/ml). Results were presented as mean ( $\pm$  SD), n=3 and n=4 in case of PEI 10 KDa standard and micelles respectively.

## **2.6 Determination of Critical Micelle Concentration (CMC)**

CMC was determined by fluorescence spectroscopy using pyrene as a fluorescent probe<sup>4</sup>. Briefly, 100  $\mu$ l of pyrene solution in methanol (12  $\mu$ M) was added into amber colored bottles and left in chemical hood overnight to allow methanol evaporation and pyrene film formation. Then varying copolymer concentrations in water (0.0001-0.5 gm/L) was prepared in triplicates and added to the pyrene film to get pyrene final concentration of (0.6  $\mu$ M). The solutions were kept on a shaker at room temperature for 24 hours. Subsequently, the fluorescence measurement was performed on F-2500 fluorescence spectrophotometer (Hitachi, Ltd. Tokyo, Japan). The measurements were done at excitation wavelengths of 334 nm and 339 nm and emission wavelength of 390 nm. The emission intensity ratio (I<sub>339</sub>/I<sub>334</sub>) was plotted against the logarithm of the copolymer concentrations. The CMC value was obtained from the intersection of the tangential lines on the curve as reported previously<sup>130</sup>. Results were reported as mean ( $\pm$  SD, n=3).



## 2.7 Preparation of siRNA Micelleplexes or Polyplexes

Micelleplexes or polyplexes were prepared according to the pre-calculated N/P ratio, which is the ratio of positively charged amine groups (N) in the polymer to the negatively charged phosphate groups (P) in siRNA. Both micelles/polymer and siRNA solutions were prepared in sterile filtered 5% glucose solution using 0.22  $\mu\text{m}$  syringe filter. Equal volumes of siRNA solution and micelles/polymer solution were efficiently mixed and pipetted many times, then incubated at room temperature for 30 min to allow efficient complexation. Micelles/polymer solutions of different concentrations were used to form micelleplexes or polyplexes at the desired various N/P ratios.

## 2.8 SYBER Gold Assay

SYBER Gold quenching assay was performed to evaluate the siRNA condensation capacity of both targeted (SMAPIE-PEI-Gal) and non-targeted (SMAPIE-PEI-N3) micelles at different N/P ratios (1, 2, 3, 4, 5, 10, 15) in comparison to PEI 25 KDa and PEI 10 KDa as controls. SYBER Gold assay was conducted according to previously reported procedure<sup>131</sup> with some modifications. For this purpose, white/opaque FluoroNunc 96 well plate was used. In each well, 50 pmol of siRNA Universal Negative Control #2 in 50  $\mu\text{L}$  of sterile 5% glucose solution was complexed with 50  $\mu\text{L}$  of micelles or polymer solution prepared at the suitable concentration in sterile 5% glucose solution to achieve the desired N/P ratio. The (100  $\mu\text{L}$ ) in each well was incubated for 30 minutes at room temperature. Then, 30  $\mu\text{L}$  of 4x SYBER Gold solution was added to each well and the plate was incubated in the dark at room temperature. After 15 minute incubation,

fluorescence was detected using a synergy 2 microplate reader (BioTek Instrument, Winooski, VT, USA) at excitation and emission wavelength of 485/20nm and 528/20nm respectively. Results were represented as mean ( $\pm$  standard deviation, n=3). Fluorescence intensity at N/P = zero (free siRNA + SYBER Gold dye) was set as 100% and relative fluorescence intensities of micelleplexes or polyplexes was obtained using the equation: [(micelleplexes or polyplexes fluorescence intensity) / (fluorescence intensity at N/P= zero)]\* 100.

### **2.9 Size and Zeta Potential Measurements: Light Scattering (LS)**

Hydrodynamic size and zeta potential measurements of siRNA free micelles, siRNA containing micelles (micelleplexes) and PEI 10 KDa polyplexes were performed in triplicates using light scattering (LS) analysis. All samples were tested in a Zetasizer Nano ZS (Malvern Instruments, Westborough, MA, USA) at 25 °C. The siRNA free micelles samples were prepared in deionized water (1mg/ml) and tested at a volume of 350  $\mu$ l and 750  $\mu$ l using disposable cuvettes for size and zeta potential determination respectively. Micelleplexes or PEI polyplexes sizes were measured by transferring 100  $\mu$ l of micelleplexes or PEI polyplexes solution in sterile filtered 5% glucose to low volume disposable cuvette, where each 100  $\mu$ l contained 20 pmol of siRNA. After size measurement, the same sample (in 100  $\mu$ l volume) was diluted with 650  $\mu$ l sterile filtered 5% glucose solution and transferred into transparent zeta cuvette for zeta potential measurements using the same instrument. The scattered light was detected at 173° backscatter angle, distilled water viscosity and refractive index of (0.8872 cP) and (1.33) respectively, were used as measuring parameters. Samples in triplicates were tested and three

measurements were performed for each sample with at least 12 runs per measurement. Size and zeta measurements Results were presented as Z-average hydrodynamic size in nanometers ( $\pm$  SD, n=3) and mean in millivolts ( $\pm$  SD, n=3), respectively.

### **2.10 Size and Morphology Measurements: Transmission Electron Microscopy (TEM)**

The size and morphology of siRNA free micelles and micelleplexes in the dry state were obtained by transmission electron microscopy TEM. TEM samples were prepared by adding a drop of siRNA free micelles solution (4mg/ml), or micelleplexes solution (prepared as described above at N/P ratio of 10 with 40 pmol siRNA Universal Negative Control #2 in total volume of 10  $\mu$ l) on a copper-coated grid (200 mesh) for 3 minutes followed by blotting the grid, and staining with 3% uranyl acetate for another 3 minutes. Finally, the grid was allowed to air dry completely before imaging. Sterile filtered 5% glucose solution was used as the dispersion medium for sample preparation. Several images at different magnifications were obtained for each sample with a transmission electron microscope (JEOL 2010 TEM, LaB6 Filament Gun, Tokyo, Japan).

### **2.11 Buffering Capacity Measurements**

An acid-base titration was performed to determine the buffering capacity of both targeted SMAPIE-PEI-Gal and non-targeted SMAPIE-PEI-N3 micelles in comparison to PEI branched polymers of different molecular weights (25, 10, 1.8 KDa) as positive controls and 150 mM NaCl solution as vehicle and negative control. The assay was done according to previously reported procedure<sup>132</sup>. Briefly, 3 mg polymer or micelles were dissolved in 15 ml of 150 mM NaCl solution

to achieve final concentration of 0.2 mg/mL. The pH of all solutions was adjusted at the beginning to 11.0 by titration against 0.1 M NaOH solution. Subsequently, titration curve was generated for each polymer or micelle by titrating their solutions with 0.1 M HCl solution at equal increments of 30  $\mu$ L till pH of 2.0. The changes in pH values were determined after each 30  $\mu$ L addition using a pH meter at room temperature. The slower the change in the pH of the solution during titration the higher its buffering capacity and vice-versa.

## **2.12 Biological Evaluation of SMAPIE-PEI-N3 and SMAPEI-PEI-Gal Micelles**

### **2.12.1 Cytotoxicity Assay Using Human Liver Cancer Cells**

The cytotoxicity of free polymers (PEI 25 KDa and PEI 10 KDa as controls) or micelles (non-targeted SMAPIE-PEI-N3 and targeted SMAPIE-PEI-Gal) was studied using MTT assay on Hep G2 human HCC cells. The Hep G2 cells were seeded in 96 well plates at cell density of 5000 cells/well in 100  $\mu$ L of DMEM growth medium containing 10% FBS and incubated for 24 hours at 37 °C in humidified air containing 5% CO<sub>2</sub>. Stock solutions of different polymers or micelles were prepared in sterile 5% glucose solution. Predetermined concentrations were obtained by serial dilution of the respective stock solutions with cell culture medium supplemented with FBS. Subsequently, 100  $\mu$ L of each serial dilution was added on the preexisting 100  $\mu$ L media in each well to achieve final polymer or micellar concentrations ranging from 400 to 1.5625  $\mu$ g/mL. The cells were incubated for 48 hours. MTT solution in phosphate buffered saline (PBS; 5 mg/mL) was then added to cells (20  $\mu$ L/well), and the plates were incubated for additional 3 hours at 37 °C and 5% CO<sub>2</sub>. Then, all the media were removed and 100  $\mu$ L of dimethyl sulfoxide

(DMSO) was added in each well and the plates were subjected to orbital shaking in the dark for 15 minutes. The DMSO solvent dissolved the purple colored formazan crystals formed in the mitochondria of live cells. The absorbance was recorded at 590 nm on a synergy 2 microplate reader (BioTek Instrument, Winooski, VT, USA). Results were presented as mean ( $\pm$  SD, n=3) of relative cell viability (%). Percentage relative cell viability = (treated cells absorbance – blank absorbance) / (untreated cells absorbance – blank absorbance) x 100. Treated and untreated cells are cells cultured in presence or absence of polymers or micelles, respectively. Blank values (controls) were attributed to the absorbance measured in wells that didn't contain cells.

### **2.12.2 Cellular Uptake Quantification by Flow Cytometry**

Flow cytometry was used to quantify the cellular uptake of the fluorescently labeled micelleplexes or polyplexes. Hep G2 cells were seeded in 24 well plates at cell density of 80,000 cells/well in 500  $\mu$ L of DMEM containing 10% FBS and incubated for 24 hours at 37 °C and 5% CO<sub>2</sub> prior to transfection. On transfection day, pre-existing medium was replaced with 350  $\mu$ L fresh media containing 10% FBS. In case of competition assay, the 350  $\mu$ L of fresh DMEM medium contained 10% FBS and 20 mM free galactosamine as a competitor of galactosamine in SMAPIE-PEI-Gal micelles. PEI 10 KDa polyplexes, targeted (SMAPIE-PEI-Gal) or non-targeted (SMAPIE-PEI-N3) micelleplexes were prepared as described above in 50  $\mu$ L of sterile 5% glucose solution at N/P ratio of 10 using fluorescent FAM<sup>™</sup>-Labeled Negative Control siRNA. The prepared polyplexes or micelleplexes were added on cells to achieve final siRNA concentration of 200 nM

per well. Untreated cells (blank) or cells treated with free siRNA served as negative controls, while cells treated with PEI 10 KDa polyplexes served as positive control. After the polyplexes or micelleplexes addition, cells were incubated at 37 °C and 5% CO<sub>2</sub> for total transfection time of 5 hours. When the transfection period ended, the transfection medium was removed, and cells were washed with 1 mL sterile PBS. 100 µL trypsin /well was added for 3 minutes to detach cells followed by addition of 900 µL fresh medium to deactivate the trypsin. Cell suspensions were collected and centrifuged at 4 °C for 5 minutes at 800 rpm, then supernatant was removed and cells were washed with 1mL sterile PBS by resuspension and re-centrifugation. Finally, cells were re-suspended in 400 µL sterile PBS for fluorescence quantification using Attune® Acoustic Focusing Flow Cytometer (Applied Biosystems, Life Technologies, Carlsbad, CA,USA). The laser beam was set at a wavelength of 488 nm for excitation and (530/30) (center/band pass) emission filter was used for emission detection. Cells were gated based on their morphology and 10,000 events were evaluated per each sample. Measurements were performed in triplicates and data analysis was performed using Attune® Cytometric Software. Data are shown as mean of median fluorescence intensity ( $\pm$  standard deviation, n=3). Statistical analysis of data was completed through one-way ANOVA and post hoc Tukey HSD test application using Vassar stats program.

### **2.12.3 Cellular Uptake and Endosomal Escape by Confocal Laser Scanning Microscopy (CLSM)**

Cellular uptake of both targeted (SMAPIE-PEI-Gal) and non-targeted (SMAPIE-PEI-N3) micelleplexes through endocytosis and the ability to achieve endosomal escape with the release of the siRNA in cytoplasm was shown by

Confocal Laser Scanning Microscopy (CLSM, Leica microsystems, Mannheim, Germany). Hep G2 cells were seeded in 4 well  $\mu$ -Slide Ph+, ibiTreat ( ibidi, Wisconsin, USA) at cell density of 35,000 cells/well in 600  $\mu$ L of FluoroBrite™ DMEM life cell fluorescence imaging medium containing 10% FBS and incubated for 24 hours at 37 °C in humidified air containing 5% CO<sub>2</sub> prior to transfection. On day of transfection pre-existing medium was replaced with 550  $\mu$ L of fresh FluoroBrite™ DMEM medium containing 10% FBS. In case of competition assay, the 550  $\mu$ L of fresh FluoroBrite™ DMEM medium contained 10% FBS and free galactosamine as a competitor of galactosamine in SMAPIE-PEI-Gal micelles. The free galactosamine was added to obtain final concentration of 100  $\mu$ g/ml in total volume of 600  $\mu$ L. Cells were transfected with micelleplexes or polyplexes at N/P ratio of 10. Polyplexes of PEI 10KDa as a positive control or micelleplexes of targeted (SMAPIE-PEI-Gal) or non-targeted (SMAPIE-PEI-N3) micelles were formed as described above using Silencer® FAM™-Labeled Negative Control siRNA in 50  $\mu$ L of sterile 5% glucose solution, which was then added to the 550  $\mu$ L of fresh medium in each well to achieve final siRNA concentration of 200 nM. Then, cells were incubated for 20 hours at 37 °C and 5% CO<sub>2</sub> before being washed with PBS PH 7.4. Subsequently, cells were incubated for 1 hour in 100 nM Lyso Tracker Deep Red dye solution in FluoroBrite™ DMEM medium containing 10% FBS to stain endosomes. Then, cells were washed with PBS PH 7.4. The nuclei were stained with 8.115  $\mu$ M Hoechst 33342 stain solution in PBS following incubation of cells with the stain at 37 °C and 5% CO<sub>2</sub> for 10 minutes. Finally, cells were washed with PBS and incubated in 700  $\mu$ L FluoroBrite™ DMEM medium

containing 10% FBS. The cells were directly imaged by live cell imaging technique on Leica TCS SP5 inverted confocal microscope (Leica microsystems, Mannheim, Germany). All images were acquired using oil immersion lens with 63X magnification / 1.4 numerical aperture. For excitation of Hoechst 33342, FAM-Labeled siRNA, and LysoTracker Deep Red Laser beams with excitation wavelengths 405nm, 488nm, and 633nm were used respectively. Merge images of the three fluorescent emissions as well as Bright field ones were recorded for each sample.

Fiji ImageJ software (Life-Line version, 2015 December 22)<sup>133,134</sup> was used for quantification of green siRNA fluorescence in the CLSM images. Fluorescence quantification was performed according to previously reported method<sup>135</sup>. Total corrected cellular fluorescence (TCCF) per cell was determined, where TCCF = integrated density obtained – (area of selected cell x fluorescence of background). After that, mean of TCCFs of all cells / image was calculated and plotted against each treatment type.

#### **2.12.4 Transfection Efficiency and Nrf2 Gene Knockdown by Western Blot Analysis**

SMAPIE-PEI-Gal micelleplexes transfection efficiency and Nrf2 gene knockdown in Hep G2 cells were evaluated using western blotting technique. Nrf2 gene knockdown mediated by Nrf2 siRNA condensing SMAPIE-PEI-Gal micelleplexes was compared to that mediated by the positive transfection control Nrf2 siRNA condensing PEI 10 KDa polyplexes. As negative controls, siRNA Universal Negative Control #2 condensing micelleplexes and polyplexes were also prepared and tested. Briefly, all micelleplexes and polyplexes were prepared at



N/P ratio of 10 as described above in total volume of 100  $\mu$ L of sterile 5% glucose solution containing 55 pmol siRNA. In 6 well plates, reverse transfection technique was applied for transfecting Hep G2 cells. In each well, 100  $\mu$ L of the micelleplexes or the polyplexes were added, followed by the addition of 1 ml Hep G2 cells suspension in complete DMEM media supplemented with 10% FBS and 1% penicillin/streptomycin at cell density 500,000 cells/ml. The final siRNA concentration in each well was 50 nM. Plates were incubated under humidified conditions at 37°C and 5% CO<sub>2</sub> for 5 hours. After 5 hours of incubation, 1.1 ml fresh complete DMEM media was added in each well to obtain final volume of 2.2 ml and cells were incubated for additional 19 hours. Subsequently, cells were collected on ice in 15 ml centrifuge tubes, centrifuged at 4°C, washed with ice cold 1x PBS solution, and then centrifuged at 4°C to get the cell pellet. Whole cell lysis buffer was then added to the cell pellets, and cells were lysed by pipetting up and down many times. Cells were incubated with the lysis buffer on an orbital rocker at 4°C for 30 minutes, then centrifuged at 120,000 rpm for 15 minutes at 4°C. The pellet was discarded and the cell lysates were collected followed by quantification of the total protein concentration in each lysate by Bradford assay using BSA as standard.

Samples were then prepared for loading in the 10% SDS-polyacrylamide gel, where lysates equivalent to 40  $\mu$ g total protein were denatured by mixing with equal volume of 2x SDS-PAGE loading buffer containing  $\beta$ -mercaptoethanol followed by heating at 95°C for 5 minutes. Denatured samples were then loaded on 10% SDS-polyacrylamide gel (SDS-PAGE) and proteins were separated by gel

electrophoresis at 120 volt for 2 hours. Once separated, the proteins were then transferred to nitrocellulose membrane at 100 volt for 1 hour on ice. The membrane was then blocked with 5% milk in TBST buffer at room temperature for 1 hour, then washed with TBST, and incubated overnight at 4 °C with 1:100 diluted Nrf2 (A-10) sc-365949 mouse monoclonal primary antibody in 5% BSA in TBST buffer. On the next day, the membrane was washed with TBST three times for 10 minutes each, followed by its incubation for 1 hour at room temperature with 1:2000 diluted goat anti-mouse IgG-HRP sc-2005 secondary antibody in 5% milk in TBST buffer. Finally, the membrane was washed in TBST three times, followed by detection of the bound secondary antibody HRP enzyme activity using chemiluminescent light based detection substrate (Super Signal West Pico chemiluminescent substrate) where the chemiluminescent immune reactive bands on the membrane were imaged using an ImageQuant LAS4000 (GE Healthcare Bio-sciences, Pittsburgh, PA, USA). Membranes were also probed with 1:500 diluted GAPDH (G-9) sc-365062 mouse monoclonal primary antibody in 5% BSA in TBST buffer in a similar manner for detecting the GAPDH protein as a loading control.

Western blot bands intensities were then quantified using Fiji ImageJ software (Life-Line version, 2015 December 22)<sup>133,134</sup>. According to previously published method, expression of Nrf2 protein reflected by the Nrf2 bands intensities was normalized to the expression of the GAPDH loading control protein of the same sample. Nrf2 Gene silencing efficiency was calculated by comparing the normalized intensity of Nrf2 of sample treated with siRNA targeting Nrf2 to the normalized intensity of Nrf2 of sample treated with negative control siRNA<sup>136</sup>. Data

from three independent experiments were shown as mean of normalized Nrf2 intensity or mean of [normalized Nrf2 intensity / normalized Nrf2 intensity in negative control siRNA treated sample] ( $\pm$  standard deviation, n=3). Statistical analysis of data was completed through t-tests application using Vassar stats program.

## CHAPTER 3 RESULTS

### 3.1. Synthesis and Characterization of SMAPIE-PEI-N3 and SMAPIE-PEI-Gal Micelles

#### 3.1.1 Synthesis of SMAPIE-PEI-N3 Micelles Forming Block Copolymer

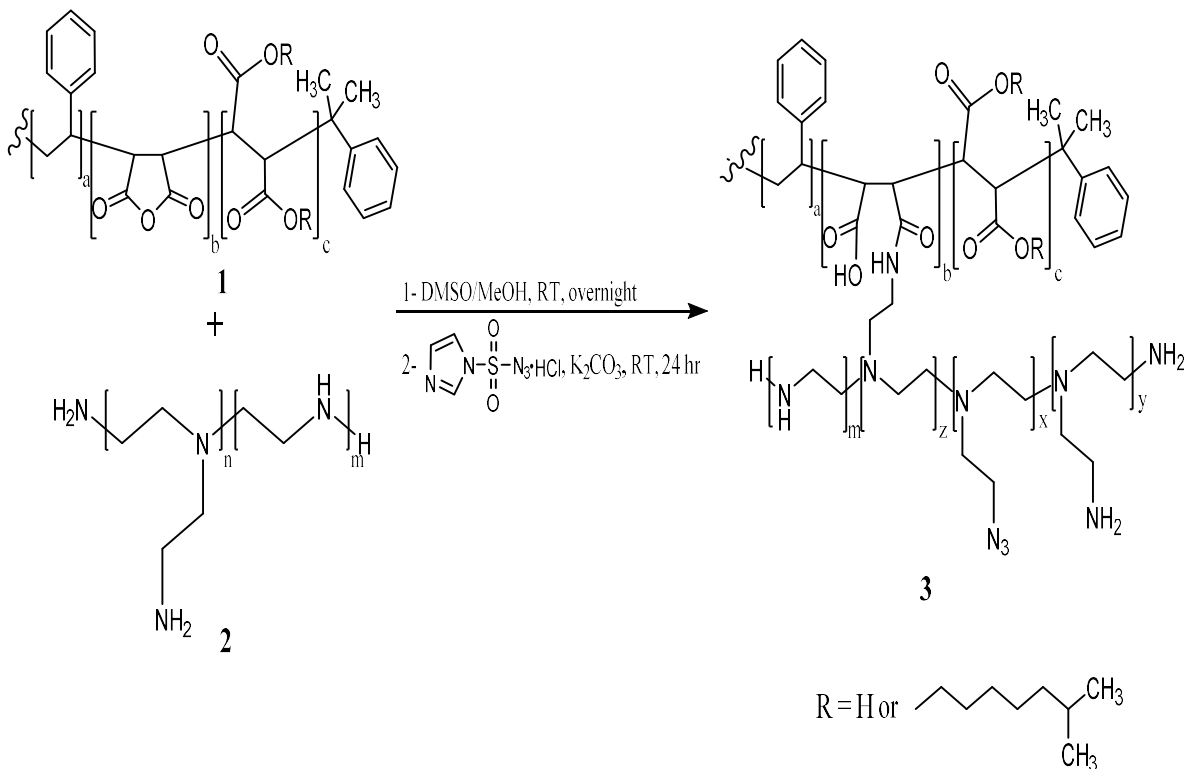
SMAPIE-PEI-N3 was synthesized in two steps by one-pot reaction (scheme 3.1). In the first step, opening of the anhydride ring in SMAPIE copolymer (**1**) by primary amine group in the branched polymer polyethylenimine (PEI) (**2**) to form amide bond linking the two polymeric chains forming the di-block copolymer SMAPIE-PEI was undertaken. In the next step, conversion of some of primary amine groups in PEI to azide groups using Imidazole-1-sulfonylazide hydrochloride reagent as a “diazo donor”, and SMAPIE-PEI-N3 micelles forming block copolymer (**3**) was obtained as the final product. The diazo-transfer reaction was completed without any copper metal catalysis. Azide decorated micelles were subsequently reacted with alkyne group in strained cyclooctyne ring through copper free “click” chemistry. The final product purification was done through membrane dialysis.

#### 3.1.2 Synthesis of Targeting Ligand Conjugated SMAPIE-PEI-Gal Micelles Forming Block Copolymer

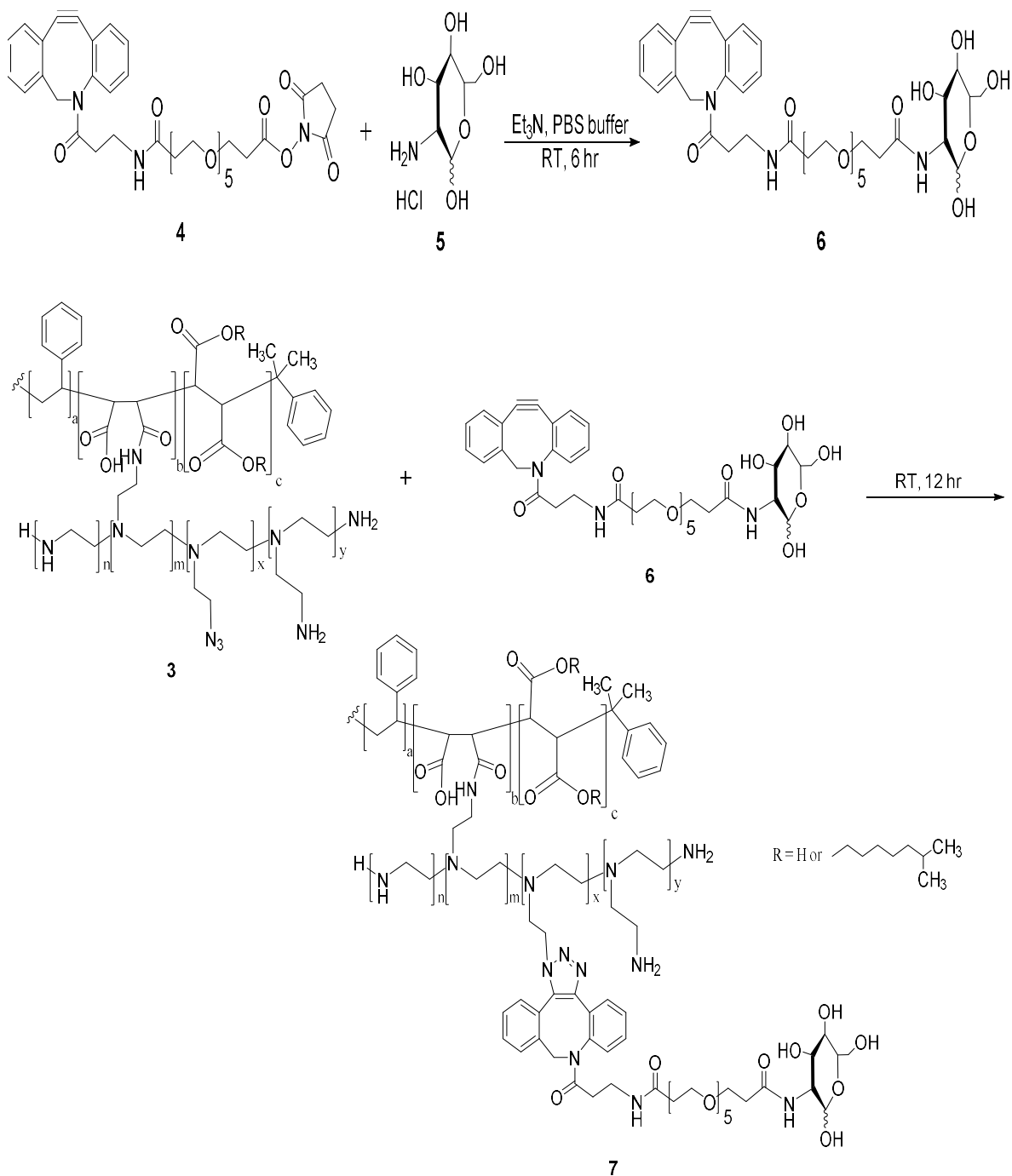
Galactosamine targeted SMAPIE-PEI-Gal micelles forming block copolymer was synthesized by copper free “click” chemistry in two steps (scheme 3.2). In the first step, the synthesis of the alkyne decorated galactosamine targeting ligand through coupling of *N*-hydroxysuccinimide part in DBCO-PEG<sub>5</sub>-NHS ester (**4**) with amine group in galactosamine.HCl (**5**) in its basic form was undertaken. The coupling reaction resulted in amide bond formation and galactosamino-PEG<sub>5</sub>-

DBCO product (**6**) was obtained. In the second step, strain-promoted alkyne-azide cycloaddition (SPAAC) reaction was undertaken between galactosamino-PEG<sub>5</sub>-DBCO product (**6**) from the first step and SMAPIE-PEI-N3 micelles forming block copolymer (**3**) to arrive at SMAPIE-PEI-Gal targeted micelles forming block copolymer (**7**). SPAAC is a well-established copper free “click” reaction between strained cyclooctyne moiety in product (**6**) and azide moiety in SMAPIE-PEI-N3 block copolymer (**3**) forming a stable triazole ring linkage. The final product purification was done through membrane dialysis.

**Scheme 3.1.** Synthesis of non-targeted SMAPIE-PEI-N3 micelles forming block copolymer (**3**)



**Scheme 3.2.** Synthesis of ligand targeted SMAPIE-PEI-Gal micelles forming block copolymer (7)



### 3.2 Size Exclusion Chromatography (SEC)

Size exclusion chromatography was run to detect the relative molecular weight of the SMAPIE-PEI-N3 micelles compared to molecular weights of protein standards. The chromatogram of SMAPIE-PEI-N3 micelles is presented in figure 3.1. The chromatogram shows unimodal molecular weight distribution. The elution volume of the micelles (78.14 mL) was used to calculate  $V_e/V_o$  (elution volume/column void volume). The micelles relative molecular weight (13474.58 Da) was obtained from standard curve of 158 KDa, 44 KDa, 17 KDa and 1.35 KDa protein standards figure 3.2.

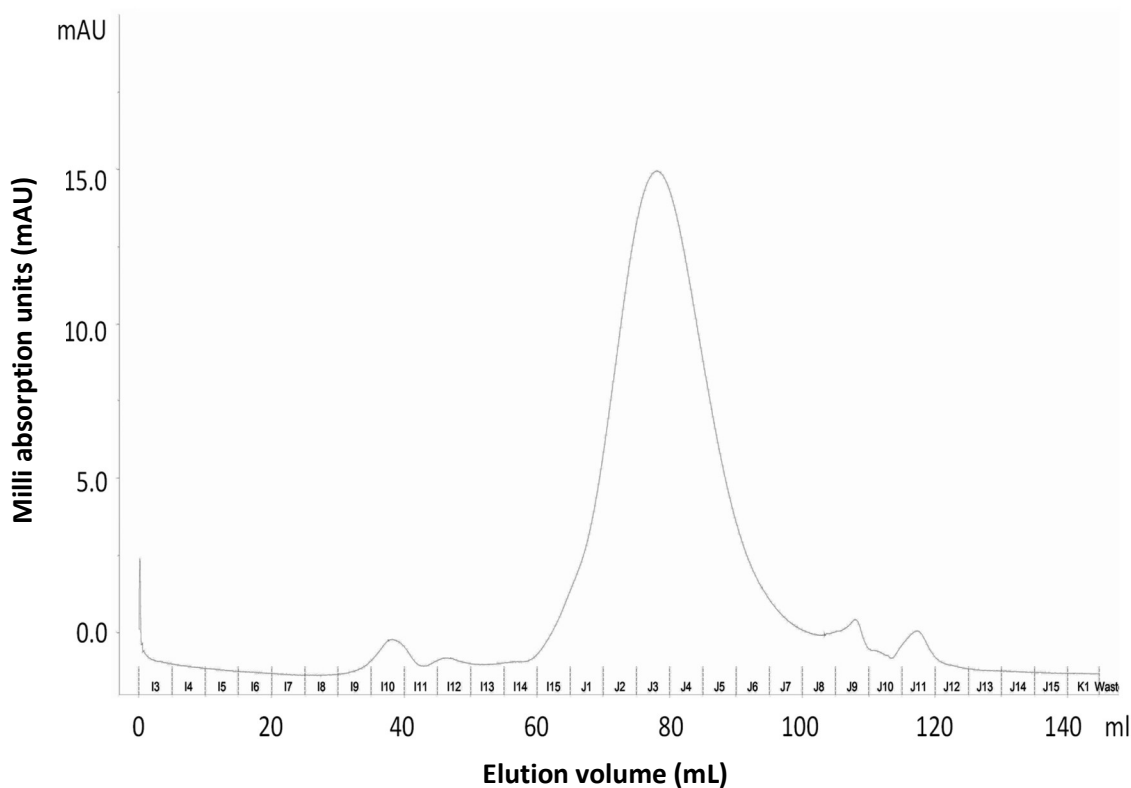


**Figure 3.1.** Size exclusion chromatogram of SMAPIE-PEI-N3 micelles.

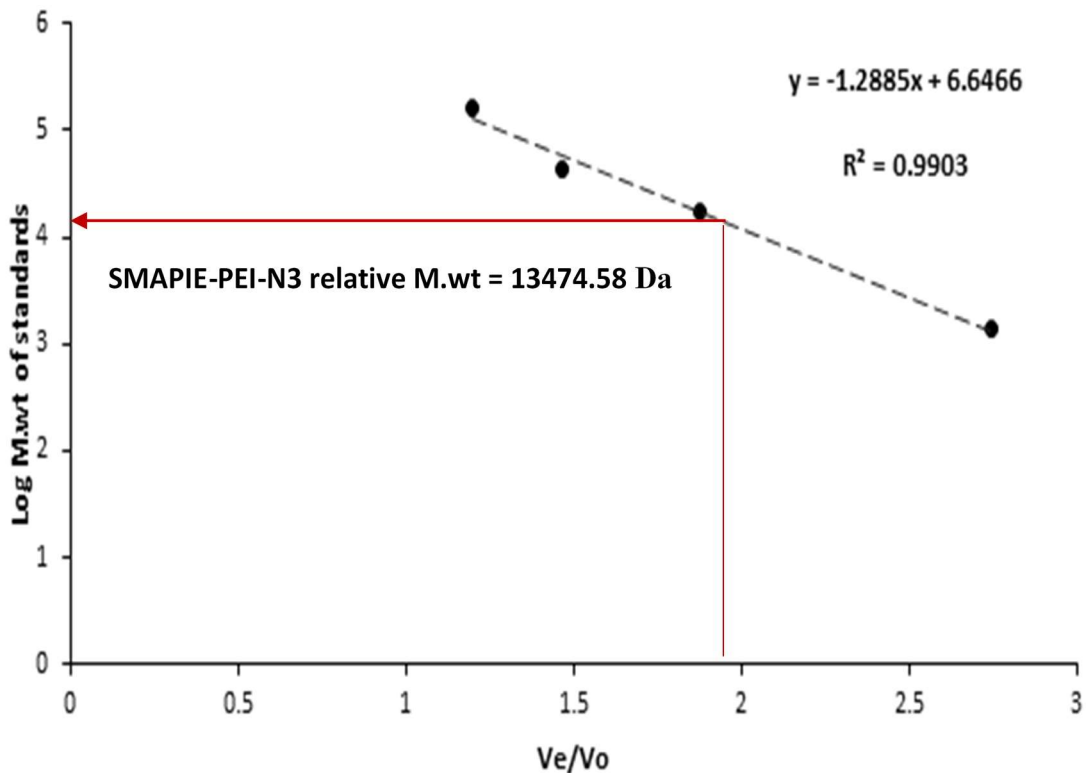


**Figure 3.2.** Standard curve of log molecular weights of protein standards versus standards  $V_e/V_o$  (elution volume/ column void volume), showing SMAPIE-PEI-N3 relative molecular weight determination.

### 3.3 Copper Assay

The relative concentration of PEI in the micelles was quantified by spectrophotometry, using a copper based assay. Copper ions successfully and specifically chelated primary amine groups in PEI polymer chains forming a blue colored complex called cuprammonium complex<sup>137</sup>. The intensity of the blue complex absorbance in the visible region was found to be in the linear range with the PEI 10 KDa various tested concentrations (2, 1, 0.5, 0.25, 0.125, 0.0625 mg/ml). As illustrated in figure 3.3, cuprammonium complex absorbance intensities obtained at varying PEI concentrations were used to construct standard curve of PEI 10 KDa as a standard. The absorbance intensities of SMAPIE-PEI-N3 and



SMAPIE-PEI-Gal complexes were applied in the standard curve equation to determine their relative PEI composition. From the results, the PEI content was found to be  $76.92 \pm 3.23\%$  (W/W) and  $54.66 \pm 5.9\%$  (W/W) for SMAPIE-PEI-N3 and SMAPIE-PEI-Gal, respectively.

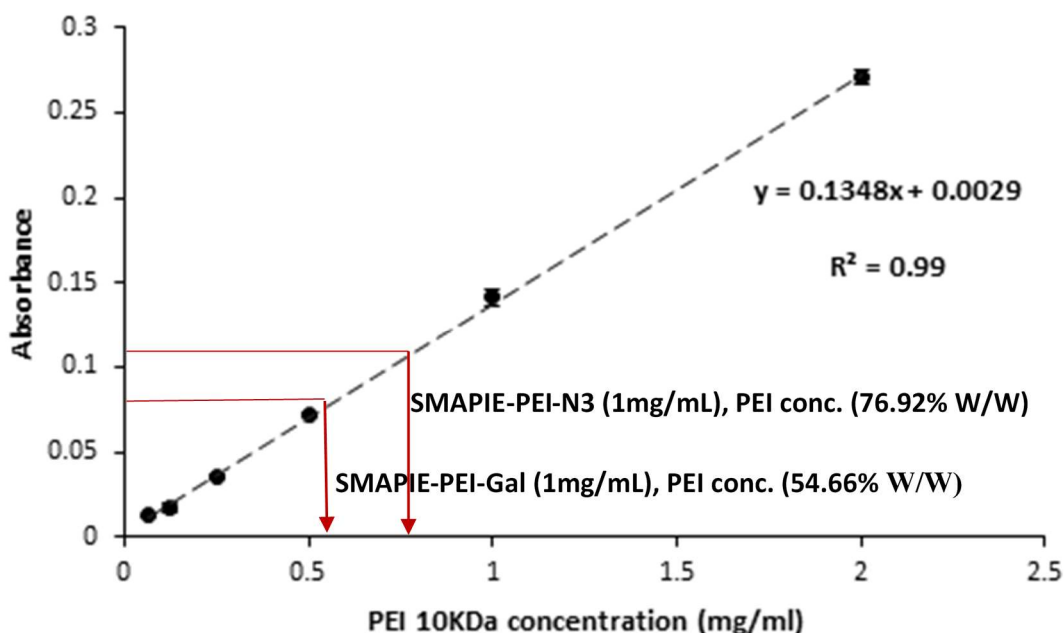


**Figure 3.3.** Standard curve of absorbance of cuprammonium complex at different PEI 10 KDa concentrations, showing PEI composition analysis of SMAPIE-PEI-N3 and SMAPIE-PEI-Gal micelles by copper assay.

### 3.4 Determination of Critical Micelle Concentration (CMC)

The ability of the amphiphilic block copolymer SMAPIE-PEI-N3 to form micelles in water was confirmed by fluorescence spectroscopy using pyrene as a fluorescent probe. Bathochromic shift in pyrene excitation wave length from 334 nm to 339 nm with increasing SMAPIE-PEI-N3 copolymer concentration from 0.0001 to 1mg/ml was detected (figure 3.4). The CMC of SMAPIE-PEI-N3 was found to be as low as 0.0112mg/ml which is  $\sim 8.6 \times 10^{-7}$  M (figure 3.5).

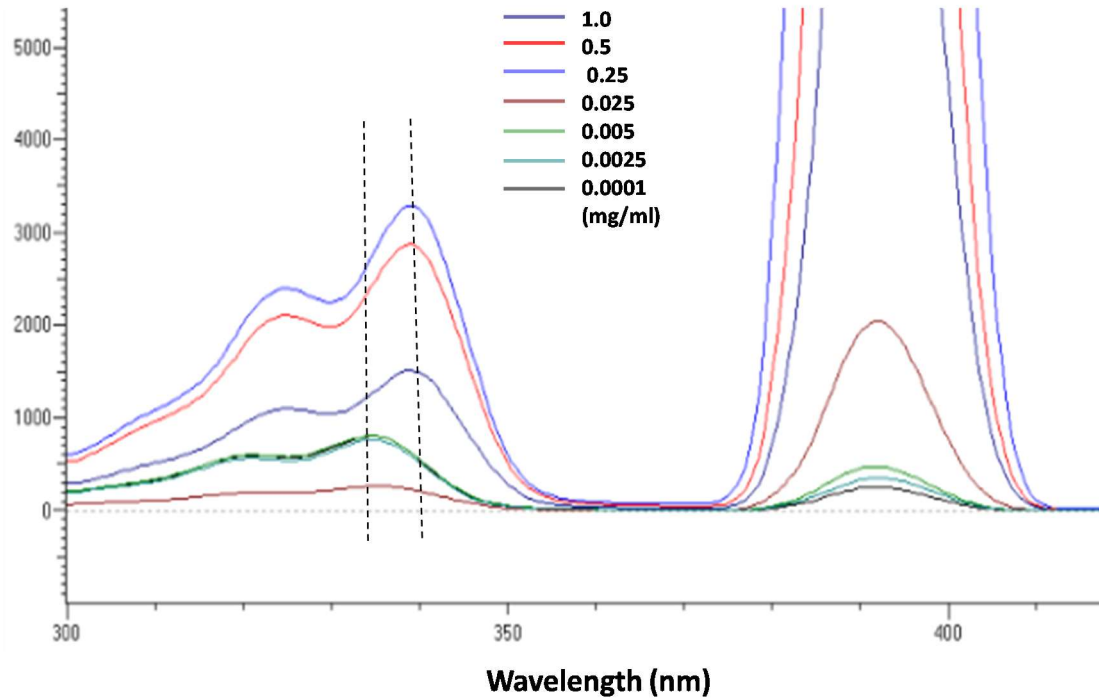


**Figure 3.4.** Fluorescence spectra of pyrene at different SMAPIE-PEI-N3 concentrations in water, showing bathochromic shift in pyrene excitation wavelength with increasing SMAPIE-PEI-N3 concentration.

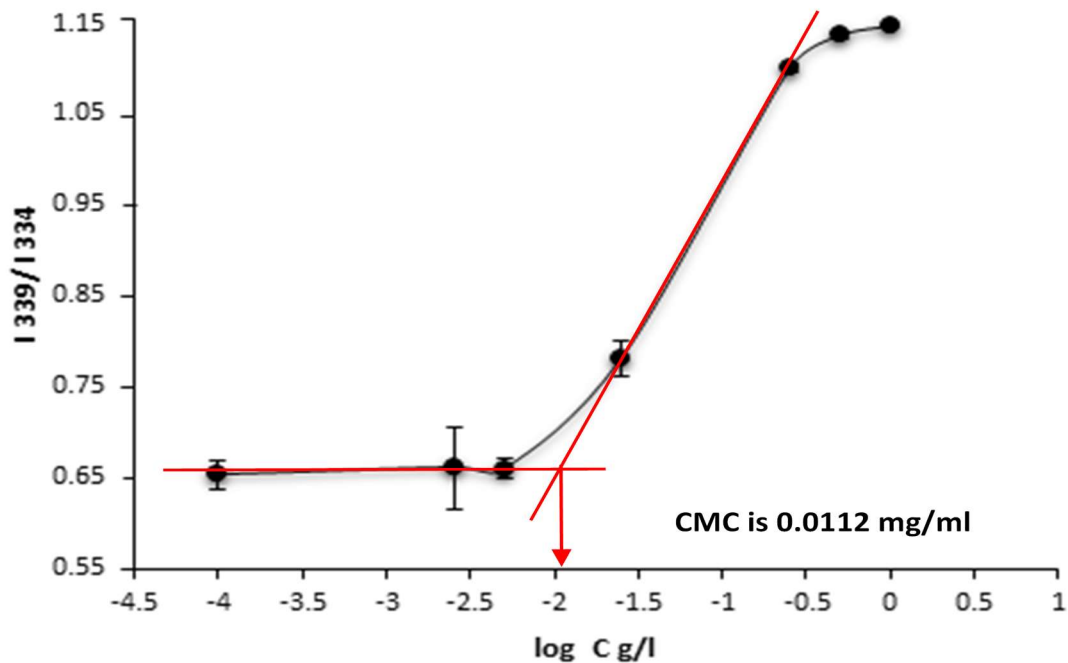


**Figure 3.5.** Critical micelle concentration (CMC) Plot of  $I_{339}/I_{334}$  emission ratio versus Log concentration of SMAPIE-PEI-N3 copolymer.

### 3.5 SYBER Gold Assay

The siRNA condensation ability of non-targeted SMAPIE-PEI-N3, and targeted SMAPIE-PEI-Gal micelles was determined by SBYER Gold fluorescence quenching assay (figure 3.6). PEI 25 KDa and PEI 10 KDa polymers were also tested as controls for comparison. Significant SBYER Gold dye fluorescence quenching indicates efficient siRNA condensation. Complete condensation of the siRNA was shown in targeted SMAPIE-PEI-Gal and non-targeted SMAPIE-PEI-N3 micelleplexes at and above N/P ratio of 4 and 7, respectively. Both PEI 25 KDa and PEI 10 KDa polymers were able to achieve complete siRNA condensation at N/P ratio of 4 and higher. Non-targeted SMAPIE-PEI-N3 micelles showed lesser siRNA complexation efficiency compared to targeted SMAPIE-PEI-Gal micelles and PEI polymers at N/P ratios lower than 10. The siRNA condensation capacity of all micelleplexes and polyplexes increased with increasing N/P ratio.

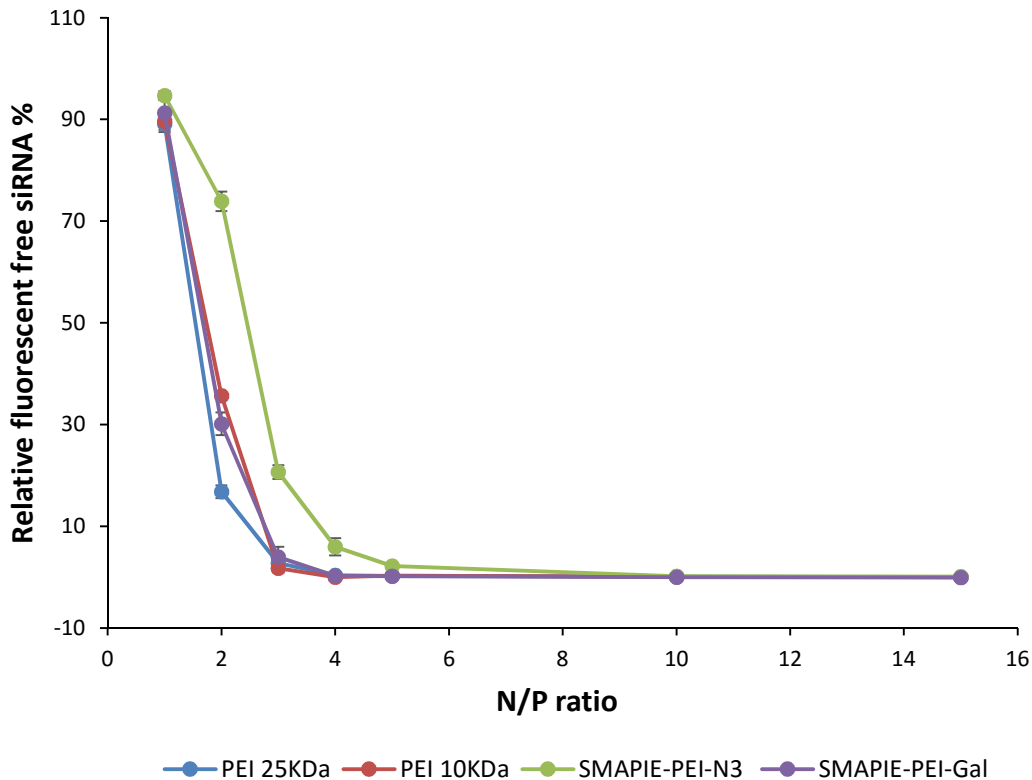


**Figure 3.6.** Condensation/Complexation behavior of polymers or micelles to siRNA by SYBER Gold fluorescence quenching assay at increasing N/P ratios.

### 3.6 Size and Zeta Potential Measurements: Light Scattering (LS)

Light scattering analysis was performed for determining the hydrodynamic size and zeta potential of plain SMAPIE-PEI-N3 (without siRNA), plain SMAPIE-PEI-Gal micelles (without siRNA) and siRNA containing targeted and non-targeted micelles (micelleplexes) as well as PEI 10 KDa polyplexes. Results were presented as mean ( $\pm$  standard deviation) from three independent experiments. Figure 3.7.A, illustrates that SMAPIE-PEI-Gal micelles exhibited larger hydrodynamic diameter of  $240 \pm 4.05$  nm than SMAPIE-PEI-N3 micelles whose size was around  $160 \pm 1.5$  nm. As shown in figure 3.7.B, both SMAPIE-PEI-N3 and SMAPIE-PEI-Gal micelles had high zeta potential of around  $38 \text{ mV} \pm 0.76$  and  $40 \pm 0.67$  mV, respectively. As summarized in table 3.1, polydispersity index (PDI)

as an indication of size distribution of SMAPIE-PEI-N3 and SMAPIE-PEI-Gal micelles was found to be  $0.25 \pm 0.01$  and  $0.42 \pm 0.03$ , respectively. Large particle sizes were observed at micelleplexes and polyplexes formed at lower N/P ratios, at N/P ratio  $< 7$  for SMAPIE-PEI-N3 micelleplexes and at N/P ratio of 3 in case of PEI polyplexes and SMAPIE-PEI-Gal micelleplexes. Apart from that, all the polyplexes and micelleplexes were around 200 nm (figure 3.8). Zeta potential of all micelleplexes and polyplexes was increased with increase in N/P ratios, with maximum zeta potential of around 23 mV at N/P ratio of 10, in case of both targeted and non-targeted micelleplexes (figure 3.9). Table 3.2 shows that the PDI (with its standard deviation) was increased mostly in the case of loosely formed large sized micelleplexes/polyplexes. However, the PDI of micelleplexes at and above N/P ratio of 7 for SMAPIE-PEI-N3 and N/P ratio of 4 for SMAPIE-PEI-Gal was  $\leq 0.39$ , indicating compact micelleplexes formation.

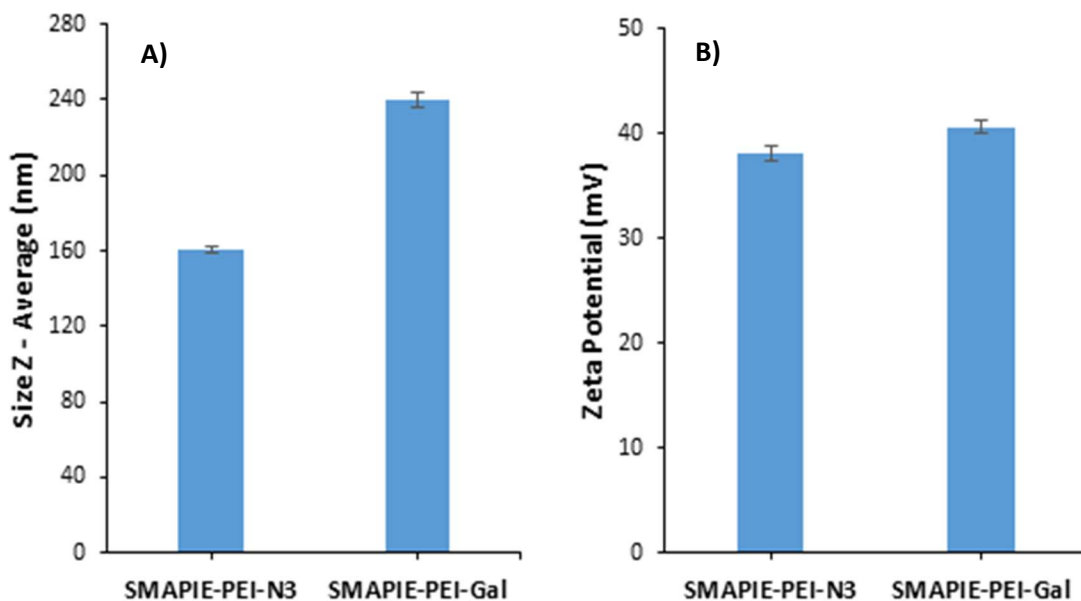


**Figure 3.7.** Hydrodynamic diameters (A) and zeta potentials (B) of plain SMAPIE-PEI-N3 and SMAPIE-PEI-Gal micelles.

**Table 3.1.** Polydispersity indexes of plain SMAPIE-PEI-N3 and SMAPIE-PEI-Gal micelles. Results are presented as average from three independent samples (n=3)  $\pm$  standard deviation.

Micelles polydispersity index (Mean $\pm$ Standard deviation, n =3)	
SMAPIE-PEI-N3	SMAPIE-PEI-Gal
0.25 $\pm$ 0.01	0.42 $\pm$ 0.03

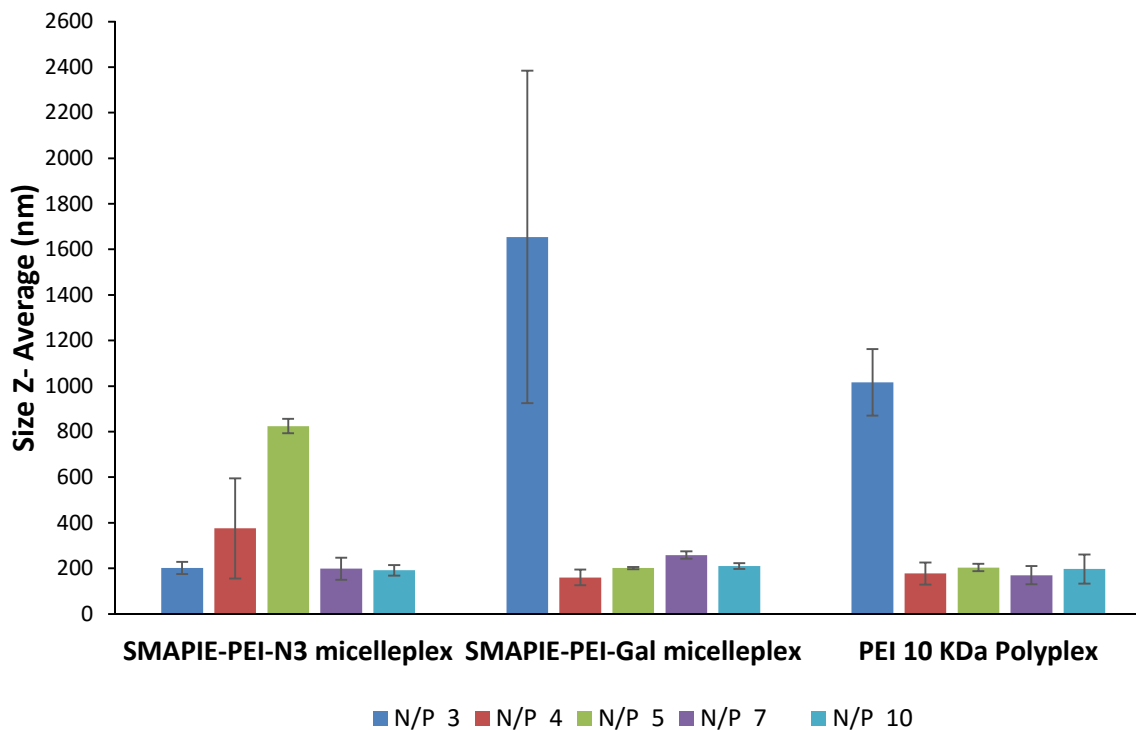


**Figure 3.8.** Hydrodynamic diameters of SMAPIE-PEI-N3/siRNA, SMAPIE-PEI-Gal/siRNA micelleplexes and PEI 10 KDa/siRNA polyplexes at the specified N/P ratios.

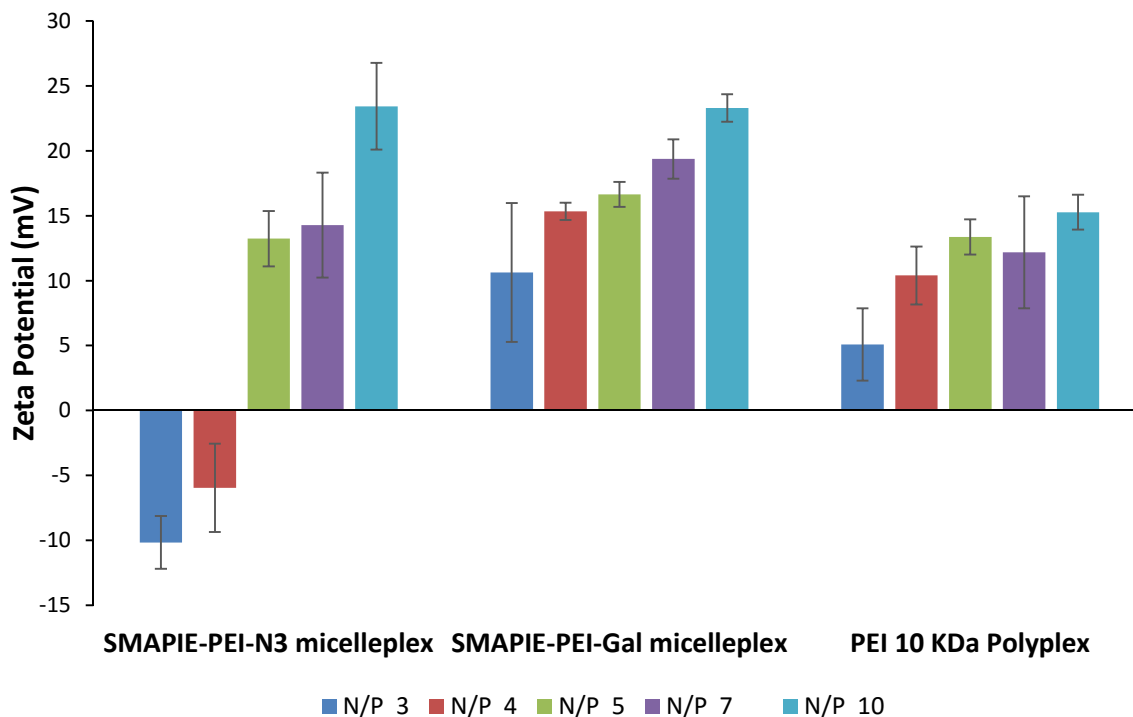


**Figure 3.9.** Zeta potentials of SMAPIE-PEI-N3/siRNA, SMAPIE-PEI-Gal/siRNA micelleplexes and PEI 10 KDa/siRNA polyplexes at the specified N/P ratios.

**Table 3.2.** Polydispersity indexes of SMAPIE-PEI-N3/siRNA, SMAPIE-PEI-Gal/siRNA micelleplexes and PEI 10 KDa/siRNA polyplexes at the specified N/P ratios. Results are presented as average from three independent samples (n=3)  $\pm$  standard deviation.

Polydispersity index (Mean $\pm$ Standard deviation, n =3)			
N/P ratio	Micelleplexes		Polyplexes
	SMAPIE-PEI-N3	SMAPIE-PEI-Gal	PEI 10 KDa
N/P = 3	0.2 $\pm$ 0.08	0.44 $\pm$ 0.49	0.49 $\pm$ 0.36
N/P = 4	0.34 $\pm$ 0.02	0.23 $\pm$ 0.09	0.28 $\pm$ 0.14
N/P = 5	0.22 $\pm$ 0.28	0.26 $\pm$ 0.03	0.35 $\pm$ 0.03
N/P = 7	0.34 $\pm$ 0.12	0.39 $\pm$ 0.03	0.31 $\pm$ 0.09
N/P = 10	0.34 $\pm$ 0.1	0.25 $\pm$ 0.11	0.45 $\pm$ 0.26

### **3.7 Size and Morphology Measurements: Transmission Electron Microscopy (TEM)**

TEM images illustrated the size and morphology of plain micelles (without siRNA) and micelleplexes (with siRNA) in the dry state (figure 3.10). Globular compact structure of darkly stained shell and white (unstained) core was obvious. SMAPIE-PEI-N3 and SMAPIE-PEI-Gal micelles (without siRNA) were of size ~100 nm and ~200 nm, respectively. At N/P ratio of 10, non-targeted micelleplexes displayed a size of ~160 nm, while galactosamine targeted micelleplexes displayed a size of ~130 nm. The TEM size, in the dry state, were relatively smaller than the ones obtained from DLS measurements, which is the hydrodynamic size.



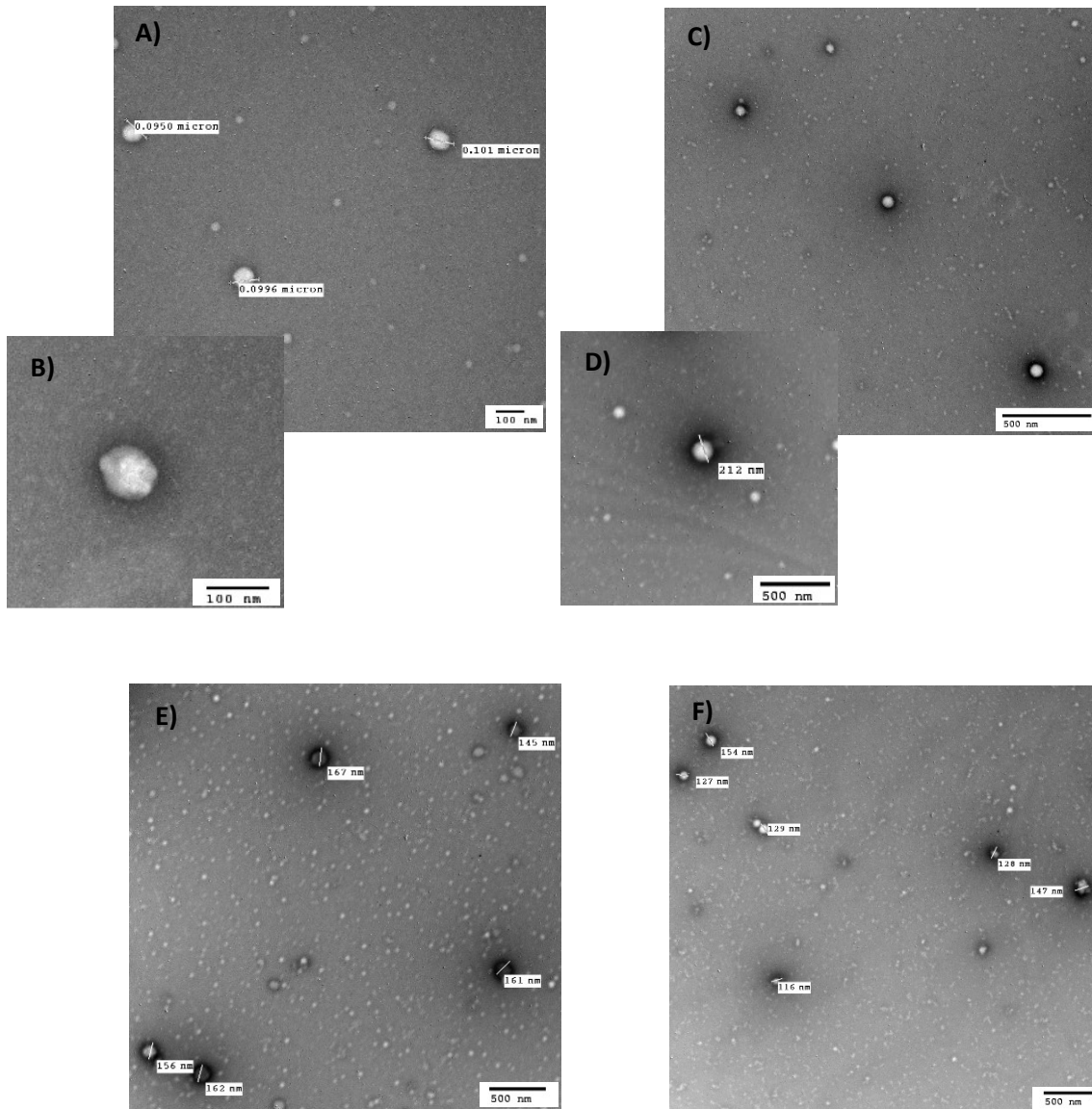


**Figure 3.10.** Transmission electron microscopy images illustrating size and morphology of SMAPIE-PEI-N3 micelles (without siRNA) (A and B), SMAPIE-PEI-Gal micelles (without siRNA) (C and D), SMAPIE-PEI-N3 micelleplexes (E), and SMAPIE-PEI-Gal micelleplexes (F). Micelleplexes were prepared at N/P ratio of 10. Micelles and micelleplexes were negatively stained with 3% uranyl acetate stain.

### 3.8 Buffering Capacity Measurements

The ability of polycationic vectors to escape out of endosomes and release their cargo into the cell cytoplasm is an important property for intracellular siRNA release and can be determined by their buffering capacity<sup>100</sup>. The buffering

capacity is evaluated by the amount of protons required for reducing pH in the endosomal pH range of (7-5.5)<sup>138</sup>. An acid-base titration experiment was performed to estimate buffering abilities of SMAPIE-PEI-N3 and SMAPIE-PEI-Gal micelles in comparison to PEI polymers and 150 mM NaCl solution (figure 3.11). During acid titration, small pH changes were observed in case of all PEI polymers, as well as, SMAPIE-PEI-N3 and SMAPIE-PEI-Gal micelles, while 150 mM NaCl solution showed an opposite scenario of abrupt pH drop. All titration curves of PEI polymers, SMAPIE-PEI-N3 and SMAPIE-PEI-Gal micelles showed two inflection points at pH ranges of (11-9) and (7-5.5). SMAPIE-PEI-N3 micelles titration data illustrated that they had a little lower proton buffering ability than SMAPIE-PEI-Gal micelles and PEI polymers of different molecular weights. On the other hand, SMAPIE-PEI-Gal micelles showed comparable buffering capacity to that of PEI polymers.

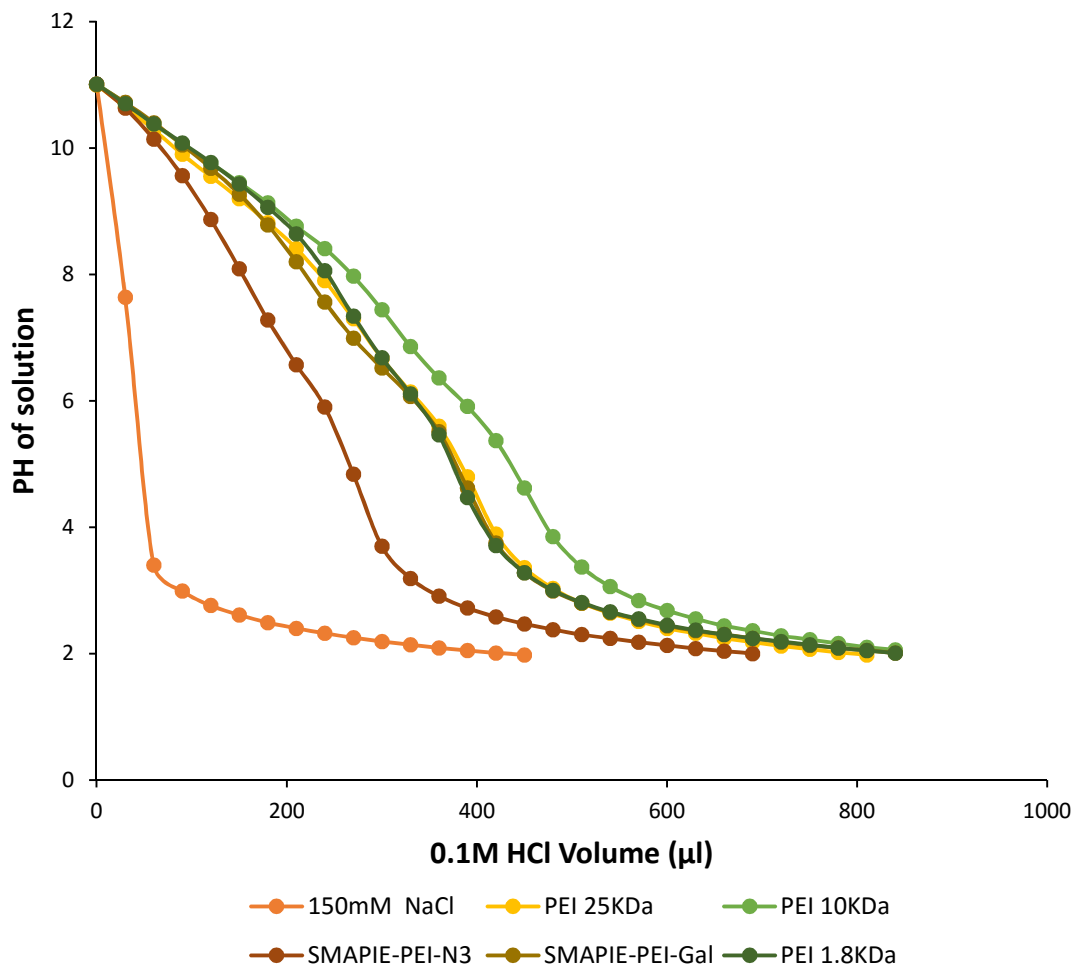


**Figure 3.11.** Acid base titration profile of non-targeted SMAPIE-PEI-N3, targeted SMAPIE-PEI-Gal micelles forming block copolymers and PEI polymers of different molecular weights (25, 10, 1.8 KDa) at pH range (11-2).

### 3.9 Biological Evaluation of SMAPIE-PEI-N3 and SMAPEI-PEI-Gal Micelles

#### 3.9.1 Cytotoxicity Assay Using Human Liver Cancer Cells

The in vitro cytotoxicity of PEI polymers, non-targeted SMAPEI-PEI-N3, and targeted SMAPEI-PEI-Gal micelles was investigated in HepG2 cells. Results demonstrated the following order: SMAPEI-PEI-Gal < PEI 10 KDa < SMAPEI-PEI-N3 < PEI 25 KDa for their cytotoxicity and inhibitory concentration  $IC_{50}$  (figure 3.12).  $IC_{50}$  values were found to be approximately 12, 70, 130, and 240  $\mu\text{g}/\text{mL}$  for PEI 25

KDa, SMAPEI-PEI-N3, PEI 10 KDa, and SMAPEI-PEI-Gal, respectively after 48 hours of incubation with cells. Cell viability was more than 80% in case of SMAPEI-PEI-N3, SMAPEI-PEI-Gal, and PEI 10 KDa at concentration below 20  $\mu\text{g/mL}$ .

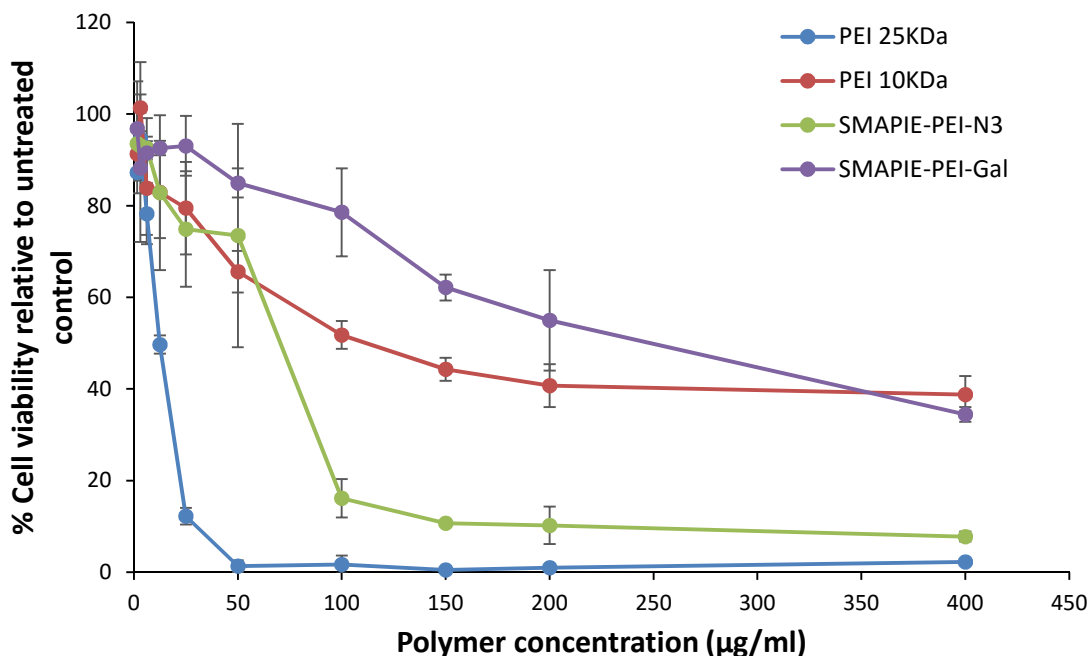


**Figure 3.12.** Plot showing cytotoxicity analysis of SMAPEI-PEI-N3, and SMAPEI-PEI-Gal copolymers in comparison with PEI 25 KDa and PEI 10 KDa as polymeric controls. Analysis was done on Hep G2 cells by MTT assay with concentration range (0 – 400  $\mu\text{g/mL}$ ) and incubation time of 48 hours.

### 3.9.2 Cellular Uptake Quantification by Flow Cytometry

SMAPEI-PEI-N3 or SMAPEI-PEI-Gal micelleplexes, and PEI 10 KDa polyplexes were prepared with fluorescent FAM-labeled siRNA at N/P ratio of 10 to evaluate and quantify their differential uptake into asialoglycoprotein receptor (ASGPR) positive Hep G2 cells. As shown in figure 3.13.A, after 5 hours incubation of the different samples with Hep G2 cells, the amount of siRNA-carrier complexes internalized into cells as reflected by the detected fluorescence intensity was in the following order : SMAPEI-PEI-Gal micelleplexes > SMAPEI-PEI-N3 micelleplexes

> PEI 10 KDa polyplexes > free FAM-labeled siRNA > untreated cells. Figure 3.13.B, demonstrates that the cellular uptake associated fluorescence intensity for SMAPIE-PEI-Gal micelleplexes in presence of 20 mM free galactosamine as competitor for ASGPRs was lower when compared to the intensity for SMAPIE-PEI-Gal micelleplexes samples lacking free galactosamine.

Statistical analysis of cellular uptake Median fluorescent intensity measurements for all the samples was summarized in figure 3.14. Data revealed no significant difference in fluorescence from free FAM-labeled siRNA cellular uptake compared to blank untreated cells. Cellular uptake of SMAPIE-PEI-N3 micelleplexes was also not significantly different from that of the positive control PEI 10 KDa polyplexes. However, targeted SMAPIE-PEI-Gal micelleplexes achieved significant increase in cellular uptake as compared to both non-targeted SMAPIE-PEI-N3 micelleplexes and PEI 10 KDa polyplexes ( $p < 0.01$ ) with 0.84 and 1.2 fold increase, respectively. The presence of free galactosamine competitor, significantly decreased the targeted SMAPIE-PEI-Gal micelleplexes cellular internalization by 0.32 fold.

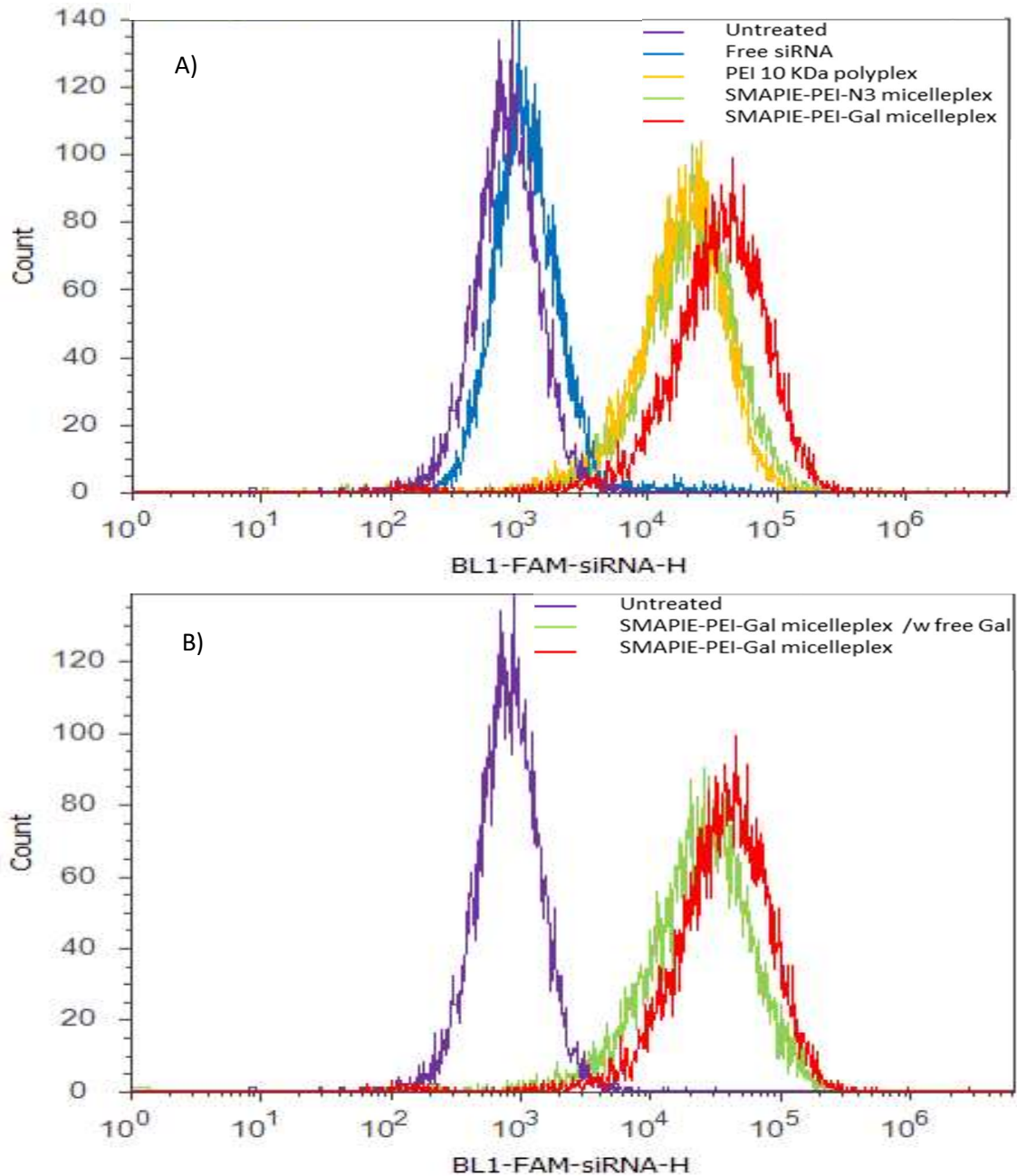


**Figure 3.13.** Histogram of flow cytometry analysis showing number of cells/channel on Y- axis versus the fluorescence intensity detected from FAM-labeled siRNA positive Hep G2 cells. A) Shows compared fluorescence intensity achieved at cellular uptake of SMAPIE-PEI-Gal or SMAPIE-PEI-N3 micelleplexes prepared with FAM-labeled siRNA, to that achieved in case of PEI 10 KDa polyplexes (positive control) and free FAM-labeled siRNA as well as untreated cells (negative controls). B) Shows different cellular uptake associated fluorescence intensity for SMAPIE-PEI-Gal micelleplexes in presence or absence of 20 mM free galactosamine as competitor.

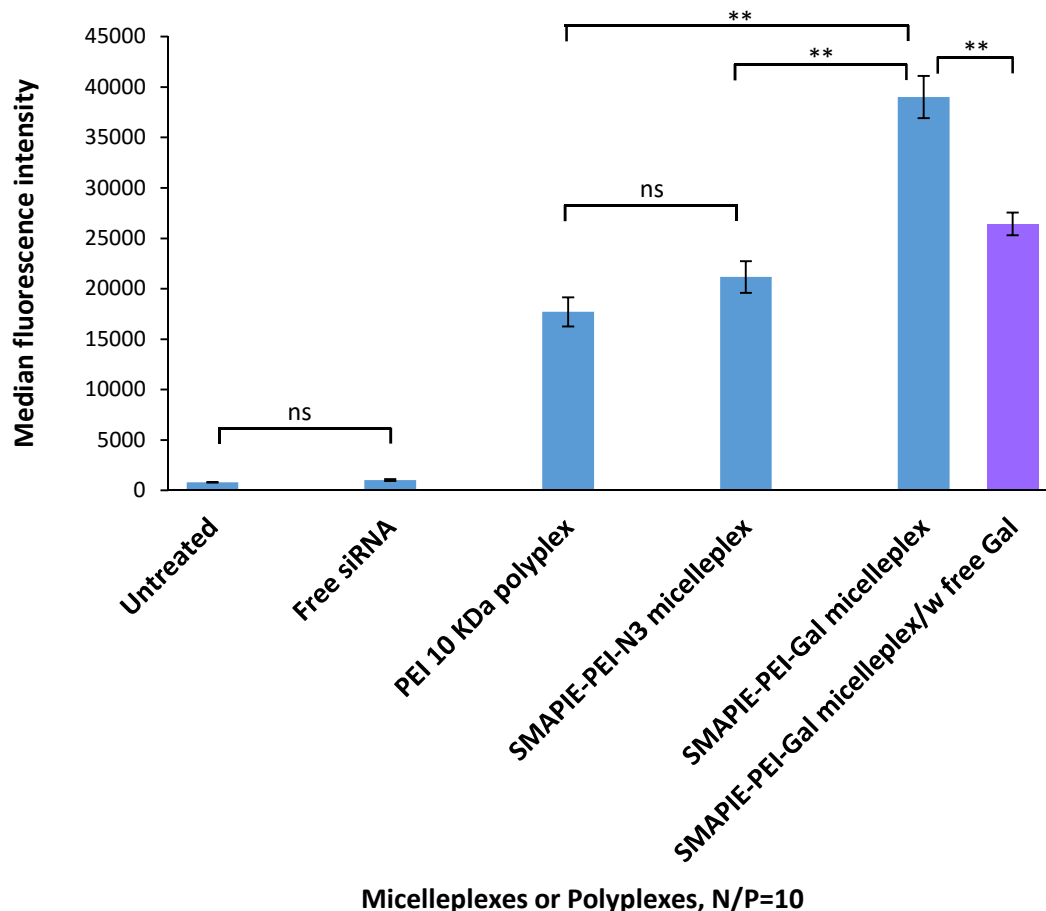


**Figure 3.14.** Plot of median fluorescent intensity of FAM- labeled siRNA positive Hep G2 cells for quantitative determination of cellular uptake of SMAPIE-PEI-N3, SMAPIE-PEI-Gal micelleplexes or polyplexes prepared with FAM-labeled siRNA at N/P ratio of 10. PEI 10 KDa polyplexes were used as positive control, while free FAM-labeled siRNA and untreated cells were as negative controls. As a competitive assay, SMAPIE-PEI-Gal micelleplexes uptake in the presence of 20 mM free galactosmine as a competitor of galactosamine in SMAPIE-PEI-Gal was detected. Results were obtained after 5 hours incubation of samples with cells, and are presented as (mean  $\pm$  standard deviation of  $n=3$ , \*\*  $p < 0.01$ , ns = none statistically significant).

### 3.9.3 Cellular Uptake and Endosomal Escape by Confocal Laser Scanning Microscopy (CLSM)

Confocal laser scanning microscopy was performed to see the ability of targeted SMAPIE-PEI-Gal and non-targeted SMAPIE-PEI-N3 micelleplexes to deliver siRNA into asialoglycoprotein receptor (ASGPR) positive Hep G2 cells as well as to determine route of their cellular uptake. PEI 10 KDa polyplexes were

used as positive control. Competition assay was conducted to study ASGPR targeting ability of SMAPIE-PEI-Gal micelleplexes in absence and presence of free galactosamine. All micelleplexes or polyplexes used for Hep G2 cells transfection were prepared with FAM-labeled siRNA at N/P ratio of 10. Live cell images were obtained 22 hours post transfection.

As shown in figure 3.15, the Hep G2 cells nuclei were stained with Hoechst 33342 stain (blue) in first row, acidic endosomal compartments with Lyso Tracker Deep Red dye (red) in second row, and FAM labeled siRNA (green) in third row. Results showed more green fluorescent siRNA within Hep G2 cell when treated with galactosamine targeted SMAPIE-PEI-Gal micelleplexes than with non-targeted SMAPIE-PEI-N3 micelleplexes or the positive control PEI 10 KDa polyplexes. In the competition assay, less green fluorescence per cell was seen in cells treated with SMAPIE-PEI-Gal micelleplexes in presence of free galactosamine compared to ones lacking free galactosamine. Although, most of the green fluorescence from the siRNA was found in the cells cytoplasm around the blue nucleus, however little amount was still co-localized with the acidic endosomes as demonstrated by yellow colored spots in merged images in fourth row. As illustrated in figure 3.16, mean of total corrected cellular fluorescence (TCCF) was calculated to quantify the green fluorescent siRNA internalized in cells with each treatment. TCCF was estimated for each cell, then the mean of all TCCFs for all cells / image was obtained. The results were found to be consistent with the ones obtained by flow cytometry quantification as mentioned above.



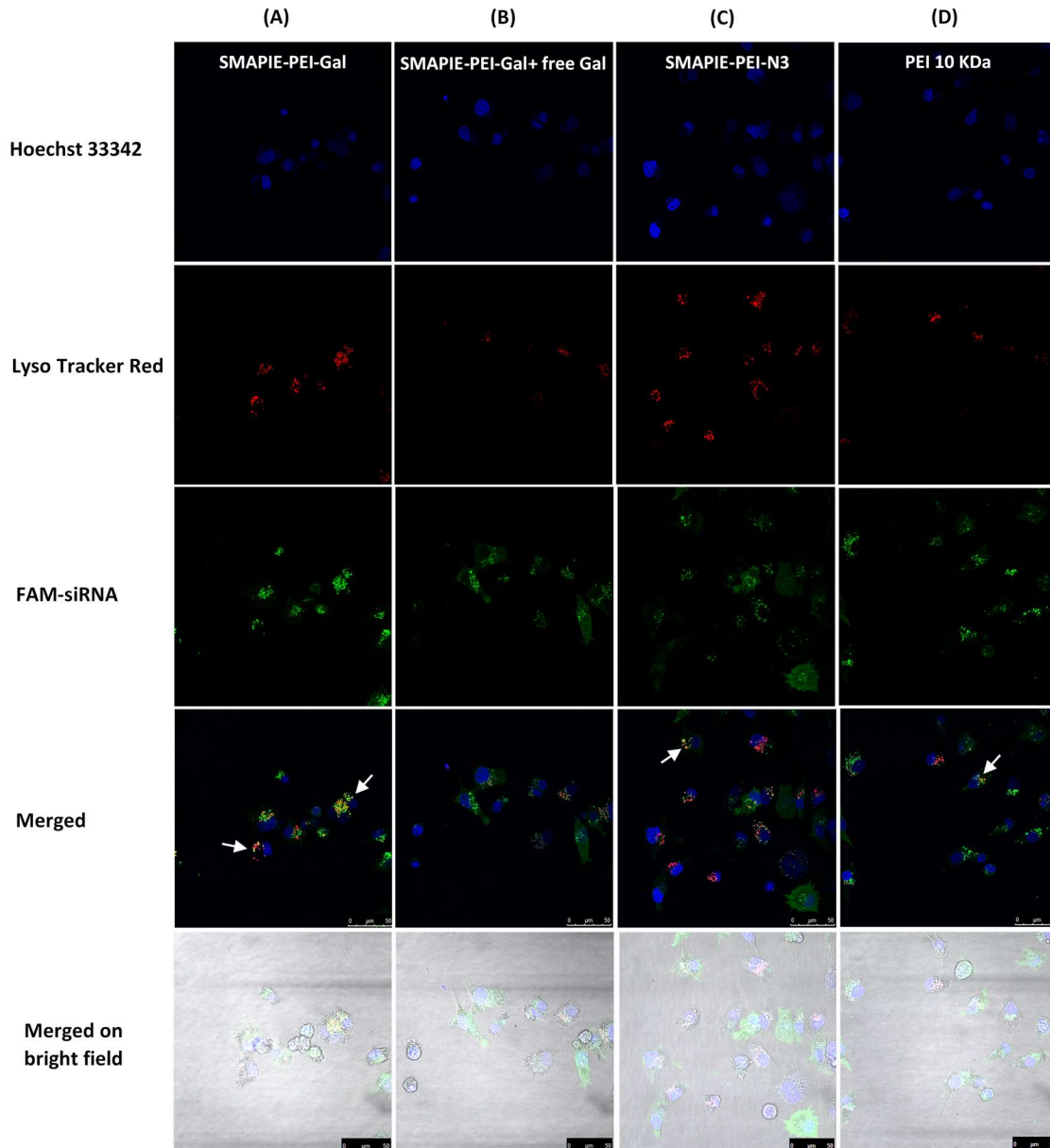


**Figure 3.15.** Confocal laser scanning microscopy images of Hep G2 cells treated with SMAPIE-PEI-Gal micelleplexes (column A), SMAPIE-PEI-Gal micelleplexes plus free galactosamine competitor (column B), SMAPIE-PEI-N3 micelleplexes (column C) and PEI 10 KDa polyplexes (column D), 22 hours after transfection. Micelleplexes or polyplexes were prepared with FAM-labeled siRNA at N/P ratio of 10. The cells nuclei were stained with Hoechst 33342 stain (blue), acidic endosomal compartments with Lyso Tracker Deep Red dye (red), and siRNA was labeled with FAM (green).

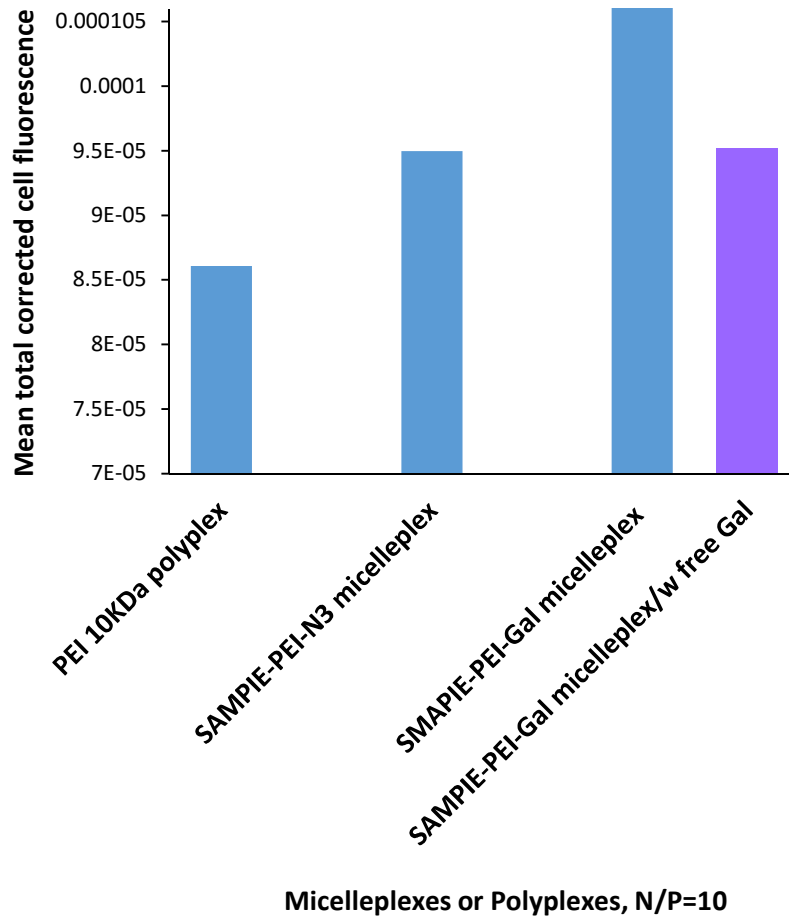


**Figure 3.16.** Plot illustrating CLSM images green fluorescence quantification. Mean total corrected cellular fluorescence (MTCCF) of internalized green fluorescent FAM -labeled siRNA complexed with micelleplexes or polyplexes in Hep G2 cells was calculated per image and plotted on Y axis against treatment type on X axis.

### 3.9.4 Transfection Efficiency and Nrf2 Gene Knockdown by Western Blot Analysis

SMAPIE-PEI-Gal micelleplexes or PEI 10 KDa polyplexes condensing 55 pmol Universal Negative Control siRNA (as negative control) or Nrf2 siRNA at N/P ratio of 10, were prepared and used for transfecting Hep G2 cells by reverse transfection technique. After 24 hours of transfection, Western blot protein expression analysis was performed to determine and quantify Nrf2 gene

knockdown mediated by SMAPIE-PEI-Gal micelleplexes compared to the positive transfection control PEI 10 KDa polyplexes.

As illustrated in figure 3.17, both Nrf2 complexing SMAPIE-PEI-Gal micelleplexes and PEI 10 KDa polyplexes mediated statistically significant Nrf2 gene knockdown ( $p < 0.05$ ). Nrf2 protein expression in cells treated with Nrf2 condensing SMAPIE-PEI-Gal micelleplexes was 0.49 fold lower than cells treated with negative control siRNA condensing SMAPIE-PEI-Gal micelleplexes. Similarly, Nrf2 protein expression in cells treated with Nrf2 condensing PEI 10 KDa polyplexes was 0.27 fold lower than cells treated with negative control siRNA condensing PEI 10 KDa polyplexes. However, the Nrf2 gene knockdown mediated by SMAPIE-PEI-Gal micelleplexes was 21% higher than that mediated by PEI 10 KDa polyplexes ( $p < 0.05$ ).

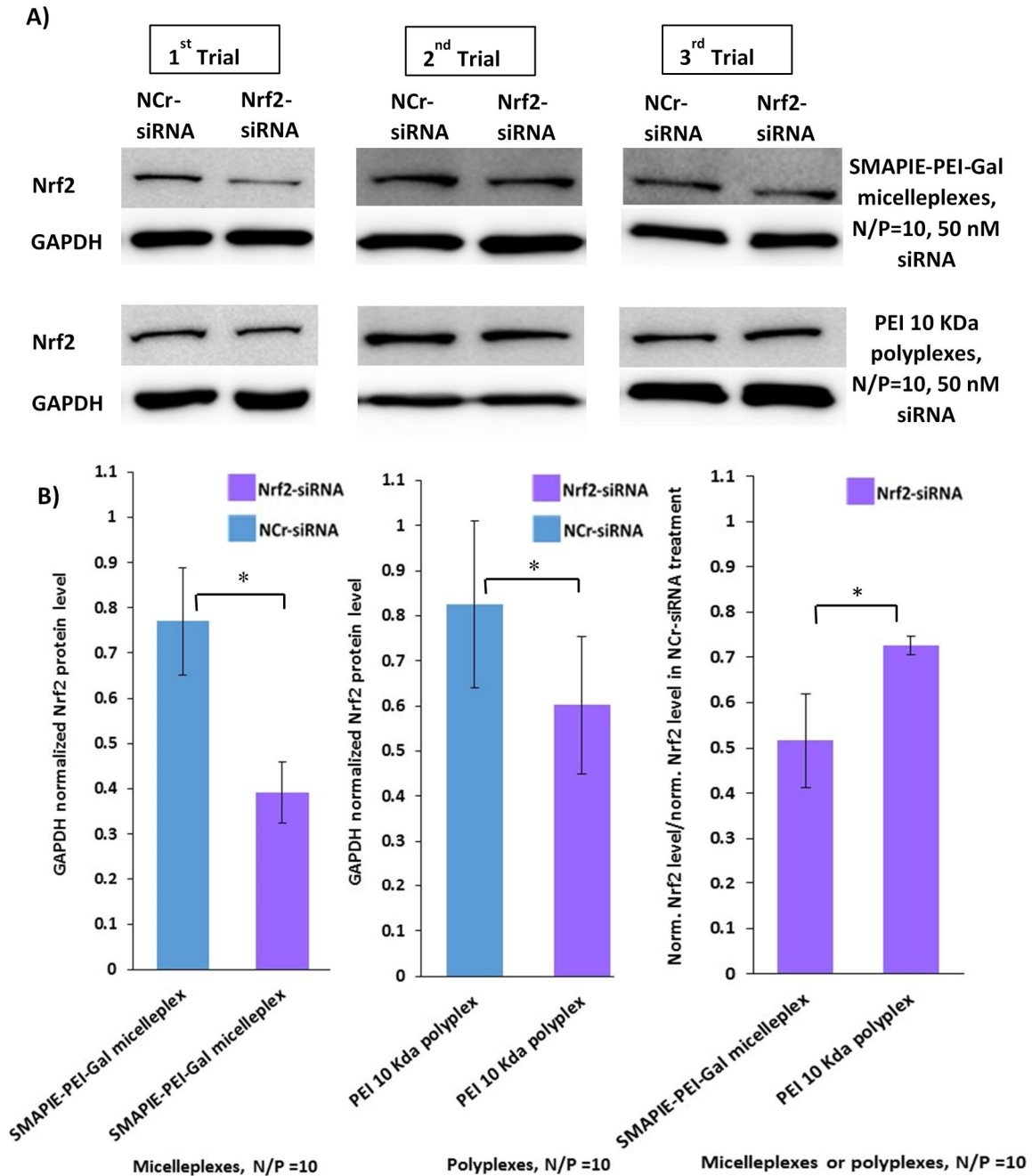


**Figure 3.17.** Western blot bands of Nrf2 and GAPDH protein levels detected in Hep G2 cells after 24 hours transfection with SMAPIE-PEI-Gal micelleplexes or PEI 10 KDa polyplexes condensing 50 nM Nrf2-siRNA or negative control siRNA (NCr-siRNA) at N/P ratio of 10 (A). Estimation of Nrf2 gene silencing efficiency accomplished by SMAPIE-PEI-Gal micelleplexes versus PEI 10 KDa polyplexes through quantification of the above western bands intensities, data presented as mean of (GAPDH normalized Nrf2 protein level/GAPDH normalized Nrf2 protein level in case of NCr-siRNA plexes treatment)  $\pm$  standard deviation,  $n=3$ , and \*  $p < 0.05$  statistical significance (B).

## CHAPTER 4 DISCUSSION

### 4.1 Synthesis and Characterization of SMAPIE-PEI-N3 and SMAPIE-PEI-Gal Micelles

#### 4.1.1 Synthesis of SMAPIE-PEI-N3 Micelles Forming Block Co-polymer

SMAPIE-PEI-N3 micelles forming block co-polymer was synthesized from SMAPIE 2.3 KDa copolymer and branched PEI 10 KDa polymer. PEI polymer of moderate molecular weight and optimal number of cationic groups was chosen for the synthesis since it has better nucleic acids condensation and transfection efficiency than the lower molecular weight ones and at the same time it induces lesser cytotoxicity compared to higher molecular weight PEI chains<sup>139</sup>. SMAPIE copolymer has hydrophobic styrene groups and iso-octyl chains that can help in self-assembly and formation of the micelles by hydrophobic interactions.

SMAPIE-PEI-N3 micelles forming block co-polymer was synthesized in two steps by one-pot reaction. The one-pot reaction module afforded several advantages including faster and easier product synthesis, lesser purification steps (no necessary purification of the intermediate and only purification was done for the final product), and hence enabled better product yield. In the first step, SMAPIE and PEI were reacted in equimolar ratio to give a water soluble diblock-copolymer. It was noted that increasing the molar ratio of SMAPIE compromised the water solubility of the so-formed diblock-copolymer. In the second step, partial conversion of primary amine groups in PEI to azide groups was achieved in order to create azide moieties for targeting ligands attachment through strain promoted alkyne azide cycloaddition (SPAAC) “click” reaction (figure 4.1), while at the same time preserving good share of the cationic amine groups for siRNA or gene

condensation and delivery. It is important to note that we succeeded to complete the diazo-transfer reaction without copper metal catalysis compared to what was previously published<sup>126</sup>. In addition, targeting ligand attachment to the block copolymer was completed using copper free “click” synthesis in order to avoid copper metal difficult purification and biological toxicity associated with trace metal impurities in the final product.

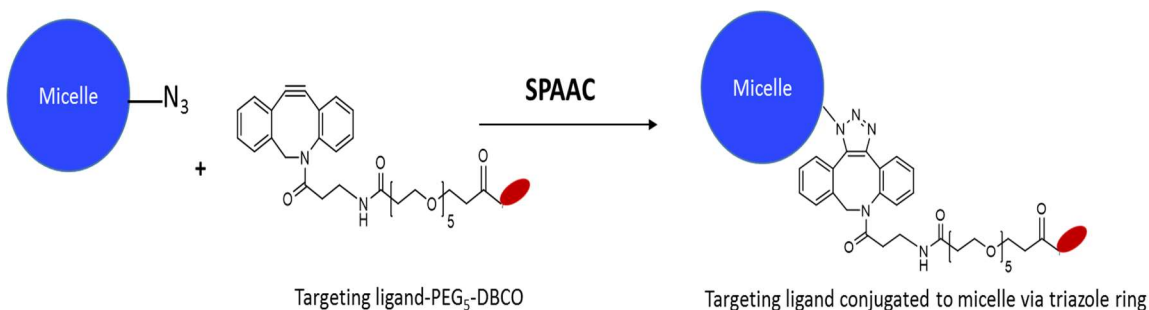
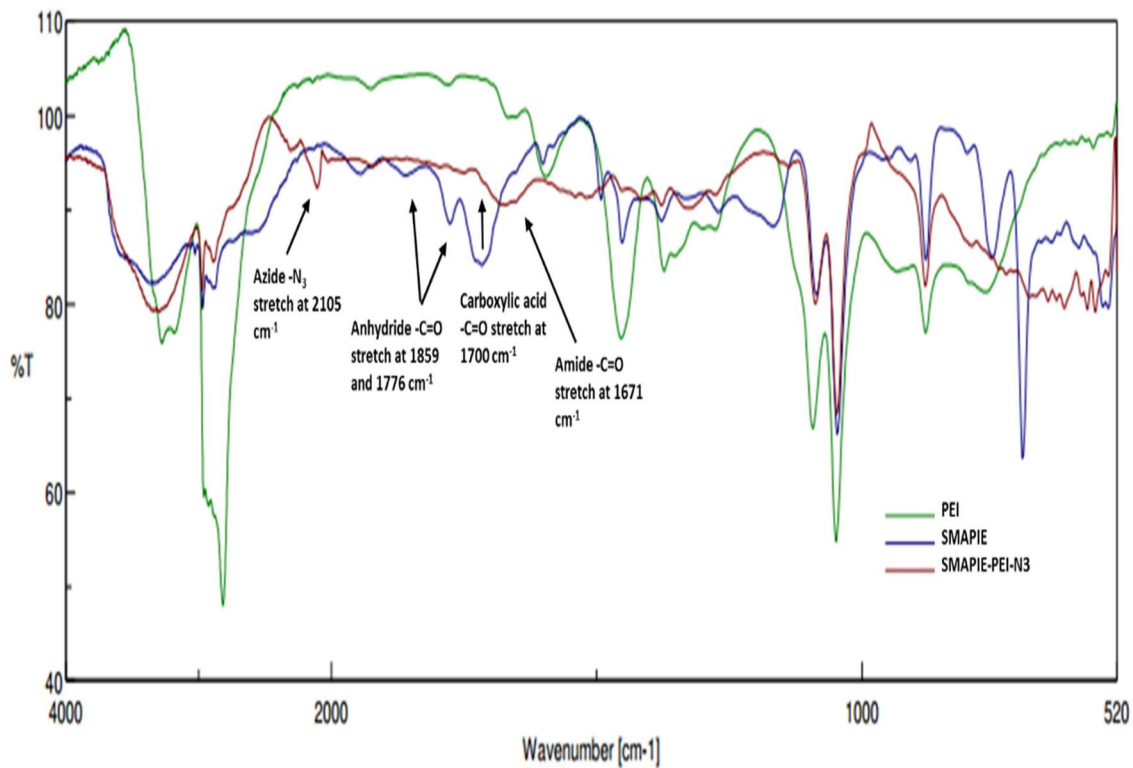


**Figure 4.1.** Illustration of targeting ligand attachment to SMAPIE-PEI-N3 micelles via strain promoted alkyne azide cycloaddition (SPAAC) “click” reaction.

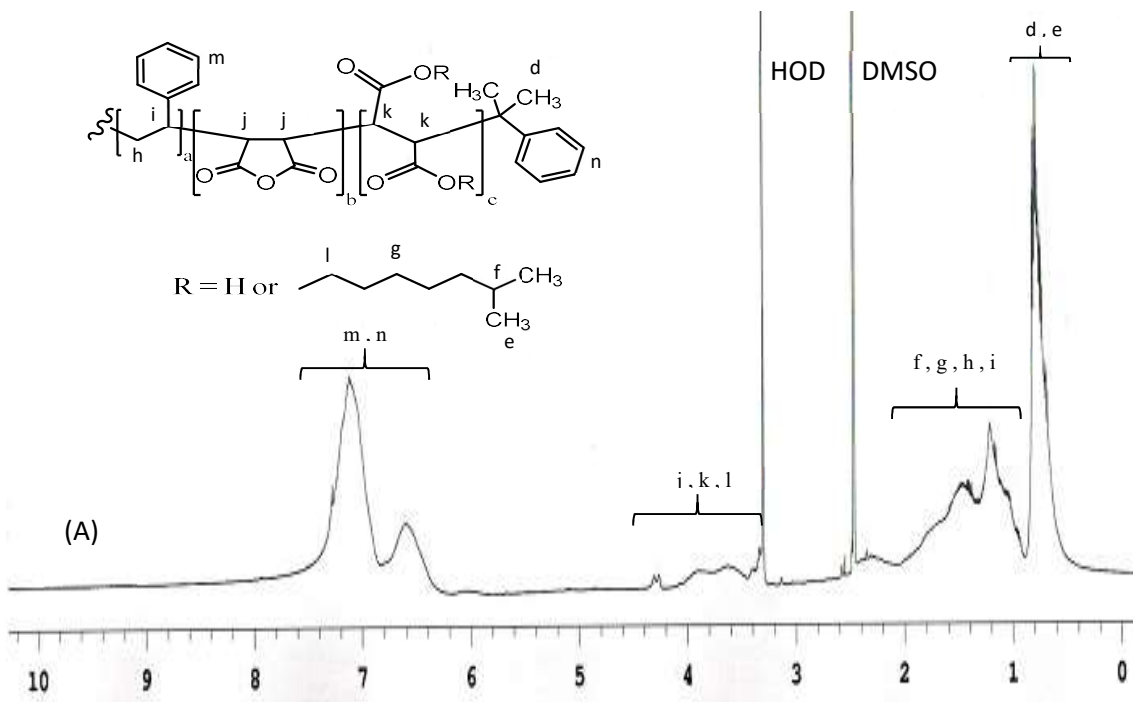
The successful synthesis of SMAPIE-PEI-N3 product was confirmed by FT/IR and <sup>1</sup>H NMR spectroscopy. FT/IR spectra (figure 4.2) showed the absence of the anhydride –C=O characteristic antisymmetric and symmetric stretch peaks in SMAPIE-PEI-N3 at 1859 cm<sup>-1</sup> and 1776 cm<sup>-1</sup> respectively with the appearance of the secondary amide–C=O stretch at 1671 cm<sup>-1</sup> indicating anhydride ring opening in SMAPIE and formation of the amide bond linker between the two polymeric chains. In addition, the azide –N<sub>3</sub> stretch at 2105 cm<sup>-1</sup> confirmed the diazo-transfer reaction.

<sup>1</sup>H NMR spectra (figure 4.3) further supported the SMAPIE-PEI-N3 copolymer synthesis. <sup>1</sup>H NMR spectra of unreacted SMAPIE and PEI chains were presented in figure 4.3.A and figure 4.3.B, respectively. <sup>1</sup>H NMR spectrum of

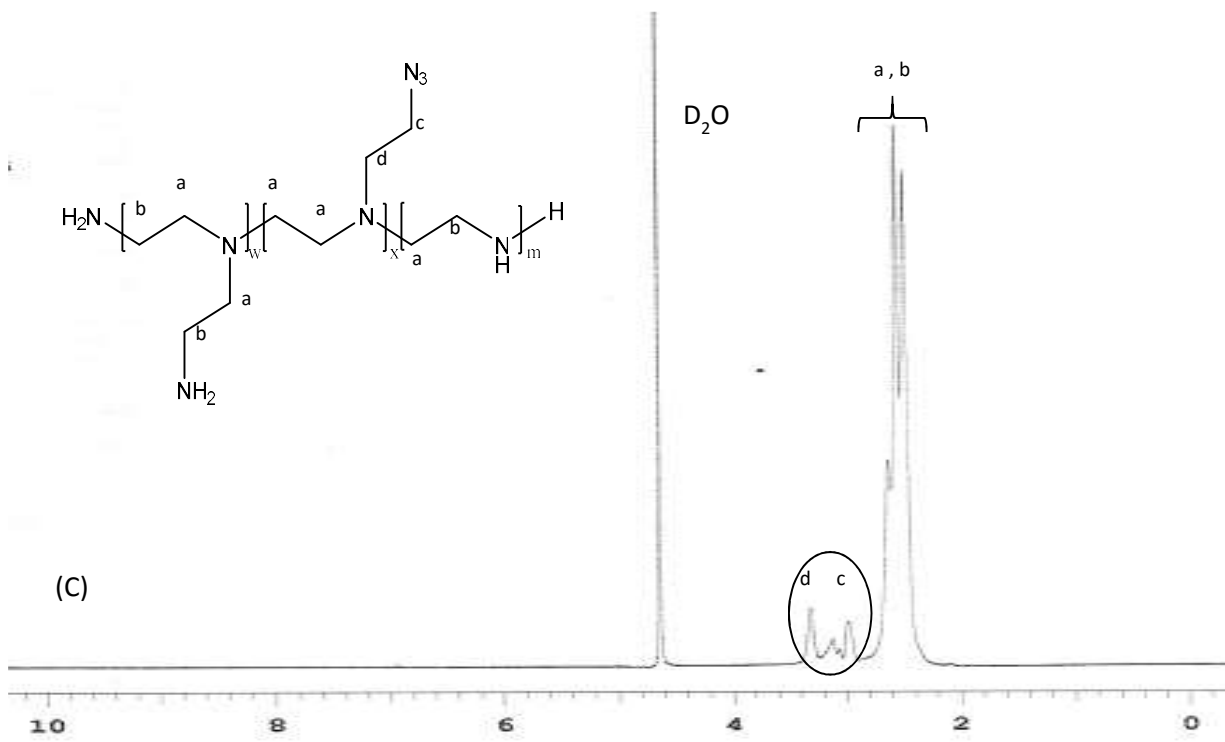
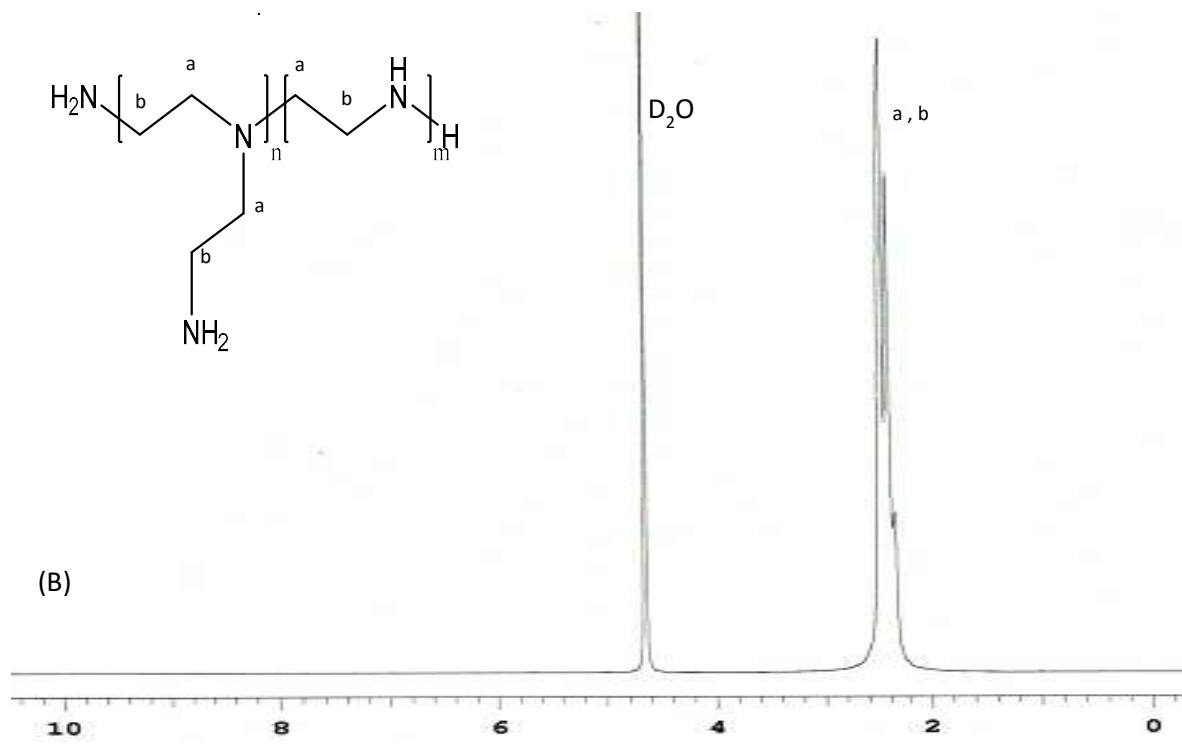
separately synthesized PEI-N3 (figure 4.3.C) illustrated the occurrence of partial azido modification of PEI chain without any other side reactions. PEI protons on carbons adjacent to unmodified amine groups (-CH<sub>2</sub>CH<sub>2</sub>NH-) were at chemical shift 2.2-3 ppm, while the protons on carbons adjacent to azide groups (-NHCH<sub>2</sub>CH<sub>2</sub>N<sub>3</sub>) and (-NHCH<sub>2</sub>CH<sub>2</sub>N<sub>3</sub>) were at chemical shift of 3 ppm and 3.3 ppm, respectively. As shown in figure 4.3.D, <sup>1</sup>H NMR spectrum of isolated SMAPIE-PEI product of the one pot reaction first step indicated grafting of SMAPIE on PEI chain. PEI (-CH<sub>2</sub>CH<sub>2</sub>NH-) characteristic peak at chemical shift 2.2-3 ppm, overlapping peaks of (-COCH- and -OCH<sub>2</sub>- in SMAPIE copolymer, and -CH<sub>2</sub>NHCO- in PEI chain) at 3.1-3.5 ppm, and the SMAPIE (C<sub>6</sub>H<sub>5</sub>-) peak in cumene terminal and styrene residues at 6.4-7.4 ppm were obviously detected. <sup>1</sup>H NMR spectrum of SMAPIE-PEI-N3 (figure 4.3.E) showed the PEI (-CH<sub>2</sub>CH<sub>2</sub>NH-) characteristic peak at chemical shift 2.2-3 ppm, overlapping peaks of (-COCH- and -OCH<sub>2</sub>- in SMAPIE copolymer, -CH<sub>2</sub>NHCO- and -NHCH<sub>2</sub>CH<sub>2</sub>N<sub>3</sub> in PEI chain) at 3.1-3.6 ppm, and the SMAPIE (C<sub>6</sub>H<sub>5</sub>-) peak in cumene terminal and styrene residues at 6.4-7.4 ppm.



**Figure 4.2.** FT/IR spectra of PEI polymer (green), SMAPIE copolymer (blue), and SMAPIE-PEI-N3 micelles forming block copolymer (red).







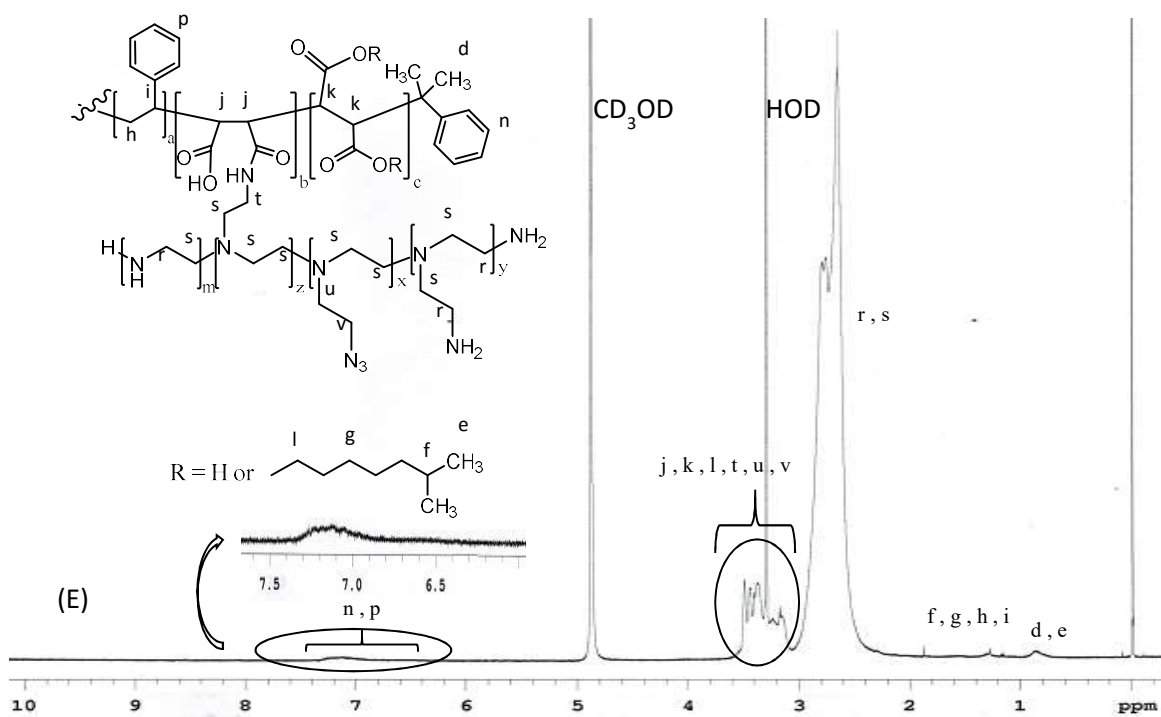
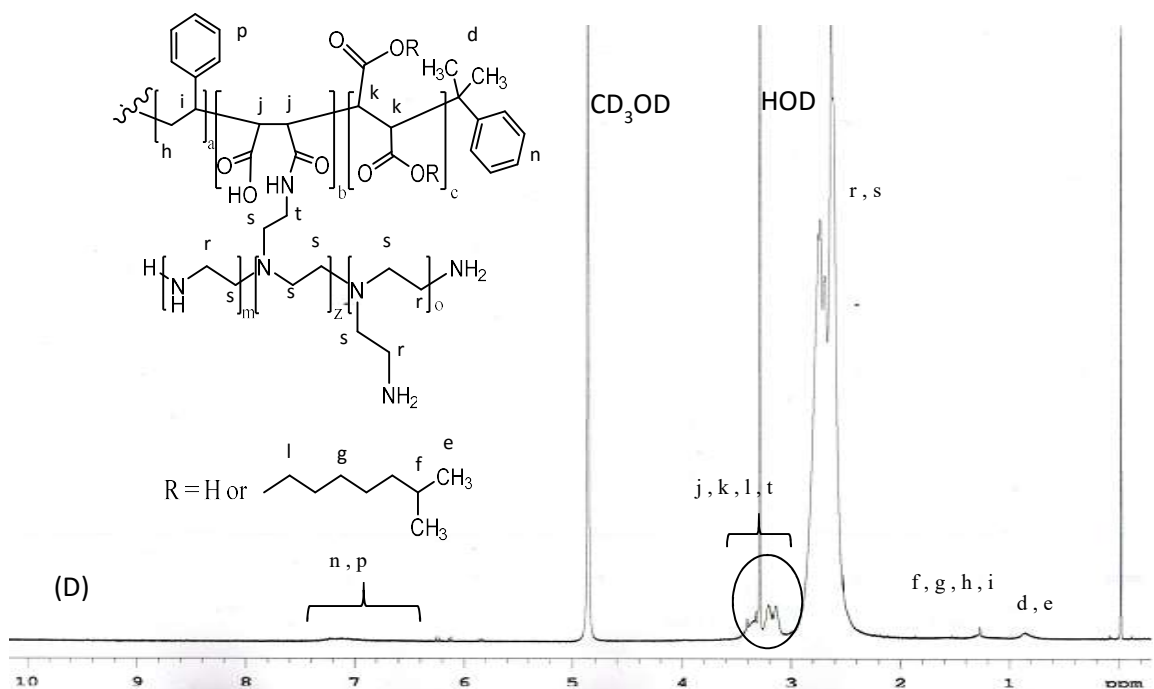


**Figure 4.3.**  $^1\text{H}$  NMR spectra of (A) SMAPIE in DMSO (B) PEI in  $\text{D}_2\text{O}$  (C) PEI-N3 in  $\text{D}_2\text{O}$  (D) SMAPIE-PEI in  $\text{CD}_3\text{OD}$  (E) SMAPIE-PEI-N3 in  $\text{CD}_3\text{OD}$ .

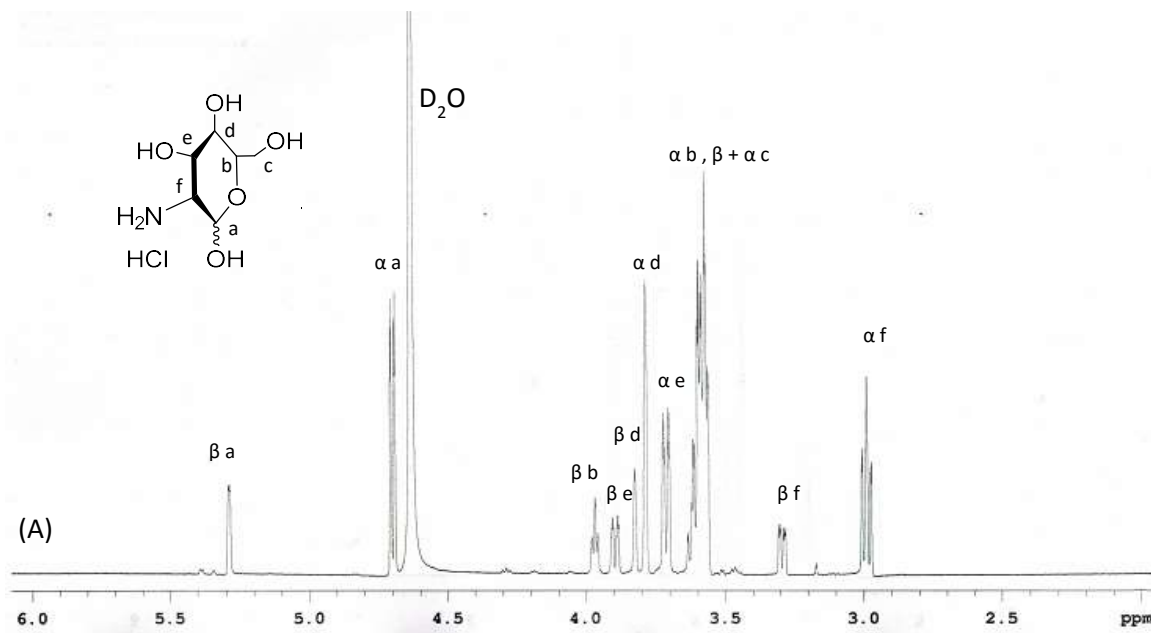
#### 4.1.2 Synthesis of Targeting Ligand Conjugated SMAPIE-PEI-Gal Micelles Forming Block Copolymer

SMAPIE-PEI-Gal (galactosamine targeted micelles forming block copolymer) was synthesized using copper free “click” chemistry in essence to obtain biocompatible micelles that can target ASGPR in hepatocellular carcinoma. During the first step, galactosamine as a targeting ligand was linked via amide bond to DBCO-PEG<sub>5</sub> moiety by amine reactive NHS coupling chemistry. The presence of PEG moiety in DBCO-PEG<sub>5</sub>-NHS ester helped to improve its water solubility and hence its reactivity. Galactosamine was added in three fold excess compared to DBCO-PEG<sub>5</sub>-NHS ester to ensure complete ester modification by the end of the reaction. Galactosamino-PEG<sub>5</sub>-DBCO (targeting) blocks was then attached to SMAPIE-PEI-N<sub>3</sub> micelles using copper free “click” chemistry.

“Click” chemistry as a synthetic tool has been extensively studied in the previous years and has several advantages including high selectivity, high reaction yield, high efficiency, fast reaction rate, mild reaction conditions and water compatibility<sup>108</sup>. “Click” chemistry, either copper catalyzed or copper free, has been used in many applications including polymer synthesis<sup>140,141</sup>, and conjugation of imaging agents or targeting ligands on nanosystems<sup>142,143</sup>. Copper free cycloaddition approach has also been used in liposomes functionalization<sup>144</sup>, DNA conjugation to nanoparticles<sup>145</sup>, and biorthogonal biomolecules labeling in living cells both in vitro and in vivo<sup>146</sup>. One major advantage of the copper free approach over the copper catalyzed one is the biocompatibility and absence of toxicity for living cells since cyclooctyne ring strain is the primary reaction promotor instead of the cytotoxic copper metal catalyst. Such reactions can thus be carried out without

the need for purification or removal of copper and highly useful for biological applications.

Successful synthesis of biocompatible SMAPIE-PEI-Gal was verified using  $^1\text{H}$  NMR spectra as shown in figure 4.4. The unreacted galactosamine protons characteristic peaks are illustrated in figure 4.4.A.  $^1\text{H}$  NMR spectrum of SMAPIE-PEI-Gal co-polymer is presented in figure 4.4.B. In addition to the characteristic peaks in SMAPIE-PEI-N3 mentioned above (figure 4.3.E), galactosamino-PEG<sub>5</sub>-DBCO attachment was confirmed by the presence of the following peaks: (-CHNH<sub>2</sub>) protons in galactosamine alpha and beta anomers and (-OCH<sub>2</sub>CH<sub>2</sub>O-) in PEG chain at 3-3.49 ppm, (-CHCHOH, -CH<sub>2</sub>OH, -CHCH<sub>2</sub>-) protons in galactosamine alpha and beta anomers at 3.5-4 ppm, (-OCHOH alpha and beta anomeric protons) in galactosamine at 4.5, 5 ppm, overlapping peaks of (-C<sub>6</sub>H<sub>4</sub> in substituted DBCO and -C<sub>6</sub>H<sub>5</sub> in cumene terminal and styrene residues) at 6.4-7.6 ppm.



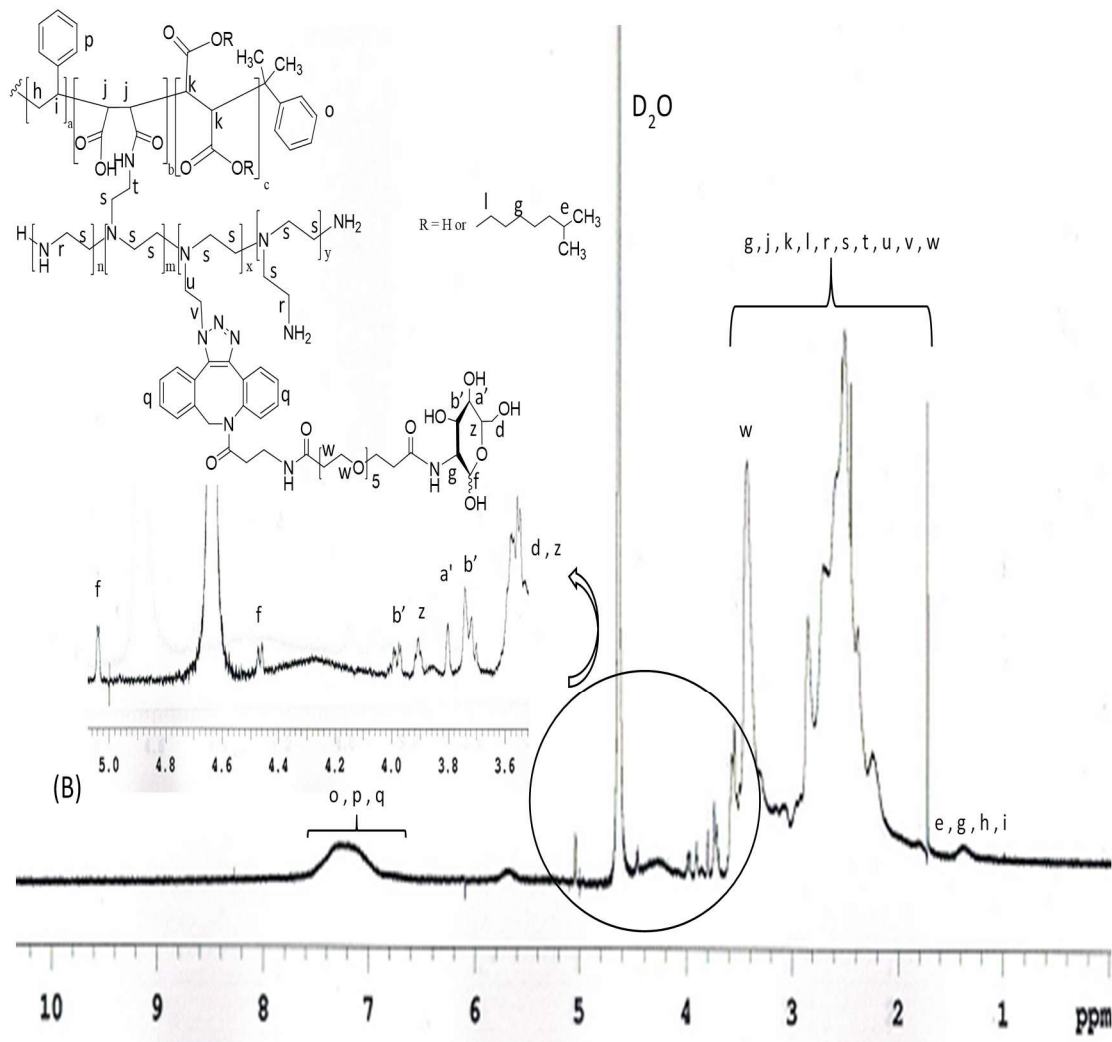


**Figure 4.4.**  $^1\text{H}$  NMR spectra of (A) Galactosamine in  $\text{D}_2\text{O}$  (B) SMAPIE-PEI-Gal in  $\text{D}_2\text{O}$ .

## 4.2 Size Exclusion Chromatography (SEC)

Size exclusion chromatography was run to detect the molecular weight of the SMAPIE-PEI-N3 micelles relative to molecular weights of standards. Gel filtration chromatography was chosen as the experimental method since SMAPIE-PEI-N3 micelles are water soluble.

The chromatogram of SMAPIE-PEI-N3 micelles (figure 3.1) revealed unimodal molecular weight distribution, indicating that the micelles were of uniform

size with low polydispersity index. The relative molecular weight of micelles obtained by substitution in the standard curve equation (figure 3.2) was 13474.58 Da. Although the molecular weight obtained is relative and not an absolute one, it nonetheless gave a good estimation of the micelle composition. From the molecular weight estimation, it can be concluded that only one chain of the 2.3 KDa SMAPIE copolymer got grafted to one chain of the 10 KDa PEI polymer in addition to the molecular weight increase as a result of partial amine groups modification to azide groups. This conclusion was in agreement with what was expected based on the polymers composition and the equimolar ratio at which the synthesis was performed. According to copolymer composition information provided by the manufacturer, SMAPIE copolymer has a molar ratio of 4:1 of styrene to anhydride units, and 75% of the anhydride rings are esterified. Molar ratio calculations indicated that each SMAPIE copolymer chain contained approximately 3 opened and 1 unopened anhydride rings. Thus, presence of only 1 unopened anhydride ring in each SMAPIE copolymer chain prevents the grafting of more than one PEI polymer chain on the same SMAPIE copolymer chain, which helped to reduce polydispersity and chances of crosslinking.

### **4.3 Copper Assay**

PEI is a cationic polymer that has been well studied for condensing negatively charged siRNAs. The role of PEI in both non-targeted SMAPIE-PEI-N3 and ASGP receptor targeted SMAPIE-PEI-Gal micelles is mainly for gene/siRNA complexation. The exact content of PEI is essential for correct calculation of

micelles amount necessary for micelleplexes formation at the desired amine groups in polymer/phosphate groups in nucleic acids (N/P) ratio.

The PEI concentration in micelles forming block co-polymer was quantified through spectrophotometry by copper chelate formation. According to previous reports, copper ions form specific blue cuprammonium complex with primary amine groups in PEI polymer<sup>137</sup>. The intensity of so-formed blue color is a reflection of the PEI concentration as long as the conditions for Beer-Lambert laws were followed. PEI chains in both SMAPIE-PEI-N3 and SMAPIE-PEI-Gal co-polymers are the only regions containing primary amine groups, and hence accurate quantification of PEI composition in both micelles can be done using copper chelation, without any interference.

As shown in figure 3.3, PEI content in SMAPIE-PEI-Gal micelles was lower than in SMAPIE-PEI-N3 micelles because of the extra galactosamino-PEG<sub>5</sub>-DBCO moieties in SMAPIE-PEI-Gal co-polymer. In line with the size exclusion chromatography, copper assay results also confirmed that only one chain of SMAPIE copolymer was grafted to one chain of PEI in SMAPIE-PEI-N3 and SMAPIE-PEI-Gal co-polymers.

#### **4.4 Determination of Critical Micelle Concentration (CMC)**

The estimation of critical micelle concentration using pyrene as a fluorescent hydrophobic probe, is a way to confirm the ability of amphiphilic copolymers to form micelles. Amphiphilic copolymers are usually block copolymers composed of hydrophilic and hydrophobic moieties that self-assemble in aqueous environment into micellar spherical core-shell structure, at concentration

exceeding the critical micelle concentration<sup>80</sup>. When CMC is reached in aqueous environment, the hydrophobic moieties of the amphiphilic copolymer start to associate with each other and away from water to reach more favorable entropy forming the micellar core while the hydrophilic moieties form the micellar shell<sup>82</sup>.

According to the SMAPIE copolymer composition information and based on molar ratio calculations, each SMAPIE chain contained around 17 styrene groups, 3 opened and 1 unopened anhydride rings. The big number of the styrene hydrophobic rings (17) together with the iso-octyl aliphatic chains esterified with the open anhydride rings participated in creation of the hydrophobic core of the SMAPIE-PEI-N3 micelles, while hydrophilic PEI polymeric chain formed the shell.

Pyrene is a fluorescent hydrophobic probe whose excitation wavelength vary depending on the hydrophobicity of the surrounding environment, where it is lower in a hydrophilic environment than in a hydrophobic one<sup>147</sup>. Bathochromic shift in pyrene excitation wave length from 334 nm to 339 nm with increasing SMAPIE-PEI-N3 copolymer concentration indicated pyrene presence in the hydrophobic core of the formed micelles when CMC was exceeded (figure 3.4).It was reported that micelles of CMC in order of  $10^{-6}$ - $10^{-7}$  M increase the blood circulation time of their cargo as they have good stability in vivo<sup>84</sup>. SMAPIE-PEI-N3 micelles was formed at low concentration and CMC was in the  $10^{-7}$  M range which indicates that SMAPIE-PEI-N3 micelles are good candidates for in vivo drug/gene delivery and can have good stability profile for in vivo applications.



#### 4.5 SYBER Gold Assay

Optimal nucleic acids complexation ability is a prerequisite for non-viral gene/siRNA vectors to achieve required gene/siRNA protection and effective cellular transfection<sup>148</sup>. Polymeric vectors based nucleic acids complexation can be evaluated using SYBER Gold assay.

SYBER Gold is a fluorescent dye that binds to both free and uncondensed siRNA and emits fluorescence, the more the siRNA gets condensed and sequestered in the micelleplexes or polyplexes the less the free siRNA available to bind to the dye and the more its fluorescence quenching<sup>149,150</sup>.

As shown in figure 3.6, the siRNA complexation capacity of all micelleplexes and polyplexes increased with increasing the N/P ratio. The reason is that, nucleic acids complexation with micelles or polymers occur through electrostatic interaction between negatively charged phosphate groups in nucleic acids and cationic groups in PEI polymeric units. As the N/P ratio increases, total cationic charge increases which allow better ionic interaction and more efficient siRNA condensation<sup>131</sup>. Non-targeted SMAPIE-PEI-N3 micelles showed lesser siRNA complexation efficiency compared to PEI polymers. It may be attributed to the presence of the negatively charged carboxylate groups in SMAPIE copolymer. According to previous study, carboxylate anions can diminish the electrostatic binding of nucleic acids to polycations<sup>138</sup>. Strikingly, galactosamino-PEG<sub>5</sub> moieties didn't hinder or weaken the siRNA access and ionic interaction with PEI segments in SMAPIE-PEI-Gal micelles, but instead, the targeted micelles showed comparable siRNA condensation capacity to PEI polymers. It was previously

reported that carbohydrates can form hydrogen bonding with nucleic acids and increase their complexation efficiency in polyplexes<sup>148</sup>. One possible explanation, in line with previous report, is that galactosamine carbohydrate residues might have an important role in improved SMAPIE-PEI-Gal micelles condensation ability by formation of hydrogen bonding with siRNAs.

#### **4.6 Size and Zeta Potential Measurements: Light Scattering (LS)**

The amphiphilic nature of SMAPIE-PEI-N3 and SMAPIE-PEI-Gal copolymers enabled them to self-assemble to form nanomicelles spontaneously in aqueous solution. The micelles can condense siRNA forming micelleplexes. Both particle size and surface charge (or zeta potential) are important aspects that affect particles cytotoxicity, localization, cellular uptake and transfection efficiency<sup>151,152</sup>. Small particles achieve better cellular uptake, and moderate positive zeta potential decreases particles aggregation and increases their colloidal stability without being highly cytotoxic<sup>149,153</sup>.

Hydrodynamic sizes of plain micelles (without loaded siRNA) and siRNA containing micelles (micelleplexes), and polyplexes were measured using dynamic light scattering (DLS) technique, while their zeta potentials were determined by electrophoretic light scattering (ELS). As shown in figure 3.7.A, hydrodynamic diameter of SMAPIE-PEI-Gal micelles was found to be larger than that of SMAPIE-PEI-N3 micelles, due to the presence of additional galactosamino-PEG<sub>5</sub> moieties. Figure 3.7.B illustrated that, both SMAPIE-PEI-Gal and SMAPIE-PEI-N3 micelles had high zeta potential of around 40 mV because of the cationic amino groups present in the PEI chain. However, siRNA complexation with both micelles

neutralized large portion of their cationic charge and hence decreased their cytotoxicity. In figure 3.8, micelleplexes and polyplexes formed at lower N/P ratios exhibited larger particle sizes as compared to the ones formed at higher N/P ratios, till complete siRNA condensation is realized<sup>154</sup>, where a size of 200 nm is noted. As presented in figure 3.9, all micelleplexes and polyplexes showed similar trend of increasing zeta potential as N/P ratio increases, which is in line with previously published reports<sup>132,143</sup>. Larger particle sizes as well as negative zeta potential indicated inefficient and loose siRNA condensation<sup>149</sup>. N/P ratio of 7 for SMAPIE-PEI-N3 and 4 for SMAPIE-PEI-Gal micelleplexes, seemed to be the most optimal N/P ratios, where the particles had the smaller size together with lesser positive surface charge. Micelleplexes and polyplexes prepared at N/P ratio of 10 were thus chosen for further experiments to allow data comparison.

As demonstrated in tables 3.1 and 3.2, micelles and micelleplexes with efficient siRNA sequestering were of moderate size distribution with  $PDI \leq 0.42$ . However, higher PDI was obtained at improper siRNA complexation due to the formation of loose aggregates with larger size.

#### **4.7 Size and Morphology Measurements: Transmission Electron Microscopy (TEM)**

Size and morphology of plain micelles and micelleplexes were determined in the dry state by transmission electron microscopy (TEM). Micelles and micelleplexes presented spherical Core/Shell structure (figure 3.10) similar to previously published results<sup>94,155</sup>. The core/shell structure presented further confirmed the ability of the amphiphilic SMAPIE-PEI co-polymer to self-assemble into micelles in aqueous environment, where the hydrophobic styrene rings and

iso-octyl chains of SMAPIE arranged to form the white/unstained core<sup>93</sup> and the hydrophilic amine groups of PEI occupied the outer shell with the dark stain. In line with earlier publication, the styrene residues aromatic interaction contributed to the formation of uniform and tightly packed dense micellar core that was more resistant to water infiltration<sup>93</sup>.

SMAPIE-PEI-Gal micelles showed larger size (~200 nm) than SMAPIE-PEI-N3 micelles (~100 nm) due to the excess molecular weight of galactosamino-PEG<sub>5</sub> moieties in SMAPIE-PEI-Gal micelles. In contrast, the SMAPIE-PEI-Gal micelleplexes exhibited smaller size than SMAPIE-PEI-N3 micelleplexes, probably due to more efficient packaging/condensation of siRNA in SMAPIE-PEI-Gal micelleplexes than in SMAPIE-PEI-N3 micelleplexes.

In the case of SMAPIE-PEI-N3 and SMAPIE-PEI-Gal micelles and micelleplexes, TEM sizes were of similar pattern with the ones obtained from DLS measurements, however they were noted to be smaller in general. This was explained by the state of micelles in which the size measurements were performed. The results are in good agreement as the hydrodynamic sizes measured by DLS are known to be larger than the dry state sizes measured by TEM.

#### **4.8 Buffer Capacity Measurements**

Drugs and nucleic acids have to evade lysosomal degradation in order to go to their sites of action in the cell. In the case of siRNAs, the gene silencing occurs in the cytoplasm and thus the siRNA has to be released in the cytoplasm for necessary action. Buffering capacity is an important measure for polycationic vectors that allows endosomal escape of the cargo. The buffering capacity is

evaluated by the amount of protons necessary for reducing the pH in the endosomal pH range of 7-5.5<sup>138</sup>.

PEI based cationic polymeric vectors have been shown to have optimal buffering capacity as a result of having many protonatable amine groups in their backbone<sup>156</sup>. According to the proton sponge hypothesis, amine groups in PEI get protonated and increase osmotic pressure in endosomes leading to their membrane rupture and release of drug/nucleic acids in cytoplasm<sup>157</sup>.

Acid base titrations are perfect evaluators of the buffering capacity. Good buffering capacity is indicated by slow, rather than steep change in pH, upon addition of the same amount of HCl to polymeric solutions during titration<sup>158</sup>.

As shown in figure 3.11, a sharp drop in pH was seen during acid titration of 150 mM NaCl solution (the negative control), which had no buffering capacity. On the other hand, all the positive control PEI polymers, as well as SMAPIE-PEI-N3 and SMAPIE-PEI-Gal micelles exhibited small pH changes with acid addition indicating their good buffering capacity. Two inflection points of slow pH changes were seen in titration curves of the polymers and the micelles as a result of having different types of protonatable amine residues (primary, secondary, and tertiary). This was in agreement with previous reports<sup>159,160</sup>. SMAPIE-PEI-N3 micelles showed lower buffer capacity compared to PEI because of the partial azide modification in SMAPIE-PEI-N3 polyethylenimine segment, which decreased the number of available protonatable amine groups. Another reason is that the carboxylic acid groups in SMAPIE could protonate some PEI primary amines into ammonium groups through zwitter-ion formation. According to a previous study,

ammonium groups can suppress protonation of surrounding amine groups<sup>161</sup>. On the other hand, SMAPIE-PEI-Gal micelles were very similar to PEI polymers and better than SMAPIE-PEI-N3 micelles in their buffering capacity. Triazole rings conjugating galactosamino PEG<sub>5</sub> moieties in SMAPIE-PEI-Gal micelles had amine groups which participate in increasing the micelles buffering ability by being protonatable at 7-5.5 pH range.

#### **4.9 Biological evaluation of SMAPIE-PEI-N3 and SMAPEI-PEI-Gal micelles**

##### **4.9.1 Cytotoxicity Assay Using Human Liver Cancer Cells**

Cytotoxicity is one of the most important aspects in the evaluation of non-viral gene/siRNA vectors composed of cationic polymers for safe gene therapy. Cytotoxicity of non-targeted SMAPIE-PEI-N3, and targeted SMAPIE-PEI-Gal micelles forming block co-polymers were investigated in Hep G2 cells. PEI polymers were studied as controls for comparison.

As shown in figure 3.12, SMAPIE-PEI-Gal < PEI 10 KDa < SMAPIE-PEI-N3 < PEI 25 KDa in order of their cytotoxicity and IC<sub>50</sub>. PEI 25KDa was more cytotoxic than PEI 10 KDa due to its higher cationic charge density, which interacts with the cell membrane and causes cell necrosis<sup>139</sup>. In line with previously reported studies, galactosamino-PEG<sub>5</sub> moieties in SMAPIE-PEI-Gal micelles lead to reduction in cytotoxicity by 2-fold as compared to PEI 10 KDa and by 3-fold as compared to SMAPIE-PEI-N3 micelles due to possible shielding of cationic PEI groups<sup>132,150</sup>. Unexpectedly, SMAPIE-PEI-N3 was more cytotoxic than PEI 10 KDa, but this might be explained by the conformation of the cationic groups in the shell of the micelles that might arrange in a way that increased their electrostatic interaction

with the negatively charged cell membrane and induced more toxicity. However, addition of targeting ligand or other functional moieties to SMAPIE-PEI-N3 micelles block copolymer can reduce its cytotoxicity as proven in case of SMAPIE-PEI-Gal copolymer.

SMAPIE-PEI-N3 micelles, SMAPIE-PEI-Gal micelles, and PEI 10 KDa polymer were complexed with siRNA to form less cytotoxic micelleplexes or polyplexes used subsequently in cellular uptake or transfection evaluation experiments. The reason for the lesser cytotoxicity is because the negatively charged siRNA gets condensed by ionic interaction with a portion of the cationic groups in the micelles or PEI 10 KDa polymer, thus decreasing the number of the cationic groups available to interact with the cell membrane to cause cytotoxicity<sup>131,162</sup>. Although, cell viability was more than 80% in case of SMAPIE-PEI-N3, SMAPIE-PEI-Gal, and PEI 10 KDa at concentrations below 20 µg/mL, and siRNA condensation should improve the cell viability more, it is important to note that the polymers or micelles concentration used in the subsequent in vitro experiments was 6.7 µg/mL or lesser depending on the micelle or polymer type. As a result, more than 90% cell viability was ensured in all the following in-vitro experiments.

#### **4.9.2 Cellular Uptake Quantification by Flow Cytometry**

Cellular uptake is an ultimate prerequisite for specific siRNA delivery and achievement of good transfection efficiency. Naked siRNAs are degraded by serum nucleases and have poor cell membrane penetration ability. These major

obstacles of diminished stability and poor cellular uptake, ultimately result in restricted and inefficient delivery<sup>71,163</sup>.

Polycationic vectors have shown promising potentials for resolving the siRNA delivery problems. Polycationic vectors such as PEI can electrostatically complex siRNA and sequester them from the enzymatic degradation by endo/exonucleases. They also improve the siRNA cargo cellular delivery through mediating endocytic cellular internalization<sup>70</sup>. Polycationic vectors functionalized with receptor specific targeting ligands help to achieve selective active targeting of siRNA therapy to affected tissues that overexpress the complementary ligand receptors and thus increase the therapeutic efficiency<sup>101,150,164</sup>.

Asialoglycoprotein (ASGP) receptors are among those targetable receptors, and are used for targeted therapy of liver cancer. ASGPRs are c-type lectin receptors<sup>165</sup> that were found to be over expressed in several human neoplastic hepatocytes<sup>118</sup> and hepatocellular carcinoma cell lines including Hep G2 and Huh7.5 cells<sup>119,120</sup>. ASGPRs selectively binds and internalize different molecules terminating with carbohydrate residues such as galactose, galactosamine, or N- acetylgalactosamine through receptor mediated endocytosis<sup>121,122</sup>.

Cellular uptake quantification and analysis using flow cytometry was conducted to evaluate the siRNA delivery ability as well as (ASGP) receptor targeting efficiency of galactosamine targeted SMAPIE-PEI-Gal micelleplexes versus the non-targeted SMAPIE-PEI-N3 ones in Hep G2 cells. PEI 10 KDa polyplexes were studied as positive transfection control for comparison, while free



siRNA and untreated cells served as negative controls. Micelleplexes or polyplexes were formed by complexation of fluorescent FAM-siRNA with SMAPIE-PEI-Gal, SMAPIE-PEI-N3 polycationic micelles and PEI 10 KDa polycationic polymer.

As illustrated in figure 3.14, statistical analysis of the median fluorescence intensities showed that naked siRNA achieved insignificant cellular uptake compared to untreated cells. This could be attributed to poor stability and inefficient cell penetration of the naked siRNA as mentioned above. On the other hand, siRNA condensation with both polycationic micelles and PEI polymer protected the siRNA and increased its cellular internalization significantly. Interestingly, cellular uptake of non-targeted SMAPIE-PEI-N3 micelleplexes was not significantly different from that of PEI 10 KDa polyplexes. One possible explanation is that, SMAPIE-PEI-N3 micelleplexes which had PEI chain residues in their micellar corona that were not decorated with targeting ligands, entered the cells via the same endocytic pathway as PEI 10 KDa polyplexes. It was previously reported that PEI polyplexes were taken up by Hep G2 cells through clathrin-mediated endocytosis<sup>166</sup>. On the other hand, galactosamine targeted SMAPIE-PEI-Gal micelleplexes showed 0.84 fold higher cellular entry than the non-targeted counterparts. In line with earlier studies, SMAPIE-PEI-Gal micelleplexes were taken up by Hep G2 cells through receptor mediated endocytosis, since the galactosamine targeting ligands bind to the overexpressed ASGPRs facilitating the micelleplexes cellular internalization selectively in huge quantities<sup>124,125</sup>. This pathway was further confirmed by the significant decrease in the cellular uptake of

SMAPIE-PEI-Gal micelleplexes in the presence of free galactosamine as competitive control. The free galactosamine didn't prevent SMAPIE-PEI-Gal micelleplexes internalization completely since it only competed for the ASGP receptors (without irreversibly occupying them) thereby decreasing their timely availability for SMAPIE-PEI-Gal micelleplexes. The enhanced ASGPRs targeting efficiency of SMAPIE-PEI-Gal micelleplexes suggests its potential value for selectively targeting hepatocytes for treatment of hepatocellular carcinoma and other liver diseases that overexpress the target receptors (ASGPRs).

#### **4.9.3 Cellular Uptake and Endosomal Escape by Confocal Laser Scanning Microscopy (CLSM)**

Confocal laser scanning microscopy serves as an important tool for visualization, imaging and studying of drugs / nucleic acids nanocarriers cellular uptake as well as their sub-cellular localization. The process involves the use of fluorescent labels for marking the carriers or their cargo and also for denoting/marketing the necessary cellular compartments.

Confocal laser scanning microscopy was performed to study the ability of both targeted SMAPIE-PEI-Gal and non-targeted SMAPIE-PEI-N3 micelleplexes to deliver siRNA to cytoplasm of asialoglycoprotein receptor (ASGPR) positive Hep G2 cells as well as the route of cellular uptake. PEI 10 KDa polyplexes were used as positive control. ASGPR targeting efficiency of SMAPIE-PEI-Gal micelleplexes was evaluated in absence and presence of free galactosamine as competitor ligand of ASGPRs.

Micelleplexes or polyplexes were prepared with FAM-labeled siRNA at N/P ratio of 10. The cells nuclei were stained with Hoechst 33342 stain (blue), acidic

endosomal compartments with Lyso Tracker Deep Red dye (red), and siRNA was labeled with FAM (green).

As shown in figure 3.15, the sub-cellular localization of the green fluorescent siRNA was in the cytoplasm around the blue nucleus or in the red endosomal compartments at 22 hours post transfection. The co-localization of siRNA (green) and endosomes (red) as denoted by yellow colored regions in the merged images indicated that the siRNA complexes underwent cell entry through endocytosis. SMAPIE-PEI-N3 micelleplexes and PEI 10 KDa polyplexes most likely entered through non-specific endocytosis due to electrostatic interaction of their cationic charge with the anionic plasma membrane as noted before<sup>71</sup>. On the other hand, and in concordance with the flow cytometry results, galactosamine targeted SMAPIE-PEI-Gal micelleplexes were taken up into Hep G2 cells that overexpress ASGPRs primarily via receptor mediated endocytosis. Indeed, the galactosamine ASGPRs targeting effect in SMAPIE-PEI-Gal micelleplexes was proven by the huge reduction in the micelleplexes uptake with free galactosamine competitor presence in the transfection medium as reflected by the lowering of green fluorescence intensity (figures 3.15 and 3.16).

As illustrated in the CLSM images, most of the green siRNA spots were present in the cytoplasm compared to very little amount remaining entrapped in the endosomes. This was true in the case of targeted SMAPIE-PEI-Gal micelleplexes and PEI 10 KDa polyplexes, while for the non-targeted SMAPIE-PEI-N3 micelleplexes, more portion of the siRNA remained in the endosomes compared to that released in the cytoplasm at the same time point. This result

could be attributed to the previously found low buffering capacity of SMAPIE-PEI-N3 micelles versus SMAPIE-PEI-Gal micelles and PEI 10 KDa polymer (figure 3.11). In line with previous findings<sup>70,132,167</sup>, the high buffering ability of SMAPIE-PEI-Gal micelleplexes and PEI 10KDa polyplexes increased their endosomal escape, which consequently increased the available siRNA for gene silencing through binding to the RNA induced silencing complex (RISC) in the cytoplasm causing the required RNA interference. This suggests that SMAPIE-PEI-Gal micelleplexes could achieve better transfection efficiency and specific gene knockdown than the non-targeted SMAPIE-PEI-N3 micelleplexes.

#### **4.9.4 Transfection Efficiency and Nrf2 Gene Knockdown by Western Blot analysis**

SMAPIE-PEI-Gal micelleplexes transfection efficiency and ability to deliver siRNA to Hep G2 cells in an effective manner was evaluated using western blot analysis. Effective siRNA delivery is a prerequisite for achieving efficient gene knockdown, which is the ultimate goal of siRNA therapy.

Nrf2 gene was chosen as target gene for the study due to its established role in promoting HCC cells proliferation, invasion, metastasis, and chemoresistance, as documented in previous publications<sup>49,57,58</sup>. Nrf2 downregulation or inhibition was proven to resensitize HCC cells to many anticancer drugs including 5-fluorouracil (5-FU), cisplatin, and doxorubicin<sup>57-59</sup>. As a result, Nrf2 protein is a potential therapeutic target in HCC management.

SMAPIE-PEI-Gal micelleplexes and PEI 10 KDa polyplexes were prepared by complexing Nrf2-siRNA or negative control non-target specific siRNA (NCR-siRNA) at N/P ratio of 10. PEI 10 KDa was used as positive transfection control,

while micelleplexes or polyplexes condensing NCr-siRNA were used as negative controls for comparison. Hep G2 cells were chosen for the study as it was reported to be positive for Nrf2 expression with Nrf2 main localization in the cytoplasm<sup>168</sup>. Hep G2 cells were transfected for 24 hours with micelleplexes or polyplexes containing 50 nM siRNA through reverse transfection technique as Hep G2 cells are among the “hard to transfect” cell lines<sup>169</sup> and reverse transfection was reported to achieve superior results as compared to the traditional transfection methodology. The Nrf2 protein half-life was reported to be very short (less than 20 minutes)<sup>170</sup>, consequently similar to previous publication, the transfection time in the study was set to 24 hours after which immunoblotting was performed for Nrf2 protein level measurement and gene knockdown assessment<sup>171</sup>.

As demonstrated from the results (figure 3.17), after 24 hours of transfection, both Nrf2 condensing SMAPIE-PEI-Gal micelleplexes and PEI 10 KDa polyplexes succeeded to achieve statistically significant ( $p < 0.05$ ) Nrf2 gene knockdown and Nrf2 protein translation interference by around 49% and 27% respectively. In line with previously obtained cellular uptake, buffering capacity and endosomal escape data, these results confirmed the ability of SMAPIE-PEI-Gal micelles to effectively deliver siRNA in HCC cells in effective quantity, with effective endosomal escape and high availability for incorporation in the cytoplasmic silencing machinery in order to produce efficient gene knockdown. Interestingly, SMAPIE-PEI-Gal micelleplexes exhibited statistically significant and superior Nrf2 gene knockdown when compared with that observed with PEI 10 KDa polyplexes, ( $p < 0.05$ ). This could be explained by the efficient ASGPRs based internalization

and targeting ability and the higher cellular uptake of SMAPIE-PEI-Gal micelleplexes than PEI 10 KDa polyplexes as illustrated before. In conclusion, SMAPIE-PEI-Gal micelles forming block copolymer is a promising vector for delivering Nrf2 siRNA, promoting sequence specific gene knockdown in Hep G2 liver cancer cells. The newly synthesized micelle forming block co-polymer thus holds potential to serve as targeted nanocarrier delivery system to counteract the chemoresistance of HCCs.

## SUMMARY

In this study, we successfully synthesized micellar polymeric nanodelivery system that can be used as multifunctional modular platform in cancer therapy and/or diagnosis. The micelles (SMAPIE-PEI-N3) were constructed from poly(Styrene-co-maleic anhydride, partial iso-octyl ester) co-polymeric chain (SMAPIE) grafted to branched polyethylenimine 10 KDa polymeric chain (PEI) in which primary amine groups were partially modified into azide groups (N3). Different targeting ligands and imaging agents can be conjugated to SMAPIE-PEI-N3 micelles simultaneously or individually by applying copper free “click” chemistry strategies, for targeting various resistant and metastatic cancers overexpressing complementary receptors. In this study, as a proof-of-concept, galactosamine decorated micelles (SMAPIE-PEI-Gal) were synthesized to efficiently target asialoglycoprotein (ASGP) receptors overexpressed in liver cancers.

The successful synthesis of targeted and non-targeted micelles forming block copolymers was confirmed by <sup>1</sup>H NMR and FT/IR. The relative molecular weight and PEI composition of the micelles were determined using size exclusion chromatography and copper chelation assay, respectively. Critical micelle concentration of SMAPIE-PEI-N3 micelles was determined using pyrene as a fluorescent probe and was found to be as low as 0.0112 mg/ml, indicating its potential to be of high stability even on dilution in vivo. In terms of the siRNA condensation ability evaluated by the SYBER Gold fluorescent dye, SMAPIE-PEI-Gal micelles were found to be of more efficient siRNA condensation capacity than SMAPIE-PEI-N3 micelles at N/P ratio lower than 10. The hydrodynamic size of

SMAPIE-PEI-N3 and SMAPIE-PEI-Gal micelles was around 160 nm and 240 nm respectively with moderate polydispersity index, but they had high zeta potential of about 40 mV. On the other hand, SMAPIE-PEI-N3 and SMAPIE-PEI-Gal micelleplexes exhibited decreasing pattern of hydrodynamic size with increasing N/P ratio and achieved more complete siRNA condensation. The size of 200 nm at N/P ratio of 10 is optimum for EPR mediated passive accumulation in cancer tissues. SMAPIE-PEI-N3 and SMAPIE-PEI-Gal micelleplexes zeta potential decreased as a consequence of siRNA condensation as compared to the highly cationic plain micelles. Transmission electron microscopy (TEM) images demonstrated the spherical core/shell morphology of both the plain micelles and the siRNA complexing micelleplexes. In terms of buffering capacity and endosomal escape potential, SMAPIE-PEI-Gal micelles were of high buffer capacity comparable to that of PEI polymers. However it was found that SMAPIE-PEI-Gal was superior to SMAPIE-PEI-N3 micelles in buffering ability. Cytotoxicity evaluation of both targeted and non-targeted micelles in Hep G2 cells showed more than 80% cell viability at concentrations below 20  $\mu\text{g/ml}$ , however much better cell viability was observed in the transfection experiments as only a total polymer concentration of 6.7  $\mu\text{g/ml}$  or lesser was used/needed.

Cellular uptake of SMAPIE-PEI-Gal micelleplexes via the ASGP receptor mediated endocytosis was confirmed by the free galactosamine competition assay results. In contrast to galactosamine targeted SMAPIE-PEI-Gal micelleplexes, cellular uptake of non-targeted SMAPIE-PEI-N3 micelleplexes and PEI polyplexes could be attributed to the cationic charge mediated non-specific endocytosis



demonstrated in the co-localization of some SMAPIE-PEI-N3 micelleplexes and PEI polyplexes with endosomes, as illustrated by CLSM. Quantification of cellular uptake of PEI 10 KDa polyplexes, SMAPIE-PEI-N3 micelleplexes, and SMAPIE-PEI-Gal micelleplexes in Hep G2 cells by flow cytometry showed statistically significant and superior cellular internalization by SMAPIE-PEI-Gal micelleplexes, ( $p < 0.01$ ). Indeed, SMAPIE-PEI-Gal micelleplexes cellular uptake was higher than that of SMAPIE-PEI-N3 micelleplexes and PEI 10 KDa polyplexes by 0.84 and 1.2 folds respectively, due to the overexpression of ASGPRs in HCC cells.

In conclusion, as noted from all the above data, SMAPIE-PEI-Gal micelles forming block copolymer showed better physical and biological characteristics than SMAPIE-PEI-N3 copolymer. As a result, SMAPIE-PEI-Gal micelles were chosen to further study their siRNA transfection efficiency and ability to achieve effective gene knockdown. As expected, SMAPIE-PEI-Gal micelleplexes successfully mediated significant 0.49 fold Nrf2 gene knockdown in ASGPRs overexpressing Hep G2 cells. The Nrf2 gene knockdown was 21% higher than the one mediated by the positive transfection control PEI 10 KDa polyplexes at statistical significance of ( $p < 0.05$ ). These results emphasize that SMAPIE-PEI-Gal is a promising candidate for siRNA delivery to HCC. Its application to knockdown Nrf2 gene, can counteract the “dark side” of Nrf2 in HCC, where it decreases HCC cells survival and chemoresistance, warranting further investigations.

In future experiments, SMAPIE-PEI-Gal micelles can be studied both in vitro and in vivo for co-delivery of chemotherapeutic agent and Nrf2 or MDR1 siRNA to

overcome chemoresistance and achieve synergistic control on tumor growth in HCC.

The scope of study could be extended by employing SMAPIE-PEI-N3 as a modular micellar block co-polymer through attachment of different targeting ligands or imaging agents and studying the potential of the so-formed micelles/micelleplexes to achieve targeted therapy of different types of cancer.

**REFERENCES**

1. Pérez-Herrero, E. & Fernández-Medarde, A. Advanced targeted therapies in cancer: Drug nanocarriers, the future of chemotherapy. *Eur. J. Pharm. Biopharm.* **93**, 52–79 (2015).
2. Hanahan, D. & Weinberg, R. A. Hallmarks of cancer: the next generation. *Cell* **144**, 646–74 (2011).
3. Marx, J. *et al.* Debate surges over the origins of genomic defects in cancer. *Science* **297**, 544–6 (2002).
4. Kulis, M. & Esteller, M. DNA methylation and cancer. *Adv. Genet.* **70**, 27–56 (2010).
5. Jones, P. A. & Baylin, S. B. The fundamental role of epigenetic events in cancer. *Nat. Rev. Genet.* **3**, 415–28 (2002).
6. You, J. S. & Jones, P. A. Cancer genetics and epigenetics: two sides of the same coin? *Cancer Cell* **22**, 9–20 (2012).
7. Sadikovic, B., Al-Romaih, K., Squire, J. A. & Zielenska, M. Cause and consequences of genetic and epigenetic alterations in human cancer. *Curr. Genomics* **9**, 394–408 (2008).
8. *National Center for Health Statistics. Health, United States, 2015: With Special Feature on Racial and Ethnic Health Disparities. Hyattsville, MD. 2016.*
9. Siegel, R. L., Miller, K. D. & Jemal, A. Cancer statistics, 2016. *CA. Cancer J. Clin.* **66**, 7–30
10. DeVita, V. T. & Rosenberg, S. A. Two Hundred Years of Cancer Research.

- New England Journal of Medicine* **366**, 2207–2214 (2012).
11. Chabner, B. A. & Roberts, T. G. Chemotherapy and the war on cancer. *Nat Rev Cancer* **5**, 65–72 (2005).
  12. Ferlay, J. *et al.* Cancer incidence and mortality worldwide: Sources, methods and major patterns in GLOBOCAN 2012. *Int. J. Cancer* **136**, E359–E386 (2015).
  13. Ryerson, A. B. *et al.* Annual Report to the Nation on the Status of Cancer, 1975-2012, featuring the increasing incidence of liver cancer. *Cancer* **122**, 1312–1337 (2016).
  14. *American Cancer Society. Cancer Facts & Figures 2016. Atlanta: American Cancer Society; 2016.*
  15. Lu, J.-W. *et al.* Zebrafish as a disease model for studying human hepatocellular carcinoma. *World J. Gastroenterol.* **21**, 12042–58 (2015).
  16. El-Serag, H. B. Hepatocellular carcinoma: an epidemiologic view. *J. Clin. Gastroenterol.* **35**, S72–8 (2002).
  17. Kew, M. C. & Popper, H. Relationship between hepatocellular carcinoma and cirrhosis. *Semin. Liver Dis.* **4**, 136–46 (1984).
  18. Poustchi, H., Sepanlou, S., Esmaili, S., Mehrabi, N. & Ansarymoghadam, A. Hepatocellular carcinoma in the world and the middle East. *Middle East J. Dig. Dis.* **2**, 31–41 (2010).
  19. Schwartz, M., Roayaie, S. & Konstadoulakis, M. Strategies for the management of hepatocellular carcinoma. *Nat. Clin. Pract. Oncol.* **4**, 424–32 (2007).

20. Janevska, D., Chaloska-Ivanova, V. & Janevski, V. Hepatocellular Carcinoma: Risk Factors, Diagnosis and Treatment. *Open access Maced. J. Med. Sci.* **3**, 732–6 (2015).
21. Livraghi, T. Radiofrequency ablation, PEIT, and TACE for hepatocellular carcinoma. *J. Hepatobiliary. Pancreat. Surg.* **10**, 67–76 (2003).
22. Shiina, S. *et al.* A randomized controlled trial of radiofrequency ablation with ethanol injection for small hepatocellular carcinoma. *Gastroenterology* **129**, 122–30 (2005).
23. Llovet, J. M. *et al.* Arterial embolisation or chemoembolisation versus symptomatic treatment in patients with unresectable hepatocellular carcinoma: a randomised controlled trial. *Lancet (London, England)* **359**, 1734–9 (2002).
24. Mazzaferro, V. *et al.* Liver transplantation for the treatment of small hepatocellular carcinomas in patients with cirrhosis. *N. Engl. J. Med.* **334**, 693–9 (1996).
25. Zhu, A. X. Systemic therapy of advanced hepatocellular carcinoma: how hopeful should we be? *Oncologist* **11**, 790–800 (2006).
26. Capone, F. *et al.* Synergistic antitumor effect of Doxorubicin and tacrolimus (FK506) on hepatocellular carcinoma cell lines. *ScientificWorldJournal.* **2014**, 450390 (2014).
27. Wrzesinski, S. H., Taddei, T. H. & Strazzabosco, M. Systemic therapy in hepatocellular carcinoma. *Clin. Liver Dis.* **15**, 423–41, vii–x (2011).
28. Deng, G.-L., Zeng, S. & Shen, H. Chemotherapy and target therapy for

- hepatocellular carcinoma: New advances and challenges. *World J. Hepatol.* **7**, 787–98 (2015).
29. Kato, A. *et al.* Multidrug resistance gene (MDR-1) expression as a useful prognostic factor in patients with human hepatocellular carcinoma after surgical resection. *J. Surg. Oncol.* **78**, 110–5 (2001).
  30. Huang, M. & Liu, G. The study of innate drug resistance of human hepatocellular carcinoma Bel7402 cell line. *Cancer Lett.* **135**, 97–105 (1999).
  31. Kim, D. *et al.* Antitumor activity of sorafenib-incorporated nanoparticles of dextran/poly(dl-lactide-co-glycolide) block copolymer. *Nanoscale Res. Lett.* **7**, 91 (2012).
  32. Luqmani, Y. A. Mechanisms of drug resistance in cancer chemotherapy. *Med. Princ. Pract.* **14 Suppl 1**, 35–48 (2005).
  33. Rebucci, M. & Michiels, C. Molecular aspects of cancer cell resistance to chemotherapy. *Biochemical Pharmacology* **85**, 1219–1226 (2013).
  34. Wu, C.-P., Hsieh, C.-H. & Wu, Y.-S. The emergence of drug transporter-mediated multidrug resistance to cancer chemotherapy. *Mol. Pharm.* **8**, 1996–2011 (2011).
  35. Gottesman, M. M., Fojo, T. & Bates, S. E. Multidrug resistance in cancer: role of ATP-dependent transporters. *Nat. Rev. Cancer* **2**, 48–58 (2002).
  36. Luqmani, Y. A. Mechanisms of drug resistance in cancer chemotherapy. *Med. Princ. Pract.* **14 Suppl 1**, 35–48 (2005).
  37. Pawlak, W., Zolnierek, J., Sarosiek, T. & Szczylik, C. Antisense therapy in

- cancer. *Cancer Treat. Rev.* **26**, 333–50 (2000).
38. Zhang, D. D., Lo, S.-C., Cross, J. V, Templeton, D. J. & Hannink, M. Keap1 is a redox-regulated substrate adaptor protein for a Cul3-dependent ubiquitin ligase complex. *Mol. Cell. Biol.* **24**, 10941–53 (2004).
  39. Furukawa, M. & Xiong, Y. BTB protein Keap1 targets antioxidant transcription factor Nrf2 for ubiquitination by the Cullin 3-Roc1 ligase. *Mol. Cell. Biol.* **25**, 162–71 (2005).
  40. Zhang, D. D. & Hannink, M. Distinct cysteine residues in Keap1 are required for Keap1-dependent ubiquitination of Nrf2 and for stabilization of Nrf2 by chemopreventive agents and oxidative stress. *Mol. Cell. Biol.* **23**, 8137–51 (2003).
  41. Dinkova-Kostova, A. T. *et al.* Direct evidence that sulfhydryl groups of Keap1 are the sensors regulating induction of phase 2 enzymes that protect against carcinogens and oxidants. *Proc. Natl. Acad. Sci. U. S. A.* **99**, 11908–13 (2002).
  42. Hirotsu, Y. *et al.* Nrf2-MafG heterodimers contribute globally to antioxidant and metabolic networks. *Nucleic Acids Res.* **40**, 10228–39 (2012).
  43. Hayes, J. D., McMahon, M., Chowdhry, S. & Dinkova-Kostova, A. T. Cancer chemoprevention mechanisms mediated through the Keap1-Nrf2 pathway. *Antioxid. Redox Signal.* **13**, 1713–48 (2010).
  44. Lau, A., Villeneuve, N. F., Sun, Z., Wong, P. K. & Zhang, D. D. Dual roles of Nrf2 in cancer. *Pharmacol. Res.* **58**, 262–70 (2008).
  45. Jaramillo, M. C. & Zhang, D. D. The emerging role of the Nrf2-Keap1

- signaling pathway in cancer. *Genes Dev.* **27**, 2179–2191 (2013).
46. Onodera, Y. *et al.* NRF2 immunolocalization in human breast cancer patients as a prognostic factor. *Endocr. Relat. Cancer* **21**, 241–252 (2014).
  47. Kang, H. J. *et al.* HER2 confers drug resistance of human breast cancer cells through activation of NRF2 by direct interaction. *Sci. Rep.* **4**, 7201 (2014).
  48. Columbano, A. *et al.* Mutations of Nrf2 are an early and frequent event in the development of rat hepatocellular carcinoma. *FASEB J.* **29**, 147.10 (2015).
  49. Zhang, M. *et al.* Nrf2 is a potential prognostic marker and promotes proliferation and invasion in human hepatocellular carcinoma. *BMC Cancer* **15**, 531 (2015).
  50. Zhang, P. *et al.* Loss of Kelch-like ECH-associated protein 1 function in prostate cancer cells causes chemoresistance and radioresistance and promotes tumor growth. *Mol. Cancer Ther.* **9**, 336–46 (2010).
  51. Shibata, T. *et al.* Genetic alteration of Keap1 confers constitutive Nrf2 activation and resistance to chemotherapy in gallbladder cancer. *Gastroenterology* **135**, 1358–1368, 1368.e1–4 (2008).
  52. Kim, Y. R. *et al.* Oncogenic NRF2 mutations in squamous cell carcinomas of oesophagus and skin. *J. Pathol.* **220**, 446–51 (2010).
  53. Lister, A. *et al.* Nrf2 is overexpressed in pancreatic cancer: implications for cell proliferation and therapy. *Mol. Cancer* **10**, 37 (2011).
  54. Singh, A. *et al.* Dysfunctional KEAP1-NRF2 interaction in non-small-cell lung cancer. *PLoS Med.* **3**, e420 (2006).
  55. Reddy, N. M. *et al.* Genetic disruption of the Nrf2 compromises cell-cycle



- progression by impairing GSH-induced redox signaling. *Oncogene* **27**, 5821–32 (2008).
56. Mitsuishi, Y. *et al.* Nrf2 redirects glucose and glutamine into anabolic pathways in metabolic reprogramming. *Cancer Cell* **22**, 66–79 (2012).
  57. Zhou, S., Ye, W., Duan, X., Zhang, M. & Wang, J. The noncytotoxic dose of sorafenib sensitizes Bel-7402/5-FU cells to 5-FU by down-regulating 5-FU-induced Nrf2 expression. *Dig. Dis. Sci.* **58**, 1615–26 (2013).
  58. Shi, L. *et al.* miR-340 reverses cisplatin resistance of hepatocellular carcinoma cell lines by targeting Nrf2-dependent antioxidant pathway. *Asian Pac. J. Cancer Prev.* **15**, 10439–44 (2014).
  59. Gao, A.-M. *et al.* Apigenin sensitizes doxorubicin-resistant hepatocellular carcinoma BEL-7402/ADM cells to doxorubicin via inhibiting PI3K/Akt/Nrf2 pathway. *Carcinogenesis* **34**, 1806–1814 (2013).
  60. Ma, R.-Q. *et al.* [Expression and distribution of Nrf2 in several hepatocellular carcinoma cell lines]. *Xi Bao Yu Fen Zi Mian Yi Xue Za Zhi* **27**, 608–10 (2011).
  61. Wang, J., Lu, Z., Wientjes, M. G. & Au, J. L.-S. Delivery of siRNA therapeutics: barriers and carriers. *AAPS J.* **12**, 492–503 (2010).
  62. Aleku, M. *et al.* Atu027, a liposomal small interfering RNA formulation targeting protein kinase N3, inhibits cancer progression. *Cancer Res.* **68**, 9788–98 (2008).
  63. Davis, M. E. The first targeted delivery of siRNA in humans via a self-assembling, cyclodextrin polymer-based nanoparticle: from concept to clinic.

- Mol. Pharm.* **6**, 659–68 (2009).
64. Davis, M. E. *et al.* Evidence of RNAi in humans from systemically administered siRNA via targeted nanoparticles. *Nature* **464**, 1067–1070 (2010).
  65. Rand, T. A., Ginalski, K., Grishin, N. V & Wang, X. Biochemical identification of Argonaute 2 as the sole protein required for RNA-induced silencing complex activity. *Proc. Natl. Acad. Sci. U. S. A.* **101**, 14385–9 (2004).
  66. Rand, T. A., Petersen, S., Du, F. & Wang, X. Argonaute2 cleaves the anti-guide strand of siRNA during RISC activation. *Cell* **123**, 621–9 (2005).
  67. Ameres, S. L., Martinez, J. & Schroeder, R. Molecular basis for target RNA recognition and cleavage by human RISC. *Cell* **130**, 101–12 (2007).
  68. Matranga, C., Tomari, Y., Shin, C., Bartel, D. P. & Zamore, P. D. Passenger-strand cleavage facilitates assembly of siRNA into Ago2-containing RNAi enzyme complexes. *Cell* **123**, 607–20 (2005).
  69. van de Water, F. M. *et al.* Intravenously administered short interfering RNA accumulates in the kidney and selectively suppresses gene function in renal proximal tubules. *Drug Metab. Dispos.* **34**, 1393–7 (2006).
  70. Whitehead, K. A., Langer, R. & Anderson, D. G. Knocking down barriers: advances in siRNA delivery. *Nat. Rev. Drug Discov.* **8**, 129–138 (2009).
  71. Akhtar, S. & Benter, I. F. Nonviral delivery of synthetic siRNAs in vivo. *J. Clin. Invest.* **117**, 3623–32 (2007).
  72. Kawakami, S. & Hashida, M. Targeted delivery systems of small interfering RNA by systemic administration. *Drug Metab. Pharmacokinet.* **22**, 142–51

- (2007).
73. Aigner, A. Delivery systems for the direct application of siRNAs to induce RNA interference (RNAi) in vivo. *J. Biomed. Biotechnol.* **2006**, 71659 (2006).
  74. Mishra, D., Hubenak, J. R. & Mathur, A. B. Nanoparticle systems as tools to improve drug delivery and therapeutic efficacy. *J. Biomed. Mater. Res. A* **101**, 3646–60 (2013).
  75. Markman, J. L., Rekechenetskiy, A., Holler, E. & Ljubimova, J. Y. Nanomedicine therapeutic approaches to overcome cancer drug resistance. *Adv. Drug Deliv. Rev.* **65**, 1866–1879 (2013).
  76. Wang, X. *et al.* The development of site-specific drug delivery nanocarriers based on receptor mediation. *J. Control. Release* **193**, 139–153 (2014).
  77. van der Meel, R., Vehmeijer, L. J. C., Kok, R. J., Storm, G. & van Gaal, E. V. B. Ligand-targeted particulate nanomedicines undergoing clinical evaluation: Current status. *Adv. Drug Deliv. Rev.* **65**, 1284–1298 (2013).
  78. Peer, D. *et al.* Nanocarriers as an emerging platform for cancer therapy. *Nat. Nanotechnol.* **2**, 751–60 (2007).
  79. Zou, H., Wang, Z. & Feng, M. Nanocarriers with tunable surface properties to unblock bottlenecks in systemic drug and gene delivery. *J. Control. Release* **214**, 121–133 (2015).
  80. Torchilin, V. P. Micellar nanocarriers: pharmaceutical perspectives. *Pharm. Res.* **24**, 1–16 (2007).
  81. Kim, S., Shi, Y., Kim, J. Y., Park, K. & Cheng, J.-X. Overcoming the barriers in micellar drug delivery: loading efficiency, in vivo stability, and micelle-cell

- interaction. *Expert Opin. Drug Deliv.* **7**, 49–62 (2010).
82. Oerlemans, C. *et al.* Polymeric micelles in anticancer therapy: targeting, imaging and triggered release. *Pharm. Res.* **27**, 2569–89 (2010).
  83. Lu, Y. & Park, K. Polymeric micelles and alternative nanonized delivery vehicles for poorly soluble drugs. *Int. J. Pharm.* **453**, 198–214 (2013).
  84. Blanco, E., Kessinger, C. W., Sumer, B. D. & Gao, J. Multifunctional micellar nanomedicine for cancer therapy. *Exp. Biol. Med. (Maywood)*. **234**, 123–31 (2009).
  85. Kwon, G. S. & Kataoka, K. Block copolymer micelles as long-circulating drug vehicles. *Adv. Drug Deliv. Rev.* **16**, 295–309 (1995).
  86. Patil, R. *et al.* Temozolomide delivery to tumor cells by a multifunctional nano vehicle based on poly( $\beta$ -L-malic acid). *Pharm. Res.* **27**, 2317–29 (2010).
  87. Zhu, L., Perche, F., Wang, T. & Torchilin, V. P. Matrix metalloproteinase 2-sensitive multifunctional polymeric micelles for tumor-specific co-delivery of siRNA and hydrophobic drugs. *Biomaterials* **35**, 4213–4222 (2014).
  88. Xiong, X.-B. & Lavasanifar, A. Traceable multifunctional micellar nanocarriers for cancer-targeted co-delivery of MDR-1 siRNA and doxorubicin. *ACS Nano* **5**, 5202–13 (2011).
  89. Chen, W. *et al.* Co-Delivery of Doxorubicin and siRNA with Reduction and pH Dually Sensitive Nanocarrier for Synergistic Cancer Therapy. *Small* **10**, 2678–2687 (2014).
  90. Li, J., Wang, Y., Zhu, Y. & Oupický, D. Recent advances in delivery of drug–nucleic acid combinations for cancer treatment. *J. Control. Release* **172**,

- 589–600 (2013).
91. Chen, G. *et al.* Multi-functional self-fluorescent unimolecular micelles for tumor-targeted drug delivery and bioimaging. *Biomaterials* **47**, 41–50 (2015).
  92. Xiao, Y. *et al.* Multifunctional unimolecular micelles for cancer-targeted drug delivery and positron emission tomography imaging. *Biomaterials* **33**, 3071–3082 (2012).
  93. Baranello, M. P., Bauer, L. & Benoit, D. S. W. Poly(styrene-alt-maleic anhydride)-based diblock copolymer micelles exhibit versatile hydrophobic drug loading, drug-dependent release, and internalization by multidrug resistant ovarian cancer cells. *Biomacromolecules* **15**, 2629–41 (2014).
  94. Han, J., Silcock, P., McQuillan, A. J. & Bremer, P. Self-organization of dipeptide-grafted polymeric nanoparticles film: A novel method for surface modification. *Eur. Polym. J.* **46**, 1824–1832 (2010).
  95. Zovko, M., Barbarić, M., Zorc, B., Hafner, A. & Filipović-Grcić, J. Synthesis of fenoprofen and gemfibrozil styrene-maleic acid copolymer conjugates. *Acta Pharm.* **55**, 169–76 (2005).
  96. Maeda, H., Ueda, M., Morinaga, T. & Matsumoto, T. Conjugation of poly(styrene-co-maleic acid) derivatives to the antitumor protein neocarzinostatin: pronounced improvements in pharmacological properties. *J. Med. Chem.* **28**, 455–61 (1985).
  97. Mu, Y. *et al.* Bioconjugation of laminin peptide YIGSR with poly(styrene co-maleic acid) increases its antimetastatic effect on lung metastasis of B16-BL6 melanoma cells. *Biochem. Biophys. Res. Commun.* **255**, 75–9 (1999).

98. Greish, K., Sawa, T., Fang, J., Akaike, T. & Maeda, H. SMA-doxorubicin, a new polymeric micellar drug for effective targeting to solid tumours. *J. Control. Release* **97**, 219–30 (2004).
99. Daruwalla, J. *et al.* In vitro and in vivo evaluation of tumor targeting styrene-maleic acid copolymer-pirarubicin micelles: Survival improvement and inhibition of liver metastases. *Cancer Sci.* **101**, 1866–74 (2010).
100. Boussif, O. *et al.* A versatile vector for gene and oligonucleotide transfer into cells in culture and in vivo: polyethylenimine. *Proc. Natl. Acad. Sci. U. S. A.* **92**, 7297–301 (1995).
101. Urban-Klein, B., Werth, S., Abuharbeid, S., Czubayko, F. & Aigner, A. RNAi-mediated gene-targeting through systemic application of polyethylenimine (PEI)-complexed siRNA in vivo. *Gene Ther.* **12**, 461–6 (2005).
102. Ge, Q. *et al.* Inhibition of influenza virus production in virus-infected mice by RNA interference. *Proc. Natl. Acad. Sci. U. S. A.* **101**, 8676–81 (2004).
103. Morille, M., Passirani, C., Vonarbourg, A., Clavreul, A. & Benoit, J.-P. Progress in developing cationic vectors for non-viral systemic gene therapy against cancer. *Biomaterials* **29**, 3477–96 (2008).
104. Kircheis, R., Wightman, L. & Wagner, E. Design and gene delivery activity of modified polyethylenimines. *Adv. Drug Deliv. Rev.* **53**, 341–358 (2001).
105. Behr, J. The proton sponge: a trick to enter cells the viruses did not exploit. *Int. J. Chem.* **2**, 34–36 (1997).
106. Dachs, G. U., Dougherty, G. J., Stratford, I. J. & Chaplin, D. J. Targeting gene therapy to cancer: a review. *Oncol. Res.* **9**, 313–25 (1997).

107. Agard, N. J., Prescher, J. A. & Bertozzi, C. R. A strain-promoted [3 + 2] azide-alkyne cycloaddition for covalent modification of biomolecules in living systems. *J. Am. Chem. Soc.* **126**, 15046–7 (2004).
108. Best, M. D. Click chemistry and bioorthogonal reactions: unprecedented selectivity in the labeling of biological molecules. *Biochemistry* **48**, 6571–84 (2009).
109. Totobenazara, J. & Burke, A. J. New click-chemistry methods for 1,2,3-triazoles synthesis: recent advances and applications. *Tetrahedron Lett.* **56**, 2853–2859 (2015).
110. Dube, D. H., Prescher, J. A., Quang, C. N. & Bertozzi, C. R. Probing mucin-type O-linked glycosylation in living animals. *Proc. Natl. Acad. Sci. U. S. A.* **103**, 4819–24 (2006).
111. Prescher, J. A., Dube, D. H. & Bertozzi, C. R. Chemical remodelling of cell surfaces in living animals. *Nature* **430**, 873–877 (2004).
112. Dieterich, D. C. *et al.* Labeling, detection and identification of newly synthesized proteomes with bioorthogonal non-canonical amino-acid tagging. *Nat. Protoc.* **2**, 532–40 (2007).
113. Baskin, J. M. *et al.* Copper-free click chemistry for dynamic in vivo imaging. *Proc. Natl. Acad. Sci. U. S. A.* **104**, 16793–7 (2007).
114. Weisbrod, S. H. & Marx, A. Novel strategies for the site-specific covalent labelling of nucleic acids. *Chem. Commun. (Camb)*. 5675–85 (2008).
115. Mocharla, V. P. *et al.* In Situ Click Chemistry: Enzyme-Generated Inhibitors of Carbonic Anhydrase II. *Angew. Chemie Int. Ed.* **44**, 116–120 (2005).

116. Roman Manetsch, † *et al.* In Situ Click Chemistry: Enzyme Inhibitors Made to Their Own Specifications. (2004).
117. Huang, B. *et al.* The facile synthesis of multifunctional PAMAM dendrimer conjugates through copper-free click chemistry. *Bioorg. Med. Chem. Lett.* **22**, 3152–3156 (2012).
118. Trerè, D. *et al.* The asialoglycoprotein receptor in human hepatocellular carcinomas: its expression on proliferating cells. *Br. J. Cancer* **81**, 404–8 (1999).
119. Singh, M. & Ariatti, M. Targeted gene delivery into HepG2 cells using complexes containing DNA, cationized asialoorosomucoid and activated cationic liposomes. *J. Control. Release* **92**, 383–394 (2003).
120. Peng, D.-J. *et al.* Inhibition of hepatocarcinoma by systemic delivery of Apoptin gene via the hepatic asialoglycoprotein receptor. *Cancer Gene Ther.* **14**, 66–73 (2007).
121. Lee, R. T., Lin, P. & Lee, Y. C. New synthetic cluster ligands for galactose/N-acetylgalactosamine-specific lectin of mammalian liver. *Biochemistry* **23**, 4255–61 (1984).
122. Pathak, P. O. *et al.* Cholesterol anchored arabinogalactan for asialoglycoprotein receptor targeting: synthesis, characterization, and proof of concept of hepatospecific delivery. *Carbohydr. Res.* **408**, 33–43 (2015).
123. Julyan, P. J. *et al.* Preliminary clinical study of the distribution of HPMA copolymers bearing doxorubicin and galactosamine. *J. Control. Release* **57**, 281–90 (1999).



124. Shen, Z. *et al.* A galactosamine-mediated drug delivery carrier for targeted liver cancer therapy. *Pharmacol. Res.* **64**, 410–9 (2011).
125. Wang, Y.-C., Liu, X.-Q., Sun, T.-M., Xiong, M.-H. & Wang, J. Functionalized micelles from block copolymer of polyphosphoester and poly(epsilon-caprolactone) for receptor-mediated drug delivery. *J. Control. Release* **128**, 32–40 (2008).
126. Goddard-Borger, E. D. & Stick, R. V. An efficient, inexpensive, and shelf-stable diazotransfer reagent: Imidazole-1-sulfonyl azide hydrochloride. *Org. Lett.* **9**, 3797–3800 (2007).
127. Duan, X. *et al.* Amphiphilic graft copolymer based on poly(styrene-co-maleic anhydride) with low molecular weight polyethylenimine for efficient gene delivery. *Int. J. Nanomedicine* **7**, 4961–4972 (2012).
128. Park, I.-K. *et al.* Glucosylated polyethylenimine as a tumor-targeting gene carrier. *Arch. Pharm. Res.* **28**, 1302–10 (2005).
129. Zhang, Y., Liu, Y., Sen, S., Král, P. & Gemeinhart, R. A. Charged group surface accessibility determines micelleplexes formation and cellular interaction. *Nanoscale* **7**, 7559–64 (2015).
130. Tian, H. Y. *et al.* Biodegradable cationic PEG-PEI-PBLG hyperbranched block copolymer: synthesis and micelle characterization. *Biomaterials* **26**, 4209–17 (2005).
131. Elsayed, M. *et al.* Influence of oligospermines architecture on their suitability for siRNA delivery. *Biomacromolecules* **15**, 1299–310 (2014).
132. Lu, B. *et al.* Galactosyl conjugated N-succinyl-chitosan-graft-

- polyethylenimine for targeting gene transfer. *Mol. Biosyst.* **6**, 2529–38 (2010).
133. Schindelin, J. *et al.* Fiji: an open-source platform for biological-image analysis. *Nat. Methods* **9**, 676–82 (2012).
134. Schneider, C. A., Rasband, W. S. & Eliceiri, K. W. NIH Image to ImageJ: 25 years of image analysis. *Nat. Methods* **9**, 671–675 (2012).
135. McCloy, R. A. *et al.* Partial inhibition of Cdk1 in G 2 phase overrides the SAC and decouples mitotic events. *Cell Cycle* **13**, 1400–12 (2014).
136. Liang, W., Mason, A. J. & Lam, J. K. W. Western blot evaluation of siRNA delivery by pH-responsive peptides. *Methods Mol. Biol.* **986**, 73–87 (2013).
137. Wen, T., Qu, F., Li, N. B. & Luo, H. Q. A facile, sensitive, and rapid spectrophotometric method for copper(II) ion detection in aqueous media using polyethyleneimine. *Arab. J. Chem.* (2013).
138. Oskuee, R. K., Dehshahri, A., Shier, W. T. & Ramezani, M. Alkylcarboxylate grafting to polyethylenimine: a simple approach to producing a DNA nanocarrier with low toxicity. *J. Gene Med.* **11**, 921–32 (2009).
139. Fischer, D., Bieber, T., Li, Y., Elsässer, H. P. & Kissel, T. A novel non-viral vector for DNA delivery based on low molecular weight, branched polyethylenimine: effect of molecular weight on transfection efficiency and cytotoxicity. *Pharm. Res.* **16**, 1273–9 (1999).
140. Shi, Y., Cao, X. & Gao, H. The use of azide-alkyne click chemistry in recent syntheses and applications of polytriazole-based nanostructured polymers. *Nanoscale* **8**, 4864–81 (2016).

141. Liu, J. *et al.* Novel reduction-responsive cross-linked polyethylenimine derivatives by click chemistry for nonviral gene delivery. *Bioconjug. Chem.* **21**, 1827–35 (2010).
142. Zong, H., Goonewardena, S. N., Chang, H.-N., Otis, J. B. & Baker, J. R. Sequential and parallel dual labeling of nanoparticles using click chemistry. *Bioorg. Med. Chem.* **22**, 6288–96 (2014).
143. Liu, L., Zheng, M., Renette, T. & Kissel, T. Modular synthesis of folate conjugated ternary copolymers: polyethylenimine-graft-polycaprolactone-block-poly(ethylene glycol)-folate for targeted gene delivery. *Bioconjug. Chem.* **23**, 1211–20 (2012).
144. Oude Blenke, E. *et al.* Liposome functionalization with copper-free ‘click chemistry’. *J. Control. Release* **202**, 14–20 (2015).
145. Calabrese, C. M. *et al.* Biocompatible infinite-coordination-polymer nanoparticle-nucleic-acid conjugates for antisense gene regulation. *Angew. Chem. Int. Ed. Engl.* **54**, 476–80 (2015).
146. Chang, P. V *et al.* Copper-free click chemistry in living animals. *Proc. Natl. Acad. Sci. U. S. A.* **107**, 1821–6 (2010).
147. Aguiar, J., Carpena, P., Molina-Bolívar, J. A. & Carnero Ruiz, C. On the determination of the critical micelle concentration by the pyrene 1:3 ratio method. *J. Colloid Interface Sci.* **258**, 116–122 (2003).
148. Thapa, B., Kumar, P., Zeng, H. & Narain, R. Asialoglycoprotein Receptor-Mediated Gene Delivery to Hepatocytes Using Galactosylated Polymers. *Biomacromolecules* **16**, 3008–20 (2015).

149. Nadithe, V. *et al.* Screening nylon-3 polymers, a new class of cationic amphiphiles, for siRNA delivery. *Mol. Pharm.* **12**, 362–74 (2015).
150. Liu, L. *et al.* Efficient and Tumor Targeted siRNA Delivery by Polyethylenimine-graft-polycaprolactone-block-poly(ethylene glycol)-folate (PEI-PCL-PEG-Fol). *Mol. Pharm.* **13**, 134–43 (2016).
151. Honary, S. & Zahir, F. Effect of Zeta Potential on the Properties of Nano-Drug Delivery Systems - A Review (Part 1). *Trop. J. Pharm. Res.* **12**, 255–264 (2013).
152. Ogris, M. *et al.* The size of DNA/transferrin-PEI complexes is an important factor for gene expression in cultured cells. *Gene Ther.* **5**, 1425–33 (1998).
153. Park, M. R. *et al.* Degradable polyethylenimine-alt-poly(ethylene glycol) copolymers as novel gene carriers. *J. Control. Release* **105**, 367–80 (2005).
154. Yao, H. *et al.* The gene transfection efficiency of a folate-PEI600-cyclodextrin nanopolymer. *Biomaterials* **30**, 5793–803 (2009).
155. Han, J., Silcock, P., McQuillan, A. J. & Bremer, P. Preparation and characterization of poly(styrene-alt-maleic acid)-b-polystyrene block copolymer self-assembled nanoparticles. *Colloid Polym. Sci.* **286**, 1605–1612 (2008).
156. Dominska, M. & Dykxhoorn, D. M. Breaking down the barriers: siRNA delivery and endosome escape. *J. Cell Sci.* **123**, 1183–9 (2010).
157. Boussif, O. *et al.* A versatile vector for gene and oligonucleotide transfer into cells in culture and in vivo: polyethylenimine. *Proc. Natl. Acad. Sci. U. S. A.* **92**, 7297–7301 (1995).

158. Tseng, W.-C., Fang, T.-Y., Su, L.-Y. & Tang, C.-H. Dependence of transgene expression and the relative buffering capacity of dextran-grafted polyethylenimine. *Mol. Pharm.* **2**, 224–32 (2005).
159. Koper, G. J. M., van Duijvenbode, R. C., Stam, D. D. P. W., Steuerle, U. & Borkovec, M. Synthesis and Protonation Behavior of Comblike Poly(ethyleneimine). *Macromolecules* **36**, 2500–2507 (2003).
160. Khazaie, Y. *et al.* Poly[N-(2-aminoethyl)ethyleneimine] as a new non-viral gene delivery carrier: the effect of two protonatable nitrogens in the monomer unit on gene delivery efficiency. *J. Pharm. Pharm. Sci. a Publ. Can. Soc. Pharm. Sci. Société Can. des Sci. Pharm.* **17**, 461–74 (2014).
161. Liu, Y. & Reineke, T. M. Poly(glycoamidoamine)s for gene delivery. structural effects on cellular internalization, buffering capacity, and gene expression. *Bioconjug. Chem.* **18**, 19–30 (2007).
162. Wang, J., Dou, B. & Bao, Y. Efficient targeted pDNA/siRNA delivery with folate-low-molecular-weight polyethyleneimine-modified pullulan as non-viral carrier. *Mater. Sci. Eng. C* **34**, 98–109 (2014).
163. Jafari, M. *et al.* Serum stability and physicochemical characterization of a novel amphipathic peptide C6M1 for siRNA delivery. *PLoS One* **9**, e97797 (2014).
164. Schiffelers, R. M. *et al.* Cancer siRNA therapy by tumor selective delivery with ligand-targeted sterically stabilized nanoparticle. *Nucleic Acids Res.* **32**, e149 (2004).
165. Rotundo, R. F., Rebres, R. A., Mckeown-Longo, P. J., Blumenstock, F. A. &

- Saba, T. M. Circulating cellular fibronectin may be a natural ligand for the hepatic asialoglycoprotein receptor: possible pathway for fibronectin deposition and turnover in the rat liver. *Hepatology* **28**, 475–85 (1998).
166. Rejman, J., Bragonzi, A. & Conese, M. Role of clathrin- and caveolae-mediated endocytosis in gene transfer mediated by lipo- and polyplexes. *Mol. Ther.* **12**, 468–74 (2005).
167. Shi, J. *et al.* Influence of histidine incorporation on buffer capacity and gene transfection efficiency of HPMA-co-oligolysine brush polymers. *Biomacromolecules* **14**, 1961–70 (2013).
168. Ma, R.-Q. *et al.* [Expression and distribution of Nrf2 in several hepatocellular carcinoma cell lines]. *Xi Bao Yu Fen Zi Mian Yi Xue Za Zhi* **27**, 608–10 (2011).
169. Cemazar, M., Hreljac, I., Sersa, G. & Filipic, M. Construction of EGFP Expressing HepG2 Cell Line Using Electroporation. 128–131 (2009).
170. Kobayashi, A. *et al.* Oxidative stress sensor Keap1 functions as an adaptor for Cul3-based E3 ligase to regulate proteasomal degradation of Nrf2. *Mol. Cell. Biol.* **24**, 7130–9 (2004).
171. Zhang, N. *et al.* Nrf2 signaling contributes to the neuroprotective effects of urate against 6-OHDA toxicity. *PLoS One* **9**, e100286 (2014).

**ABSTRACT****TARGETED DELIVERY OF NRF2 siRNA USING MODULAR POLYMERIC MICELLAR NANODELIVERY SYSTEM FOR EFFICIENT TARGET GENE KNOCKDOWN IN HEPATOCELLULAR CARCINOMA**

by

**SHAIMAA YOUSEF****August 2016****Advisor:** Dr. Arun Iyer**Major:** Pharmaceutical Sciences (Pharmaceutics)**Degree:** Master of Sciences

Tumor selective drug delivery as well as chemotherapy associated multi drug resistance (MDR) pose tremendous hurdles for effective cancer therapy. In this regard, designing multifunctional nanocarriers loaded with drug/gene payloads and engineered with tumor targeting ligands can serve as a modular platform for targeted drug/gene delivery. In this study we undertook the synthesis of a self-assembling block copolymer constructed using poly(styrene-co-maleic anhydride, partial iso-octyl ester) (SMAPIE) and branched polyethylenimine (PEI) as building blocks and evaluated its micelle forming ability, siRNA complexation and siRNA delivery potentials. In addition, we engineered galactosamine decorated nanomicelles using modular “*click*” chemistry based approaches for evaluating the targeted delivery of Nrf2 siRNA to Hep G2 liver cancer cells overexpressing asialoglycoprotein receptors (ASGPRs). Our results demonstrate that the

galactosamine decorated nanocarriers could effectively deliver Nrf2 siRNA into Hep G2 liver cancer cells resulting in efficient target gene knockdown, evincing its potential for targeted liver cancer therapy.



## **AUTOBIOGRAPHICAL STATEMENT**

### **SHAIMAA YOUSEF**

#### **EDUCATION**

##### **M.Sc. (2014-2016)**

Pharmaceutical Sciences, Wayne State University, Detroit, Michigan, USA.

##### **B.Sc. (2005-2010)**

Pharmacy and Pharmaceutical Sciences (excellent cumulative grade with honors),  
Faculty of Pharmacy, Cairo University, Cairo, Egypt.

#### **PROFESSIONAL MEMBERSHIPS AND AFFILIATIONS**

- Registered Pharmacist in Egypt (since 2010).
- Member of general syndicate of pharmacists, Cairo, Egypt (since 2010).

#### **SCHOLARSHIPS AND AWARDS**

- The Frank O. Taylor endowed scholarship, Wayne State University (2016).
- The Graduate School Graduate Professional Scholarship, Wayne State University (2015-2016).
- Minapharm pharmaceutical company award for top graduates (2010).
- EIPICO pharmaceutical company award for top graduates (2010).
- Faculty of Pharmacy, Cairo University Dean's award for the top students (2006, 2007, 2008, and 2009).

#### **PRESENTATION**

Shaimaa Yousef, and Arun K. Iyer, "Multifunctional polymeric nanodelivery system as a modular platform for targeted cancer therapy", 12<sup>th</sup> Annual Research Forum, Eugene Applebaum College of Pharmacy and Health Sciences, Wayne State University (November 4, 2015).